DEVELOPMENT OF HDAC11 INHIBITORS AND THEIR APPLICATION IN KRAS-DRIVEN CANCERS

A Dissertation

Presented to the Faculty of the Graduate School

of Cornell University

In Partial Fulfillment of the Requirements for the Degree of

Doctor of Philosophy

by

Se In Son

August 2020

DEVELOPMENT OF HDAC11 INHIBITORS AND THEIR APPLICATION IN KRAS-DRIVEN CANCERS

Se In Son, Ph. D.

Cornell University 2020

Histone deacetylase 11 (HDAC11) is the most recently discovered HDAC and the only member in Class IV HDAC. HDAC11 has diverse biological roles in the immune system, metabolic system, and tumor growth. Although it belongs to the HDAC family, HDAC11 enzymatically works as a lysine defatty acylase. Despite physiological benefits through suppression of HDAC11 activity, few inhibitors targeting HDAC11 selectively have been identified. In this thesis, I will describe developing a selective HDAC11 inhibitor, screening natural products as a potential HDAC11 inhibitor and finding potential application of HDAC11 inhibitors as a therapeutic for KRAS-driven cancers.

In Chapter 2, I describe how to develop inhibitors targeting HDAC11 selectively. Although Class I, II, and IV HDACs share the same zinc-dependent mechanism, most of previous pan-HDAC inhibitors cannot inhibit HDAC11. Therefore, I hypothesized that the catalytic pocket of HDAC11 would be distinct from Class I and II HDACs. As my HDAC11 inhibitor scaffold, Class I and II HDAC inhibitor UF010 which is a bromobenzoyl hydrazide with butyl group was chosen. And I discovered that SIS17 derived from UF010 works as a potent and bioavailable HDAC11 inhibitor.

In Chapter 3, I present an approach for the discovery of an HDAC11 inhibitor by screening natural products. First, I sorted out natural products which have a potential metal binding site. Then, I confirmed that one of the natural products, Garcinol showed similar phenotypes as HDAC11 suppression phenotypes.

Through in vitro HPLC assay and in cell SHMT2 defatty acylation assay, I concluded that Garcinol can be a potent HDAC11 inhibitor. Additionally, to confirm the selectivity of Garcinol, I tested its inhibition against defatty acylation activity of sirtuin2, sirtuin3, and HDAC8 and other deacylation activity of HDAC1, 4, and 6. Garcinol showed weak inhibition against defatty acylation activity of HDAC8 but did not inhibit other HDACs.

In Chapter 4, I elucidate how to apply an HDAC11 inhibitor as a potential therapeutic for KRAS-driven cancers. By screening various cancer cells, cancer cells which growth highly depends on KRAS showed hyper-sensitivity to SIS17 treatment. To elucidate the underlying mechanism for this phenotype, I connected CDC42 as a possible substrate related to this phenotype. CDC42 is a well-known downstream target of KRAS and is involved in the formation of the cell cytoskeleton. I discovered that the HDAC11 lysine fatty acylation site on CDC42 is important for both actin morphology and colony formation of KRAS-driven cancers.

Overall, my thesis work would describe the development of HDAC11 inhibitors in the Chemistry part and new treatment perspectives for KRAS-driven cancers using the identified HDAC11 inhibitors in the Biology part.

BIOGRAPHICAL SKETCH

Se In Son was born in South Korea and received her Bachelor's degree from Sogang University in 2013. She majored in Chemistry, graduated from her undergraduate study as *Summa Cum Laude* and awarded Dean's list from Sogang University. Her undergraduate research work was focused on the development of a nanoparticle-covered ITO glass, which can produce electricity triggered by sunlight. This work was conducted under the guidance of Prof. Young Soo Kang in Sogang University. After graduation, she continued her research work in an organic synthesis laboratory under the guidance of Prof. Won Koo Lee in Sogang University. There, she developed solvent-free synthetic methods for oxindole synthesis and synthesized aziridine-derived small molecules. She received her Master's degree in 2015. She won an outstanding graduate student award in Organic Chemistry from Sogang University and the full scholarship for her graduate study at Sogang University from Kwanjeong educational foundation. In 2015, she began her Ph.D. study in the Department of Chemistry and Chemical Biology at Cornell University and joined Prof. Hening Lin's laboratory, where she studied histone deacetylase 11 (HDAC11).

Dedicated to my parents, Hyung-Dae Son and Eun-Sook Choi,

and to my dear Heavenly Father, Lord.

ACKNOWLEDGMENTS

First, I want to thank my parents who always give me endless love and supports. Without them, I would not know how to survive in hardship. They have taught me to appreciate process instead of consequence, to be always humble, and to build my confidence inside. I feel grateful that they are my role-models and great guidance for my life. I would also like to thank my two sisters, Se-Hee and Star. There would not be enough words to describe how much I love my family.

And I would like to thank my Ph.D. advisor Prof. Hening Lin. I also appreciate my committee members, Prof. Frank Schroeder and Prof. Pamela Chang. I would have never forgotten their hospitality and kindness when I asked them to be my committees. Having two Professors whom I respect so much on my committee meant a lot to me.

I would also thank Dr. Xiaoyu Zhang who is my student mentor at the Lin lab. When I struggled during my first and second years of Ph.D., he always believed my potential, trusted me, and gave good guidance as a mentor. I could not imagine how difficult it could be to spend a lot of time for mentoring a junior student in his last year of Ph.D. He never said no when I asked him for help, and I could stay and survive in the Ph.D. program thanks to him. I appreciate his selfless mentoring, and I would acknowledge him for the rest of my career. I would also like to thank all previous/current lab members who I worked with. They are good friends and co-workers. I feel so lucky to have an opportunity to work with them.

I would also thank my previous mentors, Prof. Young Soo Kang and Prof. Won Koo Lee at Sogang University. I could pursue my career in science thanks to their

wonderful mentoring. Thanks to great education at Sogang University, I could build my passion for science. I always feel so proud to be a student of Sogang University and feel grateful to meet Professors at Sogang University.

I also thank to Cornell University and the Chemistry department. I have met a lot of nice and passionate scientists here. This place is like my first home in USA. I appreciate Cornell University and the Chemistry department to give me a chance to stay here for my Ph.D.

Last, I would like to thank my heavenly Father, Lord for everything. All glory I had and I would have dedicates to him.

TABLE OF CONTENTS

LIST OF FIGURES

CHAPTER 1

AN OVERVIEW OF HDAC11, GARCINOL AND KRAS

My thesis work is developing inhibitors targeting HDAC11, screening natural products as a potential HDAC11 inhibitor and finding its application as a potential therapeutic for KRAS-driven cancers. In this chapter, I review previous research related to HDAC11 phenotype, development of HDAC11 inhibitors, including a natural product, Garcinol, and current therapeutics for KRAS.

Introduction of HDAC11 (Histone Deacetylase 11).

Histone deacetylases (HDACs) that can remove acetyl group from histones have long been regarded as good therapeutic targets. HDACs have been known to tighten chromatin complexes and to decrease the approach of proteins which initiate transcription. HDACs have been also well-reported that they could remove acetyl groups from non-histone proteins such as α-tubulin. There are 4 classes in HDACs based on their amino acid sequence homology to the yeast original enzymes and domain organization (Figure 1.1).[1]

A.

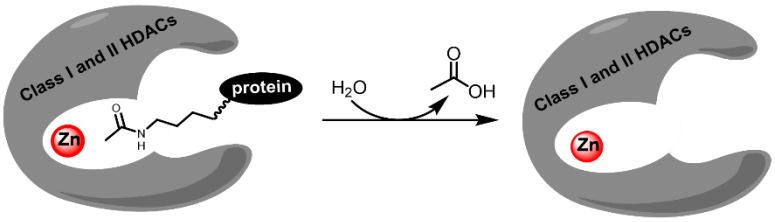

B.

Class	Members	Subcellular localization	Knockout Phenotype in mice
I	HDAC1	Nucleus	Proliferation Defects (Lethal)
	HDAC2	Nucleus	Cardiac Malformation (Lethal)
	HDAC3	Nucleus	Gastrulation Defects (Lethal)
	HDAC8	Nucleus/Cytoplasm	Craniofacial Defects (Lethal)
IIA	HDAC4	Nucleus/Cytoplasm	Chondrocyte Differentiation Defect (Lethal)
	HDAC5	Nucleus/Cytoplasm	Exacerbated Cardiac Hypertrophy after stress (Viable)
	HDAC7	Nucleus/Cytoplasm/ Mitochondria	Endothelial Dysfunction (Lethal)
	HDAC9	Nucleus/Cytoplasm	Exacerbated Cardiac Hypertrophy after stress (Viable)
IIB	HDAC6	Mostly Cytoplasm	Increased Tubulin Acetylation (Viable)
	HDAC10	Mostly Cytoplasm	Viable
III	Sirtuins in mammals (SIRT1, SIRT2, SIRT3, SIRT4, SIRT5, SIRT6, SIRT7)		Various based on each sirtuin
IV	HDAC11	Nucleus/Cytoplasm	Viable

Figure 1.1. General information on HDACs. (A) Zinc dependent deacetylation activity and mechanism of Class I and II HDACs. (B) Classes of HDACs and their localization and knockout phenotype in mice.

Class I HDACs that are homologous to yeast Rpd3 enzyme include HDAC1, 2, 3 and 8, and Class II HDACs which are homologous to yeast Hda1 enzyme comprise HDAC4, 5, 6, 7, 9, and 10. Class IV HDAC is not highly homologous with either Rpd3 or Hda1. Therefore, HDAC11 is classified in the only member of Class IV HDAC (Figure 1.1.B). Sirtuins which belong to Class III HDACs have NAD-dependent mechanism unlike other classes of HDACs.[2] Except Class III HDACs, Class I, II and IV HDACs have the zinc-dependent deacylation mechanism (Figure

1.1.A).

There also have been many efforts to figure out knockout phenotype of each HDAC in mice (Figure 1.1.B).[3] Deletion of Class I HDACs has been reported to show lethality in mice such as proliferation defects and cardiac malfunction. Knockout of Class II HDACs (HDAC4 and HDAC7) is also detrimental for mice, yet mice could be viable. On the other hand, knockout and suppression of HDAC11 have been reported to impede cancer progression and increase immune response in viral infection without harmful effects in normal cells and mice.[4] This indicates that HDAC11 inhibitors can be good drug candidates not only because of its potential as therapeutics for cancers and immune response, but also because of the non-toxicity.

Enzymatic activities of HDAC11.

HDAC11 has been discovered as a member of HDAC in 2002 and it is the most recently discovered HDAC. Therefore, its activity physiological roles remained unclear until a few years ago.

A.

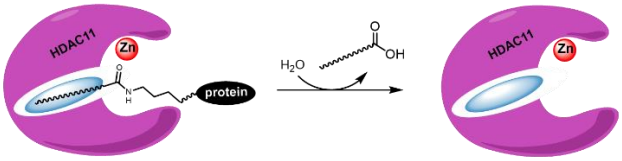

B.

Catalytic Efficiency of HDAC11 on acyl-H3K9 peptide			
Peptide	K_{cat} (S^{-1})	K_m(μM)	K_{cat}/K_m ($S^{-1}M^{-1}$)
Myr-H3K9	0.262±0.002	17.3±2.3	$1.54X10^4$
Ac-H3K9	ND	ND	~1

Figure 1.2. Activity of HDAC11. (A) Scheme of zinc dependent defatty acylation of HDAC11. (B) Kinetic data of HDAC11 in HPLC assays[5]

Recently, three research groups including our lab independently reported that HDAC11 works as a defatty-acylase (Figure 1.2.A).[5] Cao et al. examined deacylation activity of HDAC11 using acyl-H3K9 peptides. In an HPLC assay, no deacetylation activity of HDAC11 was detected while defatty acylation activity of HDAC11 was very efficient, with catalytic efficiency 15,000 higher (Figure 1.2.B). Hence, although

HDAC11 shares the same zinc dependent mechanism with Class I and II HDACs, it specifically recognizes long chain fatty acyl groups. This unique defatty acylation activity provided insight to develop a selective HDAC11 inhibitor.

Physiological role of HDAC11 and the underlying mechanisms

Physiological roles of HDAC11 have been mostly reported in the areas of immune response, metabolism, and, to a lesser extent, tumorigenesis.[5]

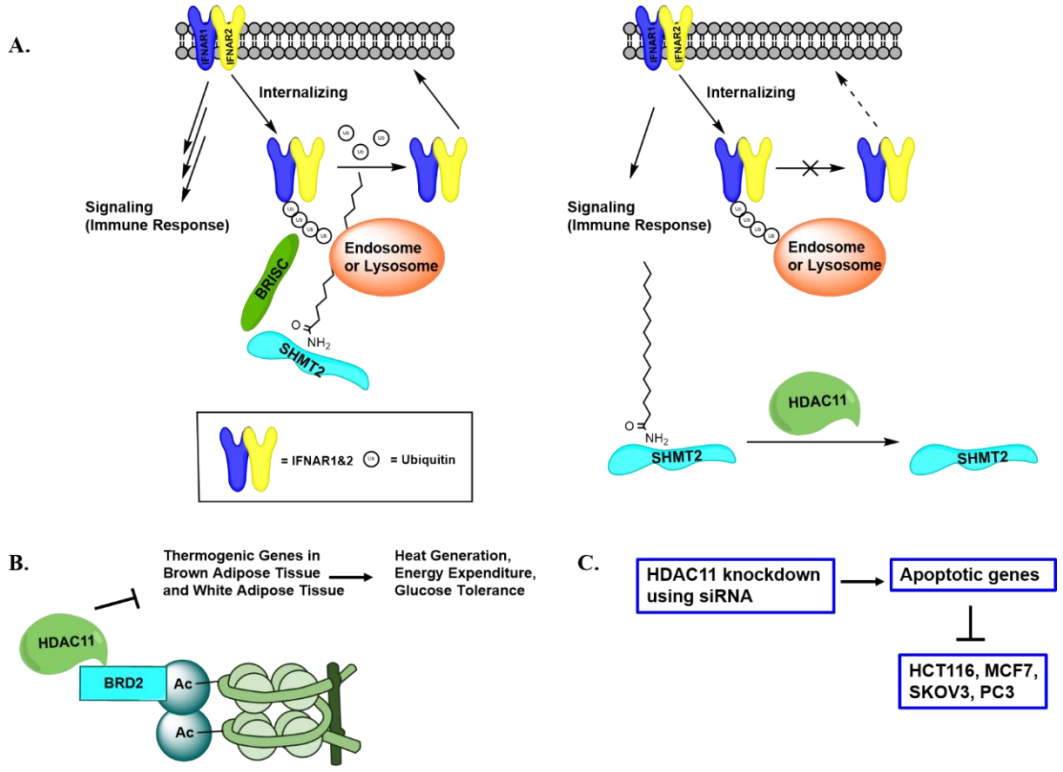

Figure 1.3. Phenotypic reports of HDAC11 suppression/depletion. (A) HDAC11 knockdown can increase fatty acylated SHMT2 level and decrease the ubiquitination of interferon alpha receptors (IFNAR1 and IFNAR2). (B) HDAC11 involves in metabolic system in mice model. (C) HDAC11 knockdown can induce apoptosis of cancer cells.

Cao at al. recently reported that suppression of HDAC11 increases type I interferon signaling in cells and in mice by promoting type I interferon receptor (IFNAR1 and IFNAR2) deubiquitination (Figure 1.3.A). In this research, the author showed in vitro

results that HDAC11 works as a defatty-acylase 15,000-fold more efficiently than as a deacetylase. Additionally, Serine hydroxy methyltransferase 2 (SHMT2) was validated as a physiological HDAC11 substrate through Stable Isotope Labeling by Amino acids in Cell culture (SILAC) proteomic experiment.[5]

Furthermore, the author showed that SHMT2 defatty acylation by HDAC11 regulates downstream genes of interferon-alpha signaling pathway in viral infection.

Besides the role of HDAC11 in virus defense, there are several reports showing that HDAC11 plays a role in regulating metabolism. One of the studies discovered that the depletion of HDAC11 in mice would stimulate brown adipose tissue (BAT) formation and beiging of white adipose tissue (WAT) (Figure 1.3.B). Bagchi et al. showed that HDAC11 knockout mice have increased thermogenic potential, decreased obesity, and increased insulin sensitivity under the high-fat diet. The underlying mechanism for this phenotype was explained by suppression of BAT transcriptional system by HDAC11 in association with BRD2 domain.[5]

Lastly, there have been a few reports that the depletion of HDAC11 inhibits cancer cell proliferation (Figure 1.3.C). Deubzer et al reported that HDAC11 was overexpressed in several carcinomas compared to normal cells and depletion of HDAC11 caused cell death in 4 different cancer cells – HCT116 Colon, PC3 Prostate, MCF7 Breast, and SKOV3 Ovarian cancers. They seeded cancer cells on plates and infected cells with siRNA (silencing RNA) of HDAC11. After 96 hrs of transfection, they measured numbers of survived cells using trypan blue reagent. To demonstrate the underlying mechanism of the phenotype, 72 and 96 hrs after seeding cancer cells in cell plates, they measured caspase 3-like activity using Annexin V staining and showed that caspase 3-like activity increased in cancer cells with HDAC11 depletion. Overall, in this study, HDAC11 depletion showed no detectable effects on normal cells while it increased cancer cell death by inducing apoptosis.[5]

Compared to other HDACs, HDAC11 is less characterized. However, HDAC11 knockout mice have been reported as viable. Additionally, HDAC11 knockdown does not inhibit normal cells to grow. Instead, HDAC11 suppression and depletion would be beneficial in tumorigenesis, immune response and metabolic disease. This justifies

the necessity of HDAC11 inhibitor development.

Reported HDAC11 inhibitors

Since the structure of HDAC11 is still unknown and the catalytic activity of HDAC11 as a defatty-acylase has been recently discovered, there have been only a few HDAC11 inhibitors reported (Figure 1.4). Moreno-Yruela et al reported HDAC11 function as a defatty-acylase in vitro along with a few HDAC11 inhibitor candidates.[5]

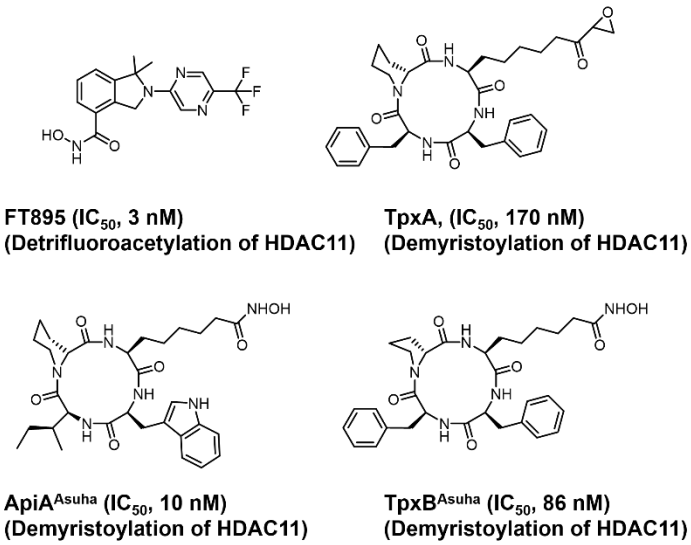

Figure 1.4. Previous HDAC11 inhibitors.

In the paper, they screened 5 commercially available pan-HDAC inhibitors – TSA, SAHA, ApiA, TpxA and TpxB. TSA and SAHA started showing moderate inhibition at concentrations higher than 32 μM (for TSA) or 164 μM (for SAHA). They also tested macrocyclic pan-HDAC inhibitors (ApiA, TpxA and TpxB) and the macrocyclic inhibitors showed potent inhibition against HDAC11 in nM range (Figure 1.4). However, since the three inhibitors have been reported to strongly inhibit other HDACs for which the knockout is lethal in mice, these inhibitors may have high toxicity due to their non-selective nature.

Forma Therapeutics also recently reported their own HDAC11 inhibitor – FT895 (Figure 1.4).[6] FT895 (N-hydroxy-2-arylisoindoline-4-carboxamide) showed potent inhibition against HDAC11 (3 nM) based on their fluorescent assay using

trifluoroacetyl fluorescent probe, which is not physiologically relevant. Thus, the IC_{50} of FT895 may not be very meaningful. FT895 showed moderate inhibition against HDAC8 but the compound showed excellent selectivity against other HDACs None the less, FT895 indeed showed the possibility to develop HDAC11-selective inhibitors without inhibiting other HDACs.

Other than FT895, there were many reports about potential HDAC11 inhibitors but most of them inhibit other HDACs more efficiently than HDAC11 and were not tested on HDAC11's defatty-acylation activity. These limited resources for HDAC11 inhibitors promoted our lab to develop potent HDAC11-selective inhibitors.

Introduction of Garcinol

My thesis work also identifies Garcinol as an HDAC11 inhibitor and thus here I will summarize literature knowledge on Garcinol.

Garcinol is a natural product and a polyisoprenylated benzophenone compound from the *Garcinia indica* fruit (Figure 1.5).[8] It has been well-known as a potent inhibitor for histone acetyltransferases (HATs), p300 (IC_{50} ~ 7 μM in vitro.) and PCAF (IC_{50} ~ 5 μM in vitro.). Garcinol regulates cell growth and division through regulating interactions with transcription factors. Garcinol also can induce caspase-3 activation and apoptosis through p300-mediated acetylation of p53.

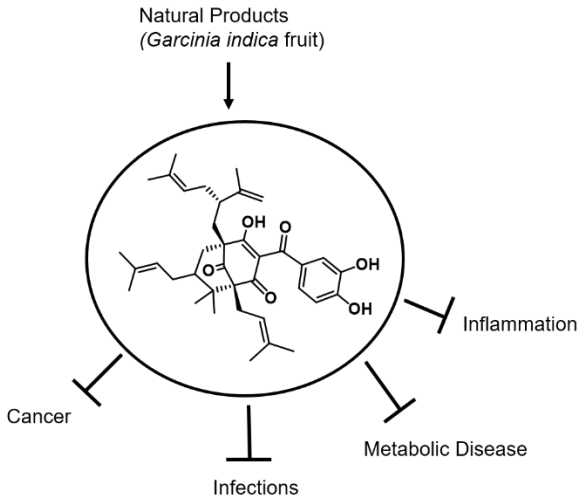

Figure 1.5. Garcinol Structure and its reported application.

Furthermore, Garcinol has been known to downregulate gene expression in HeLa cells and exhibit dose-dependent cancer cell-specific growth inhibition in MCF-7 and MDA-MB-231 breast cancer cells. Garcinol exhibits anti-carcinogenic and anti-inflammatory properties via suppression of prostaglandin E2 synthesis and 5-lipoxygenase product generation. Garcinol has also been used in a mice inflammation model.[9]

Despite all beneficial and promising results of Garcinol usage, the explanation of how Garcinol provides all these beneficial effects has been mostly based on in vitro assay results suggesting that it is a HAT inhibitor. Our lab found out that Garcinol can work as a potent HDAC11 inhibitor and this finding would not only provide another potent HDAC11 inhibitor but would also provide new insights into the underlying mechanism of Garcinol's biological activities.

Introduction of KRAS mutation in human cancers and limitation of current treatment.

RAS proteins are a family of small GTPases that are involved with transmission of cell signaling and regulation of various cell behaviors.[10]

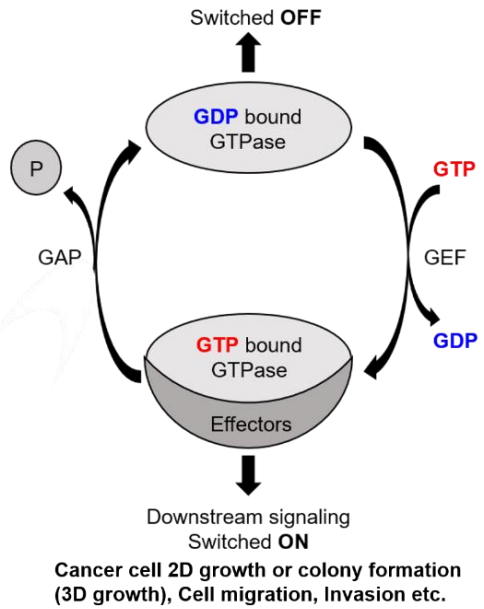

Figure 1.6. Activation and inactivation of GTPase proteins through "switch-on" and "switch-off" cycle.

GTPase proteins work as binary signaling switches with “switch-on” and “switch-off” states (Figure 1.6). During the “switch-on” status, RAS proteins are bound to guanosine triphosphate (GTP), which possesses one more phosphate group than GDP. Activation and deactivation of RAS are regulated by a cycle between the active (Switch-on) GTP-bound and inactive (Switch-off) GDP-bound forms.

When RAS gets activation signals, it passes the activation signal to effector proteins which ultimately turn on genes associated with cell proliferation and survival. Presence of Kirsten rat sarcoma viral oncogene homolog (KRAS) mutation is a prognostic biomarker in several cancer cells. The Ras family includes three kinds of RAS genes, HRAS, NRAS and KRAS (which is alternatively spliced into KRAS4A and KRAS4B). Among the three RAS genes, KRAS is the most frequently mutated in cancer cells, especially in pancreatic, colon, lung and rectal cancers (Figure 1.7.A). One mutation, G12C, a glycine to cysteine substitution at codon 12, accounts for 4% of all KRAS mutations.[11] With this mutation, the activated state (Switch-on) of KRAS is favored and eventually this mutation amplifies signaling pathways which lead to oncogenesis. Although there have been many reports and attempts to overcome the KRAS mutation-driven tumorigenesis, it is still challenging to target KRAS. Most of previous KRAS targeted inhibitors have toxicity issue since they could also target non-mutated KRAS which is required for normal cell growth.[12]

Current therapeutic strategies for RAS mutant cancers include the targeting of RAS downstream proteins such as MEK, ERK, Akt, or mTOR (Figure 1.7.B). However, the downstream proteins are important for both normal cells signaling and oncogenic signaling. Therefore, these strategies may have inevitable toxicity problems.[12] Hence, in Chapter 4, I suggest a new approach to impede transformation of KRAS mutant cancers without toxicity through HDAC11 inhibitor treatment.

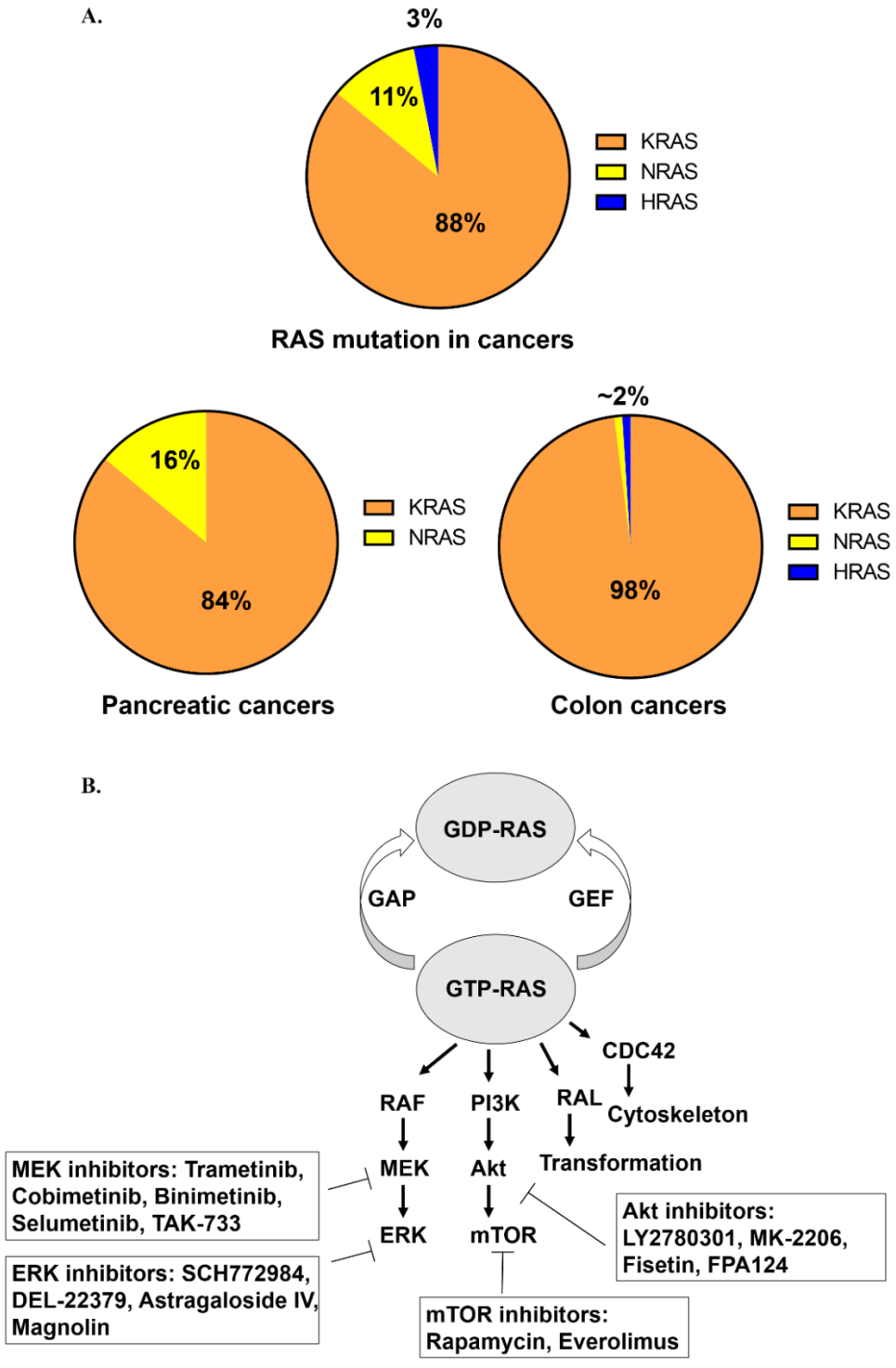

Figure 1.7. RAS mutation in cancers and potential therapeutics for RAS derived cancers. (A) Percentage of KRAS, NRAS and HRAS mutation in cancers. (B) Previous approach to treat RAS mutant cancers.

Summary of my thesis research

HDAC11 is the most recently discovered and the least studied HDAC. In recent years, it has been reported to have crucial roles in immune function, metabolism, and tumorigenesis. During my Ph.D., I have worked on developing selective HDAC11 inhibitors that do not impede other HDAC's activity and exploring natural products as potential HDAC11 inhibitors such as Garcinol. I then applied my developed inhibitors in different types of cancer cells. Surprisingly, HDAC11 inhibition potently suppressed the anchorage-independent growth of KRAS dependent pancreas and colon cancer cells. Our preliminary data suggest that HDAC11 inhibitors could be potential therapeutics for KRAS-driven cancers and may provide a possible solution for the long-term challenge of targeting KRAS.

References

1. Dokmanovic M, Clarke C, Marks PA, Histone deacetylase inhibitors: overview and perspectives, *Molecular Cancer Research,* **5**, 981–989, DOI: 10.1158/1541-7786.MCR-07-0324, (2017).
2. Bürger M, Chory J, Structural and chemical biology of deacetylases for carbohydrates, proteins, small molecules and histones, *Communications Biology*, **1**, 217, doi: 10.1038/s42003-018-0214-4, (2018).
3. Michael Haberland, Rusty L Montgomery, Eric N Olson, The Many Roles of Histone Deacetylases in Development and Physiology: Implications for Disease and Therapy, *Nat Rev Genet,* **10**, 32-42. doi: 10.1038/nrg2485, (2009).
4. Olaf Witt 1, Hedwig E Deubzer, Till Milde, Ina Oehme, HDAC Family: What Are the Cancer Relevant Targets?, *Cancer Lett.*, **277**, 8-21, doi: 10.1016/j.canlet.2008.08.016, (2009).
DOI: 10.1016/j.canlet.2008.08.016
5. Ji Cao , Lei Sun, Pornpun Aramsangtienchai, Nicole A Spiegelman, Xiaoyu Zhang, Weishan Huang, Edward Seto, Hening Lin, HDAC11 Regulates Type I Interferon Signaling Through Defatty-Acylation of SHMT2, Proc Natl Acad Sci U S A, 116, 5487-5492. doi: 10.1073/pnas.1815365116, (2019); Rushita A Bagchi, Bradley S Ferguson, Matthew S Stratton, Tianjing Hu, Maria A Cavasin, Lei Sun, Ying-Hsi Lin, Dianxin Liu, Pilar Londono, Kunhua Song, Maria F Pino, Lauren M Sparks, Steven R Smith, Philipp E Scherer, Sheila Collins, Edward Seto, Timothy A McKinsey, HDAC11 Suppresses the Thermogenic Program of Adipose Tissue via BRD2, *JCI Insight*, **3**, e120159, doi: 10.1172/jci.insight.120159, (2018); Hedwig E Deubzer 1, Marie C Schier, Ina Oehme, Marco Lodrini, Bernard Haendler, Anette Sommer, Olaf Witt, HDAC11 Is a Novel Drug Target in Carcinomas, *Int. J. Cancer.*, **132**, 2200-2208, doi: 10.1002/ijc.27876, (2013).
6. Matthew W Martin, Jennifer Y Lee, David R Lancia Jr, Pui Yee Ng, Bingsong Han, Jennifer R Thomason, Maureen S Lynes, C Gary Marshall, Chiara Conti, Alan Collis, Monica Alvarez Morales, Kshama Doshi, Aleksandra Rudnitskaya, Lili Yao,

Xiaozhang Zheng, Discovery of Novel N-hydroxy-2-arylisoindoline-4-carboxamides as Potent and Selective Inhibitors of HDAC11, *Bioorg Med Chem Lett.,* **28**, 2143-2147, doi: 10.1016/j.bmcl.2018.05.021, (2018).
7. X-J Yang 1, E Seto, HATs and HDACs: From Structure, Function and Regulation to Novel Strategies for Therapy and Prevention, *Oncogene,* **26**, 5310-5318, doi: 10.1038/sj.onc.1210599, (2007).
8. Rainer Schobert, Bernhard Biersack, Chemical and Biological Aspects of Garcinol and Isogarcinol: Recent Developments, *Chem. Biodivers.,* **16**, e1900366, doi: 10.1002/cbdv.201900366, (2019).
9. Wen-Chien Huang, Kuang-Tai Kuo, Bamodu Oluwaseun Adebayo, Chun-Hua Wang, Yu-Jen Chen, Ketao Jin, Tung-Hu Tsai, Chi-Tai Yeh, Garcinol Inhibits Cancer Stem Cell-Like Phenotype via Suppression of the Wnt/β-catenin/STAT3 Axis Signalling Pathway in Human Non-Small Cell Lung Carcinomas, *J. Nutr. Biochem.,* **54**, 140-150. doi: 10.1016/j.jnutbio.2017.12.008, (2017).
10. Dhirendra K Simanshu, Dwight V Nissley, Frank McCormick, RAS Proteins and Their Regulators in Human Disease, *Cell*, **170,** 17-33, doi: 10.1016/j.cell.2017.06.009, (2017).
11. Hilmi Kodaz, Osman Kostek, Muhammet Bekir Hacioglu, Bulent Erdogan, Cagnur Elpen Kodaz, Ilhan Hacibekiroglu, Esma Turkmen, Sernaz Uzunoglu, Irfan Cicin, Frequency of RAS Mutations (KRAS, NRAS, HRAS) in Human Solid Cancer, *EJMO*, **1**, 1-7, DOI: 10.14744/ejmo.2017.22931, (2017).
12. Pingyu Liu, YijunWang, XinLi, Targeting the untargetable KRAS in cancer therapy, *Acta. Pharm. Sin. B.*, **9**, 871-879, doi: 10.1016/j.apsb.2019.03.002, (2019)

CHAPTER 2

DEVELOPMENT OF SELECTIVE HDAC11 INHIBITORS[a]

Abstract

Mammalian histone deacetylases (HDACs) are a class of enzymes that play important roles in various biological pathways. Existing HDAC inhibitors target multiple HDACs without much selectivity. Inhibitors that target one particular HDAC will be useful for investigating the biological functions of HDACs and for developing better therapeutics. Here, we report the development of HDAC11-specific inhibitors using an activity-guided rational design approach. The enzymatic activity and biological function of HDAC11 have been little known, but recent reports suggest that it has efficient defatty-acylation activity and inhibiting it could be useful for treating a variety of human diseases, including viral infection, multiple sclerosis, and metabolic diseases. Our best inhibitor, SIS17, is active in cells and inhibited the demyristoylation of a known HDAC11 substrate, serine hydroxymethyl transferase 2 (SHMT2), without inhibiting other HDACs. The activity-guided design may also be useful for the development of isoform-specific inhibitors for other classes of enzymes.

[a] This is a revised version of our published paper: Son. et al. Activity-Guided Design of HDAC11-Specific Inhibitors, *ACS Chemical Biology*, **2019**, 14 (7), pp 1393–1397.

Introduction

Histone deacetylases are a class of zinc-dependent amide hydrolases with important biological functions. They catalyze the deacetylation of numerous substrate proteins, including histones, transcription factors, and signaling proteins and thus regulate various biological processes.[1,2] They are the targets of important anticancer natural products, such as trapoxin and trichostatin A, and clinically used synthetic anticancer drugs, such as Vorinostat and Romidepsin.[1,3,4] Because of their clinical relevance, many small molecule inhibitors are commercially available. However, most of these inhibitors target multiple HDACs and thus the biological effect of targeting a specific HDAC is not clear. It is highly possible that small molecule inhibitors that selectively inhibit only one HDAC are better therapeutics due to lower toxicity. Developing small molecules that target only one of the HDACs is key to addressing these questions.

HDAC11 is the only member in Class IV HDAC and its biological function remains largely unknown. Recently, three research teams independently discovered that HDAC11 works as a defatty-acylase instead of a deacetylase.[5-7] One physiological substrate identified is serine hydroxymethyl transferase 2 (SHMT2), an enzyme important for one-carbon metabolism.[7] Interestingly, HDAC11 and lysine fatty acylation does not affect the enzymatic activity of SHMT2.[7] Instead, they affect the ability of SHMT2 to deubiquitinate type I interferon receptor. Inhibiting HDAC11 therefore has the potential to treat diseases that involve type I interferon signaling. Along this line, there have been reports suggesting that suppression of HDAC11 could be beneficial for treating cancer,[8-10] multiple sclerosis,[11] viral infection,[7] and metabolic disease.[12,13] We therefore set out to develop HDAC11-specific inhibitors utilizing its unique activity profile, the preference for long-chain fatty acyl lysine.

Results and discussion

UF010 as a scaffold for HDAC11 Inhibitors

Although there has been no reported X-ray crystal structure of HDAC11, HDAC11 is similar to Class I HDACs.[1,4] Therefore, our HDAC11 inhibitors were designed based

on known Class I HDAC inhibitors. Known Class I HDAC inhibitors typically contain three structural motifs, a zinc binding group (ZBG), a linker, and a surface recognition group (SRG). [1,4] ZBG is mostly composed of hetero atoms which have lone pairs to chelate with zinc. The linker contains aliphatic group to connect ZBG and SRG and it mimics the side chain of lysine. Last, SRG mostly includes aromatic ring to increase π (pi)-π (pi) interaction with conserved aromatic residues on the surface of HDACs.[1,4] We first examined whether previous HDAC inhibitors could inhibit HDAC11 in vitro using an HPLC assay. However, known HDAC inhibitors such as SAHA, Mocetinostat, and Droxinostat do not inhibit HDAC11 demyristoylation activity while TSA showed weak inhibition at 50 μM. Next, since HDAC11 works as a defatty-acylase and prefers long-chain fatty acyl group, we introduced a palmitoyl group on SAHA and Mocetinostat. However, the introduction of palmitoyl group on SAHA and Mocetinostat did not improve HDAC11 inhibition (Figure 2.1).

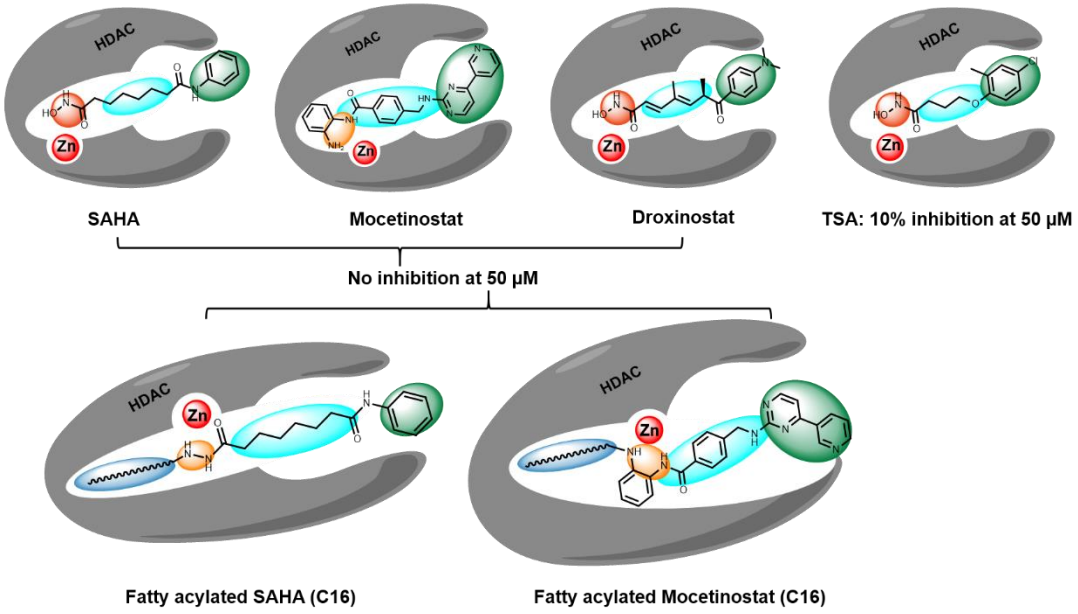

Figure 2.1. HDAC11 inhibition with previous HDAC inhibitors and fatty acylated SAHA and Mocetinostat-like molecules through in vitro HPLC assay.

It was disappointing that pan-HDAC inhibitor, SAHA, cannot inhibit HDAC11 but can inhibit other HDACs efficiently. Therefore, we analyzed conserved amino acids in

Class I, II and IV HDACs surrounding SAHA. Key amino acids such as aspartic acid and histidine residues that coordinate with zinc were conserved in ZBG area within Class I, II and IV HDACs. Aromatic acids that are located on a surface of Class I, II and IV HDACs are also conserved. In the part that recognizes the linker region of the inhibitors, however, leucine and phenyl alanine are found in Class I and II HDACs but tyrosine and arginine are found in Class IV HDAC (Figure 2.2). Although there is no structure information of HDAC11, we hypothesized that the linker part could be the distinct feature of HDAC11.[15] Therefore, we need HDAC inhibitor scaffold with different linkers. We decided to change our HDAC11 inhibitor scaffold to UF010 which does not have the linker part in its structure.

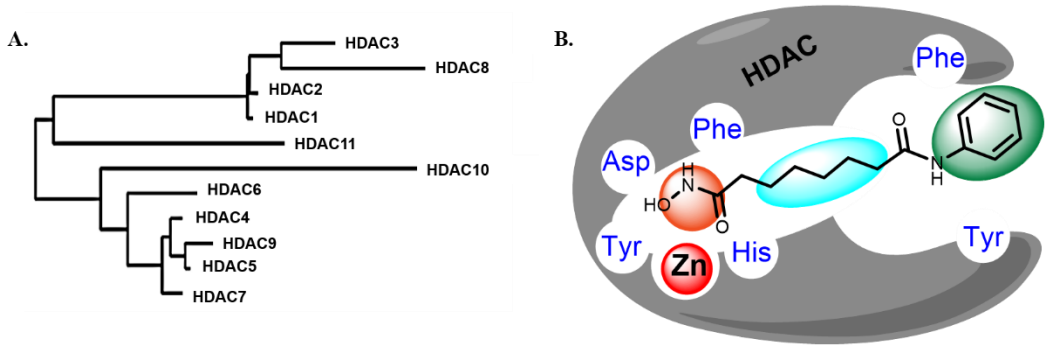

Figure 2.2. Phylogenetic tree of HDACs and conserved amino acids surrounding SAHA. (A) Reported phylogenetic tree of Class I, II and IV HDACs. (B) Conserved amino acids surrounding SAHA in Class I, II and IV HDACs.

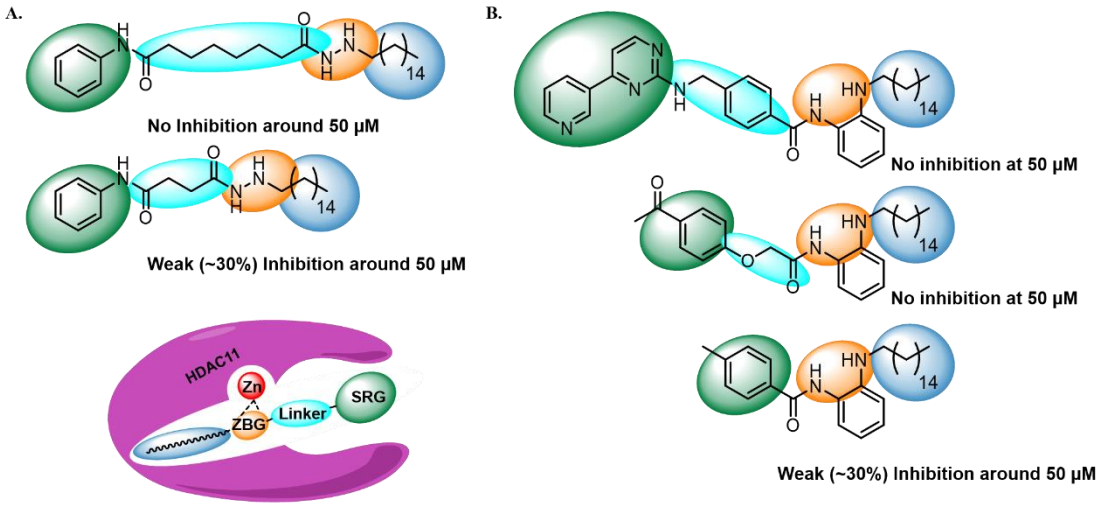

Figure 2.3. Inhibition by fatty acylated SAHA and Mocetinostat-like molecules with a different length of a linker against HDAC11.

Modification of inhibitors

We introduced a palmitoyl group instead of a butyl group on UF010.[16] The inhibition against HDAC11 was tested using the HPLC-based assay with a myristoyl-H3K9 peptide. The UF010-derived SIS4 showed modest inhibition of HDAC11 with an IC_{50} value about 35 μM (Figure 2.4.A). We then decided to further optimize SIS4 by carrying out structure-activity relationship (SAR) studies.

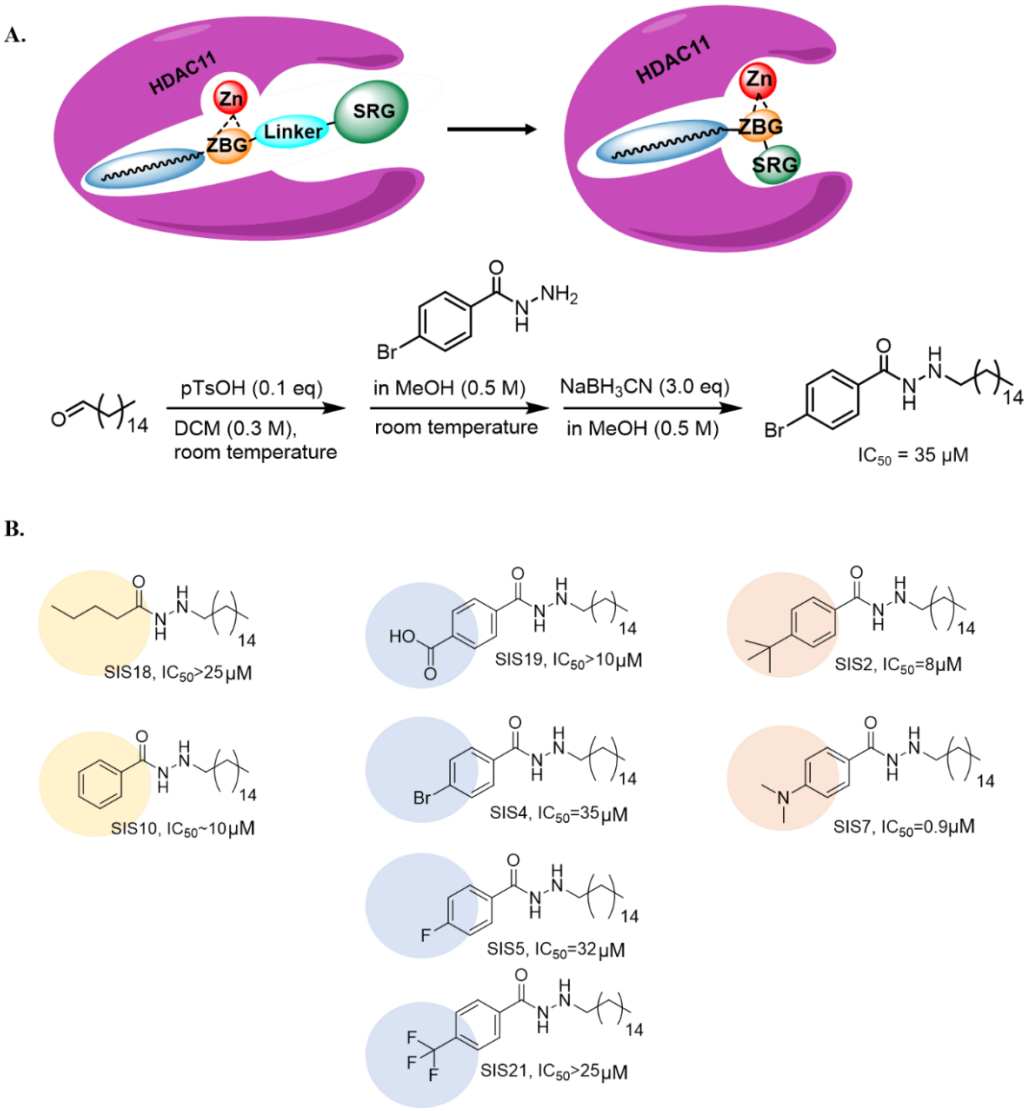

Figure 2.4. HDAC11 inhibitors derived from UF010. (A) Change HDAC11 inhibitor scaffold without a linker part and introduce long fatty acyl group into UF010. (B) IC_{50} values with different substitution on SRG.

First, we examined whether an aromatic ring (SIS10) would give better inhibition than an alkyl chain on SRG (SIS18, Figure 2.4.B). SIS10 with a phenyl ring gave around 2-fold better inhibition than SIS18 with pentyl group. Given that an existence of aromatic ring would make HDAC11 inhibition more efficiently, we put different substitutions on aromatic rings. First, electron donating groups show more potent inhibition against HDAC11 than electron withdrawing groups (Figure 2.4.B). Changing from 4-dimethylamino (SIS7) and tert-butyl (SIS2) to the bromo (SIS4), fluoro (SIS5) or trifluoromethyl (SIS21) substituents did not improve inhibition.

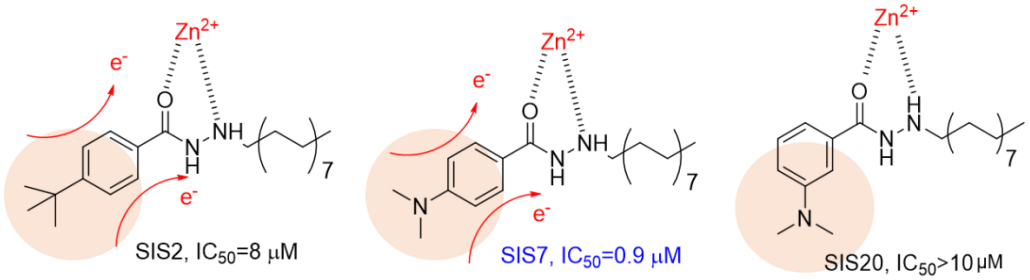

Figure 2.5. Inhibition against HDAC11 with different electron donating groups.

To make sure that the electron donating efficiency is important for HDAC11 inhibition, we side-by-side compared the strongest electron donating group (4-dimethylamino group) based on the Hammett Rule with a weaker electron donating group (tert-butyl group). Consistent with the electron donating ability, SIS2 with a tert-butyl group exhibited weaker HDAC11 inhibition than SIS7 with a 4-dimethylamino group. To further examine the electron donating efficiency contribution towards HDAC11 inhibition, we compared HDAC11 inhibition between SIS7 with 4-dimethylamino group on para position and SIS20 with 4-dimehylamino group on meta position of aromatic ring. Based on electron donation mechanism through resonance in aromatic ring, ortho- and para- positions of electron donating groups would give the most efficient electron donation towards ZBG. Indeed, SIS7

showed better HDAC11 inhibition than SIS20 (Figure 2.5).[17]

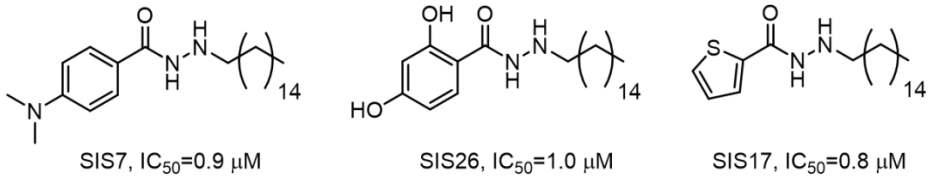

Figure 2.6. Structure and IC_{50} values of three HDAC11 inhibitors.

To obtain more HDAC11 inhibitors, 5-member aromatic ring was introduced for a new HDAC11 inhibitor (SIS17, Figure 2.6). SIS17 has HDAC11 inhibition potency similar to that of SIS7, with an IC_{50} value of 0.83 μM. We then replaced the 5-member aromatic thiophene ring in SIS17 to a pyrrole ring (SIS39). The pyrrole-containing compound SIS39 did not inhibit HDAC11. The pyrrole ring is likely less electron-donating compared to the thiophene ring due to stronger inductive effect of nitrogen atom. Alternatively, the -NH group of the pyrrole ring might be too polar to be accommodated by the HDAC11 active site.

Next, we modified the alkyl chain length on SIS17. The length of hydrophobic chain also seemed to be important, as shortening it (SIS49, SIS50 and SIS65) or lengthening it (SIS52 and SIS66) decreased the HDAC11 inhibition potency. This was consistent with the previous HDAC11 enzymatic activity profile which showed that shorter or longer acyl chains were not good substrates of HDAC11 (Figure 2.7.A).

In addition, to increase hydrophobic interaction with the hydrophobic channel that accommodates the fatty acyl groups in the catalytic pocket, branches and phenyl groups were introduced. However, inhibition against HDAC11 was decreased (Figure 2.7.B).

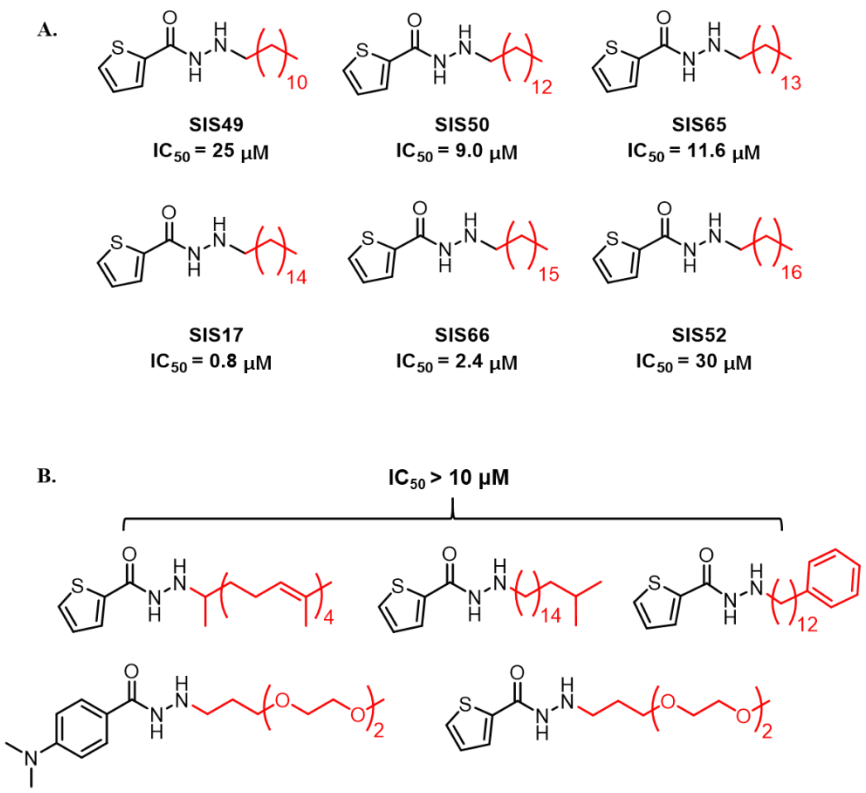

Figure 2.7. Modification of hydrophobic chain. (A) Inhibition against HDAC11 with different alkyl chain length. (B) Introduce branches and phenyl ring on alkyl chain.

In attempt to increase the solubility of compounds in cell media, we introduced PEG-3 alkyl chain based on SIS7 and SIS17 structures. However, the inhibition against HDAC11 was decreased (Figure 2.7.B).

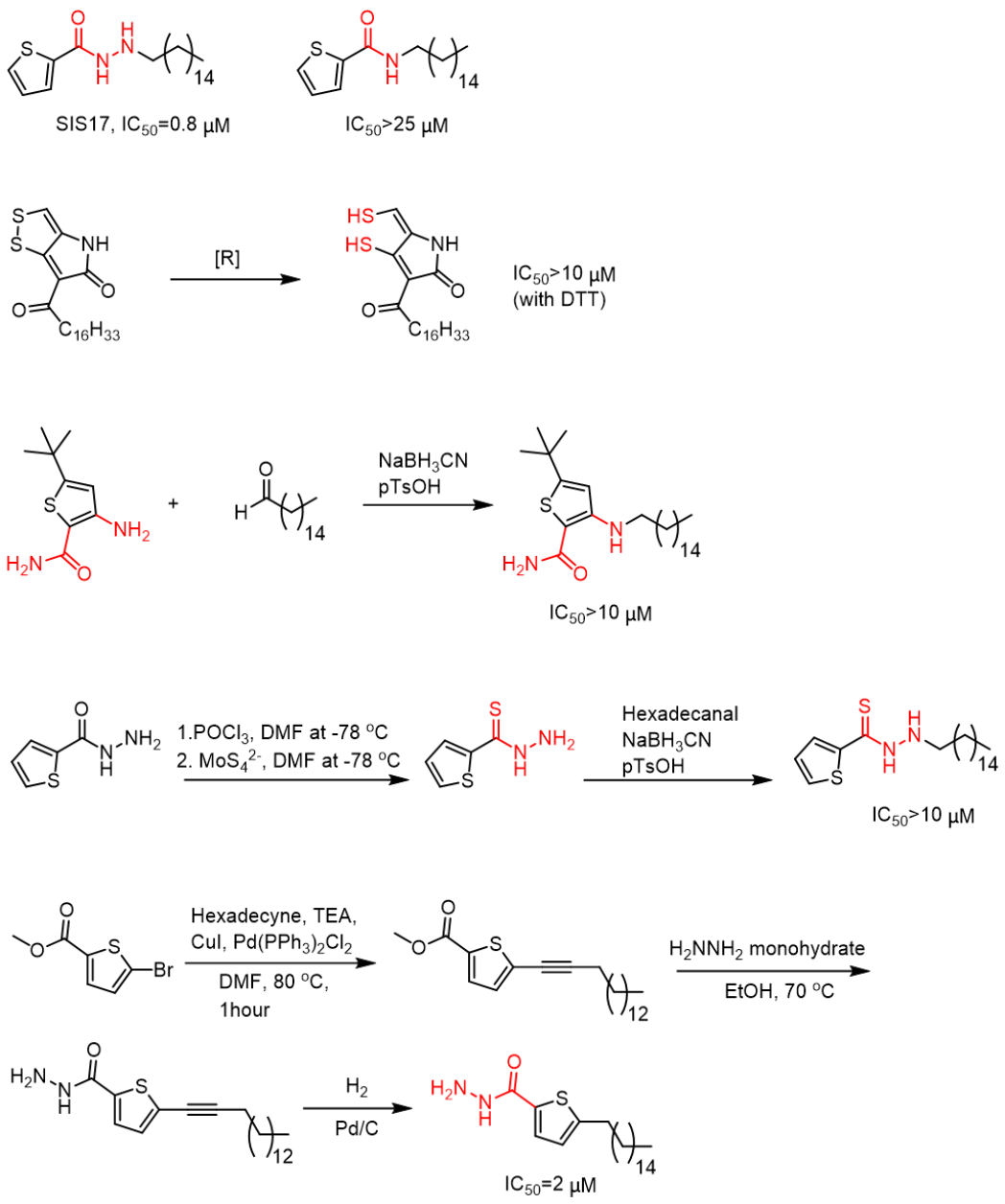

Figure 2.8. Modification of zinc binding group.

To explore other ZBGs, we also examined the requirement of the carbohydrazide moiety, the presumed zinc chelating group, for HDAC11 inhibition. Replacing the carbohydrazide with an amide led to loss of HDAC11 inhibition (Figure 2.8). Thus, the zinc chelating carbohydrazide is crucial for HDAC11 inhibition. We also explored dithiol, benzamide, thiocarbohydrazide, and carbohydrazide at a different position

(Figure 2.8) as potential ZBGs. However, none of compounds improved HDAC11 inhibition (Figure 2.8).[18]

Selectivity and Bioavailability of HDAC11 inhibitors

With the two potent HDAC11 inhibitors, SIS7 and SIS17, we then tested whether they are selective toward HDAC11. This is important as the purpose of our activity-based design was to obtain HDAC11-selective inhibitors. Furthermore, several other HDACs, including SIRT2, SIRT6, and HDAC8, have been shown to be able to remove long chain fatty acyl groups from protein lysine residues. Thus, it is important to make sure that they are not inhibited by the HDAC11 inhibitors. [20-22] To examine the selectivity of SIS7 and SIS17, we picked representative HDACs from each class, Class I (HDAC1 and HDAC8), Class II (HDAC4), and the NAD-dependent Class III (Sirtuins: SIRT1, SIRT2, SIRT3, and SIRT6). Satisfyingly, SIS7 and SIS17 did not show significant inhibition of these HDACs at 100 μM concentrations. The selectivity of these two inhibitors highlights that our activity-guided design is effective.

In the literature, only a few HDAC11 inhibitors had been reported, including palmitic acid, Trapoxin A, and FT895.[5,6,19] In our hands, palmitic acid did not show good inhibition on HDAC11 (no inhibition at 10 μM). TpxA could completely abolish HDAC11 activity at 1 μM but it is a pan-HDAC inhibitor. Forma Therapeutics recently reported an HDAC11-specific inhibitor, FT895.[19] The reported in vitro IC_{50} value is 3 nM, but it was measured using a trifluoroacetyl lysine compound, not the physiological myristoyl lysine peptide. Therefore, we synthesized FT895 and measured its IC_{50} value using the myristoyl-H3K9 in the HPLC assay (Figure 2.9 and the synthesis of FT895 is described in Supplementary data C). FT895 inhibited HDAC11 with an IC_{50} value of 0.74 μM which is slightly better than SIS7 (IC_{50} 0.91 μM) and SIS17 (IC_{50} 0.83 μM). However, it is not as selective as SIS7 or SIS17 because it also inhibited HDAC4 (IC_{50} 25 μM), and HDAC8 (IC_{50} 9.2 μM). Thus, SIS7 and SIS17 are the most selective HDAC11 inhibitors known.

Because of the lack of physiological substrates for HDAC11, none of the known

HDAC11 inhibitors had been tested in cellular assays. It was recently reported that HDAC11 defatty-acylates SHMT2, which in turn regulates type I interferon receptor signaling.[7] We thus checked whether our HDAC11 inhibitors can increase the fatty acylation level of endogenous SHMT2 using a previously established detection method. We first tested whether SIS7 and SIS17 can inhibit the demyristoylation of a myristoyl-SHMT2 peptide by HDAC11 in vitro. Using a myristoyl-SHMT2 peptide as the substrate, SIS7 and SIS17 could still inhibit HDAC11 with IC_{50} values of 1.0 μM and 270 nM, respectively, which is slightly different from that measured with myristoyl-H3K9 peptides.

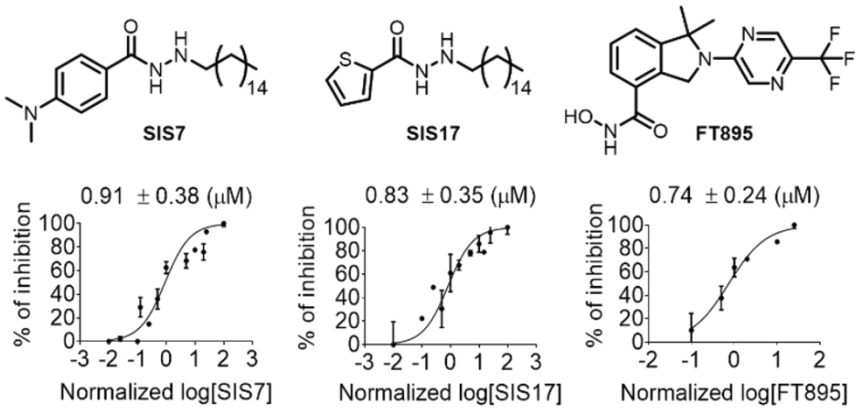

	In vitro HPLC IC_{50} [a]		
	SIS7	SIS17	FT895
HDAC1[c]	>100 μM	>100 μM	>100 μM
HDAC4[d]	>100 μM	>100 μM	~25 μM[b]
HDAC8[e]	>100 μM	>100 μM	9.2 ± 0.41 μM
SIRT1[f]	>100 μM	>100 μM	>100 μM
SIRT2[f]	>100 μM	>100 μM	>100 μM
SIRT3[f]	>100 μM	>100 μM	>100 μM
SIRT6[e]	>100 μM	>100 μM	>100 μM
HDAC11[e]	0.91 ± 0.38 μM	0.83 ± 0.35 μM	0.74 ± 0.24 μM

Figure 2.9. In vitro assay with HDAC11 inhibitors. Top: Comparing SIS7 and SIS17 to FT895 on HDAC11 inhibition using myristoyl-H3K9. IC_{50} values using myristoyl-H3K9 derived from GraphPad Prism are presented as mean values from three independent experiments. Bottom: in vitro IC_{50} values against different HDACs and

sirtuins with acyl-H3K9 peptides. [a] acyl-H3K9 peptides used. [b] FT895 inhibited 50% of HDAC4 activity at 25 μM but inhibition with higher concentration did not increase inhibition rate. [c] Deacetylation activity of enzyme tested. [d] Detrifluoroacetylation activity of enzyme tested. [e] Demyristoylation activity of enzyme tested. [f] Both deacetylation and demyristoylation activities of enzyme tested.

We then tested whether SIS7 and SIS17 could inhibit HDAC11-mediated SHMT2 defatty-acylation in cells. We treated MCF7 cells with 50 μM of an alkyne-tagged palmitic acid analog, Alk14, along with 0, 12.5, 25.0, and 50.0 μM of SIS7 or SIS17 for 6 hrs at 37^{o}C. The labeled proteins were pulled down with streptavidin beads after installation of a biotin tag with click chemistry. The amount of acylated SHMT2 was then detected by Western blot. SIS17 increased the fatty acylation level of SHMT2 significantly in MCF7 cells down to 12.5 μM demonstrating that it is cell permeable and can inhibit HDAC11 in living cells. SIS7 was less effective than SIS17 in cells (Figure 2.10.A).

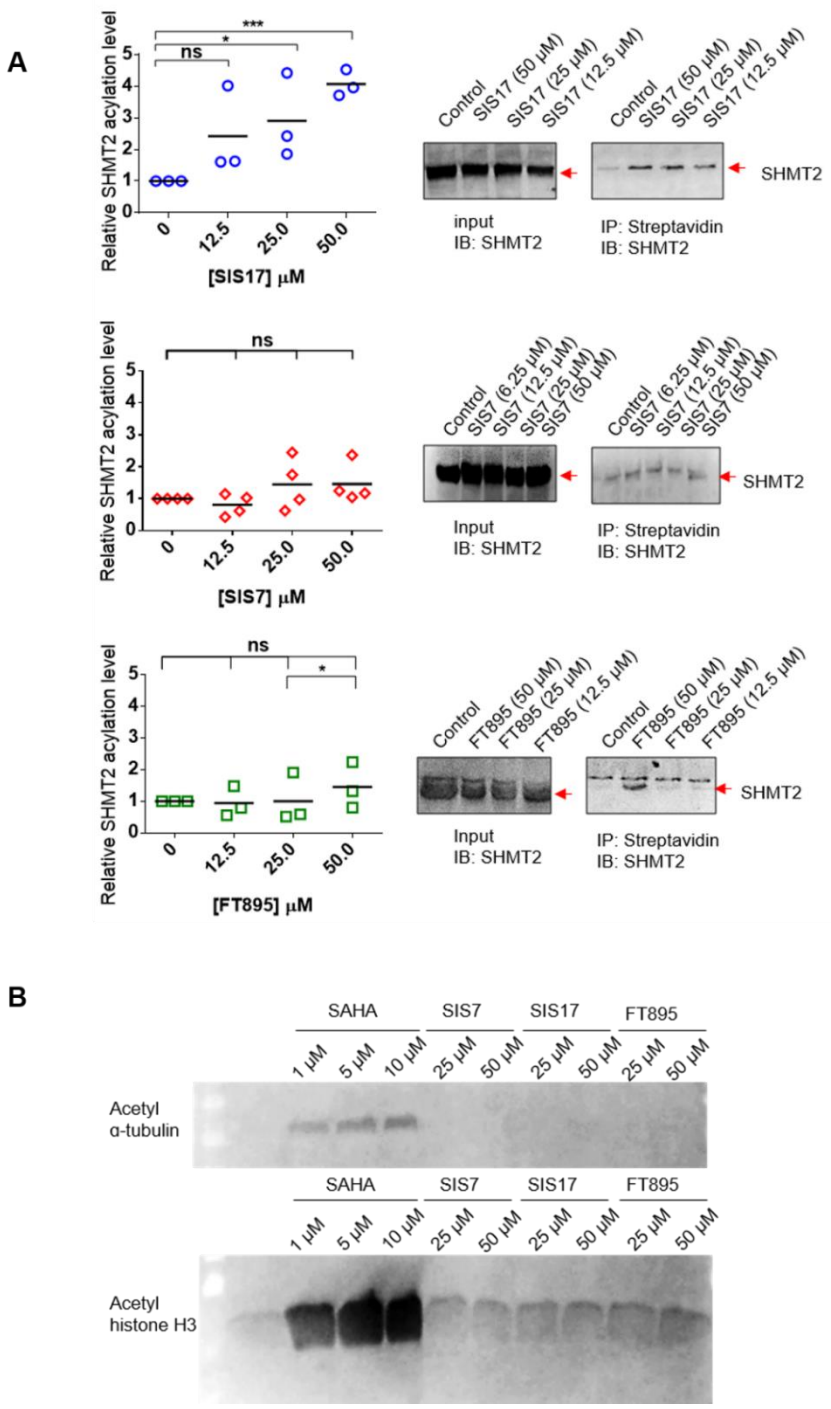

Figure 2.10. (A) Endogenous fatty acylation level graph of SHMT2 and representative western blot images with 12.5, 25.0 and 50.0 μM of SIS7, SIS17 and FT895 in MCF7. Signal intensity was quantified by ImageJ and signal of control group without inhibitor treatment set as 1.0. *, p value < 0.1, **, p value < 0.05, ***, p value < 0.01; ns, not statistically significant. (B) HDAC11 inhibitors do not affect acetylation in

cells. Immunoblot for acetyl-α-tubulin (K40) and acetyl-histone H3 in HEK 293T cells treated with inhibitors for 6 hrs. Loading for each sample was checked by blue-stained membrane.

We believe this was mainly due to cell permeability or metabolic stability. Using and LC-MS based assay, we could readily detect SIS17 in cell lysate, but not SIS7.
To further demonstrate the selectivity of these inhibitors in cells, we checked whether SIS7, SIS17, and FT895 could in-crease the acetylation level of α-tubulin and histone H3. SIS7, SIS17 and FT895 up to 50 μM did not affect the acetylation levels of α-tubulin and histone H3. In contrast, the pan-HDAC inhibitor SAHA significantly increased the acetylation levels at 1 μM (Figure 2.10.B). Thus, the selectivity of SIS7 and SIS17 for HDAC11 is maintained in cells.

Summary

Using an activity-guided rational design approach, we have developed two potent and selective inhibitors, SIS7 and SIS17, for HDAC11. In vitro, SIS7 and SIS17 are slightly less potent against HDAC11 compared to FT895 but are more selective. In cells, SIS17 appears better than FT895 and SIS7 due to increased cell permeability and/or metabolic stability. To our best knowledge, SIS17 represents the first HDAC11-selective inhibitor to show cellular effects. Given the recent increased research interest in HDAC11, we believe SIS17 will be a useful tool compound to explore the biological function and therapeutic potential of HDAC11. Furthermore, we believe this activity-guided design approach could be generally useful for the development of isoform-selective inhibitors for other families of enzymes.

Methods

General Information

Reagents. Commercially available chemicals were purchased from Sigma, Aldrich, TCI Chemicals, Alfa Aesar, Fischer, Matrix Scientific, Combi-Blocks and Cayman. Unless otherwise noted, all reagents were used without further purification. Anti-Flag affinity gel (#A2220) and anti-Flag antibody conjugated with horseradish peroxidase (#A8592) were purchased from Sigma-Aldrich. Acetyl-Histone H3 Antibody (#9675), acetyl α-tubulin (#9671) antibodies were purchased from Cell Signaling Technology. Trapoxin A (CAS 133155-89-2), SHMT2 (mSHMT Antibody (F-11): sc-390641- Non-conjugated), ß-actin antibody (SC-47778 HRP) and goat anti-mouse IgG-HRP (sc-2005) were purchased from Santa Cruz. Palmitic acid, 3× Flag peptide, and protease inhibitor cocktail were purchased from Sigma-Aldrich. ECL plus western blotting detection reagent and universal nuclease for cell lysis were purchased from Thermo Scientific Pierce. Acyl peptides (acetyl-H3K9, Free H3K9, myristoyl-H3K9, and Alk14) were synthesized according to known procedures.[24] The peptide sequence for the H3K9 peptide is KQTARK(modified)STGGWW with uncapped N-terminal and SHMT2 peptide is SDEVK(modified)AHLLAWW with capped acetyl N-terminal; K (lysine) with myristoyl group is the reported catalytic site of HDAC11.[7]

Instrumentation. High-resolution MS was obtained using DART-Orbitrap mass spectrometer. TLC plates were purchased from EDM Chemicals (TLC Silica gel 60 F254, 250 mm thickness). Flash column chromatography was performed over Silica gel 60 (particle size 0.04- 0.063 mm) from EDM Chemicals.

Proton nuclear magnetic resonance (^{1}H NMR) spectra and carbon nuclear magnetic resonance (^{13}C NMR) spectra were recorded on INOVA 400 (500 MHz) and Bruker-500 (500 MHz). Chemical shifts for protons are reported in parts per million downfield from tetramethylsilane and are referenced to the NMR solvent residual peak ($CHCl_3$ δ 7.26). Chemical shifts for carbons are reported in parts per million downfield from tetramethylsilane and are referenced to the carbon resonances of the NMR solvent ($CDCl_3$ δ 77.0). Data are represented as follows: chemical shift,

multiplicity (br = broad, s = singlet, d = doublet, t = triplet, q = quartet, m = multiplet), coupling constants in Hertz (Hz), and integration.
Analytical HPLC analysis was carried out on a SHIMADZU LC with Kinetex 5u EVO C18 100A column (100 mm × 4.60 mm, 5 μm, Phenomenex) monitoring at 215 nm and 280 nm. Solvents for analytical HPLC were water with 0.1% (v/v) trifluoroacetic acid (TFA) as solvent A and acetonitrile with 0.1% (v/v) TFA as solvent B. Compounds were analyzed at a flow rate of 0.5 mL/min.

Cell culture. HEK293T MCF7 cells were cultured in DMEM with 10% (v/v) heat-inactivated FBS. The cell lines used for experiments had been passaged no more than 20 times and all cell lines were tested for and showed no mycoplasma contamination.

Abbreviations Used. NAD - Nicotinamide adenine dinucleotide, DTT – Dithiothreitol, NMR - Nuclear Magnetic Resonance, FBS- Fetal Bovine Serum, LC-MS - Liquid chromatography–mass spectrometry, HPLC - High-Performance Liquid Chromatography, MeOH–Methanol, EtOAc–ethyl acetate, THF–tetrahydrofuran, Et_2O–diethyl ether, CH_2Cl_2–dichloromethane, TEA–triethylamine, MeCN–acetonitrile, TLC–thin layer chromatography, TsOH–*p*-toluenesulfonic acid, DMEM (Dulbecco's Modified Eagle Medium), Alk14 (Palmitic Acid Alkyne) and BCA (Bicinchoninic acid).

Expression and Purification of HDACs and Sirtuins from HEK293T Cells
Flag-tagged HDAC and Sirtuin (SIRT) expression plasmids were previously described.[2] Full-length human HDACs and sirtuins were inserted into the pCMV-Tag 4a vector with a C-terminal Flag tag. All plasmids were transfected into HEK293T cells using FuGene 6 Transfection Reagent according to the manufacturer's protocol (from Promega). Eight 10-cm plates of cells were collected by centrifugation at 500 × g for 5 min and then lysed in 2 ml of Nonidet P-40 lysis buffer (25 mM Tris-HCl, pH 7.4, 150 mM NaCl, 10% (v/v) glycerol and 1% (v/v) Nonidet P-40) with protease inhibitor cocktail (1:100 dilution) at 4 °C for 30 min. After centrifugation at 15,000 ×

g for 15 min, the supernatant was collected and incubated with 20 μL anti-Flag affinity gel at 4 °C for 2 h. The affinity gel was washed three times with 1 ml of washing buffer (25 mM Tris-HCl, pH 7.4, 150 mM NaCl, 0.2% (v/v) Nonidet P-40) and then eluted with 100 μl of 300 μM 3× FLAG peptide (dissolved in 25 mM Tris-HCl, pH 7.4, 150 mM NaCl and 10% (v/v) glycerol) twice (total 200 μL) for 1 hr each time. The eluted proteins were checked by 12% SDS-PAGE to be at least 80% pure.

HDACs and Sirtuins Deacylase Activity Assay.

***In vitro* Deacylation Assay.** All inhibitors were dissolved in DMSO. For the deacylation assay using the zinc-dependent HDACs, HDACs were incubated in 40 μL reaction mixtures (25 mM Tris-HCl, pH 8.0, 50 mM NaCl, 25 μM H3K9 myristoyl peptide) at 37 °C for 20 min with 64nM of HDAC11. To quench the reactions, 40 μL cold acetonitrile was mixed with the reaction mixture. After centrifuging at 15,000 × g for 15 min, the supernatant was collected and analyzed by HPLC using Kinetex 5u EVO C18 100A column (150 mm × 4.6 mm, Phenomenex). Solvents used for HPLC were water with 0.1% (v/v) trifluoroacetic acid (solvent A) and acetonitrile with 0.1% (v/v) trifluoroacetic acid (solvent B). The gradient for HPLC condition was 0% B for 2 min, 0–20% B in 2 min, 20–40% B in 13 min, 40–100% B in 2 min, and then 100% B for 5 min. The flow rate was 0.5 mL/min. Procedure for HPLC assay with SHMT2 myristoyl peptide is the same as H3K9 myristoyl procedure described above except 120 mins incubation time used instead of 20mins.

For the deacylation assay using sirtuins, sirtuins were incubated in 40 μL reaction mixtures (25 mM Tris-HCl, pH 8.0, 50 mM NaCl, 1 mM DTT, 1 mM NAD^+, 25 μM H3K9 acetyl or myristoyl peptide) at 37 °C for (sirtuin 1, 2 and 3 for 5 mins and sirtuin 6 for 30 mins with 2 μM). To quench the reactions, 40 μL of cold acetonitrile was mixed with the reaction mixture. After centrifuging at 15,000 g for 15 min, the supernatant was collected and analyzed by HPLC using Kinetex 5u EVO C18 100A column (150 mm × 4.6 mm, Phenomenex). Solvents used for HPLC were water with 0.1% (v/v) trifluoroacetic acid (solvent A) and acetonitrile with 0.1% (v/v) trifluoroacetic acid (solvent B). The gradient for HPLC condition was 0% B for 2 min,

0–20% B in 2 min, 20–40% B in 13 min, 40–100% B in 2 min, and then 100% B for 5 min. The flow rate was 0.5 mL/min.

The HPLC data was analyzed to get the conversation rate and inhibition rate according to the following equations:

Conversion rate = $\frac{(Area\ of\ Free\ H3K9\ UV\ peak)}{(Area\ of\ Free\ H3K9\ UV\ peak)+(Area\ of\ Acyl\ H3K9)} X\ 100\ (\%)$

Inhibition rate = {100 - $\frac{(Conversion\ rate\ of\ inhibitor-treated\ sample)}{(Conversion\ rate\ of\ sample\ with\ DMSO\ instead\ of\ inhibitor)} X100\}$ (%)

In-cell Deacetylation Assay. HEK293T cells cultured in 15-cm dishes were treated with inhibitors for 6 h. The cells were scraped off the plates and collected at 500 g for 5 min. Cells from each plate were then lysed in 200 μL of 4% SDS lysis buffer (50 mM triethanolamine at pH 7.4, 150 mM NaCl, 4% (w/v) SDS) with protease inhibitor cocktail (1:100 dilution) and nuclease (1:1000 dilution) at room temperature for 15 min. The protein concentration in the total cell lysate was determined using a BCA assay and each amount of protein was loaded onto a 15% SDS-PAGE gel and resolved. The gel was used for western blot analysis with acetyl α-tubulin and acetyl histone H3 antibodies. The loading for each sample was checked by Coomassie blue-staining the polyvinylidene fluoride (PVDF) membranes.

Western Blot. Proteins were resolved by 12% or 15% SDS-PAGE and transferred to PVDF membranes. The membrane was blocked with 5% (w/v) BSA in PBS with 0.1% (v/v) Tween-20 (TPBS) at room temperature for 60 min. The primary antibody was diluted with fresh 5% (w/v) BSA in TPBS (1:5,000 dilution for antibodies to Flag, Ac-histone H3, Ac-α-tubulin and mSHMT2) and incubated with the membrane at room temperature for 1 h or at 4 °C for 12 h. After washing the membrane three times with TPBS, the secondary antibody (1:3,000 dilution with 5% (w/v) BSA in TPBS) was added and then incubated at room temperature for 1 h. The chemiluminescence signal in the membrane was recorded after developing in ECL Plus Western Blotting detection reagents using a Typhoon 9400 Variable Mode Imager (GE Healthcare Life Sciences).

Detection of Lysine Fatty Acylation on Endogenous SHMT2 by Western Blot. MCF7 cells were treated with 50 μM of Alk14 and inhibitor or DMSO for 6 hours. Two of 80-90% confluent 15-cm MCF7 cells (approximately $2*10^6$ cells per 15-cm dish) cells were collected by centrifugation at 1000 g for 5 min and lysed in 4% SDS lysis buffer (50 mM triethanolamine at pH 7.4, 150 mM NaCl, 4% (w/v) SDS) with protease inhibitor cocktail (1:100 dilution) and nuclease (1:1000 dilution) at room temperature for 15 min. The proteins were precipitated with cold methanol (200 μL per sample), cold chloroform (75 μL per sample), and cold water (150 μL per sample). After vortexing to mix well, samples were spun down at 17,000 g for 15 min. Proteins should be located between the upper layer and bottom layer. The upper layer of the solvents was gently removed. Then 1 mL of cold methanol was added to each sample to wash the proteins by vortexing them. Samples were centrifuged at 17,000g for 5 min. The washing was repeated once more. After methanol washing, methanol was removed from tubes and protein pellets in tubes were air-dried for 5-10 min. Proteins were dissolved in 100 μL of click chemistry buffer (25 mM HEPES, pH 7.4, 150 mM NaCl, and 4% (w/v) SDS). The proteins were sonicated for 30 min at room temperature to be resolubilized. The concentration of the resolubilized proteins was determined using a BCA assay. For each sample, 800 μg of proteins were used for click chemistry (for samples that have higher protein concentration, the volume was adjusted with click chemistry buffer). Biotin-N_3 (5 μL of 5 mM solution in DMF), Tris[(1-benzyl-1H-1,2,3-triazole-4-yl)methyl]amine (5 μL of 2 mM solution in DMF), $CuSO_4$ (5 μL of 50 mM solution in H_2O) and Tris(2-carboxyethyl)phosphine (5 μL of 50 mM solution in H_2O) were added into the reaction mixture. The click chemistry reaction was allowed to proceed at 30^oC for 60 min. Proteins were then precipitated using cold methanol, chloroform (and water as described above. After washing two times with cold methanol, the proteins were resolubilized in 120 μL of 4% SDS lysis buffer. Again, the concentrations of proteins were measured by BCA, and 10 μg of proteins for each sample were set aside as input. Then, 400μg of proteins for sample was added into 10 mL of IP washing buffer (25 mM Tris-HCl pH 8.0, 150 mM NaCl, 0.2% (v/v) NP-40) (making sure that SDS is lower than 0.1% in IP washing buffer for

efficient affinity purification with streptavidin beads). Streptavidin agarose beads (Thermo Fisher, 20 µl) were added into each sample. The mixture was agitated for 1 h at room temperature. After washing the beads three times with 1 mL of IP washing buffer, 24 µL of 4% (w/v) SDS lysis buffer and 6 µL of 6× loading dye were added into each sample and boiled for 10 min. The samples and inputs were resolved using 12% SDS-PAGE gel, transferred to nitrocellulose membrane, and analyzed by western blot for SHMT2 (samples; IP) and (input). The signal was recorded using a Typhoon 9400 Variable Mode Imager (GE Healthcare Life Sciences).

Quantification of Western Blot Signal and Statistical Analysis. The SHMT2 band intensity in the western blot was quantified with ImageJ. All signals were normalized using the control signal. Statistical evaluation of imaging data was done using two-way ANOVA. Differences between two groups were examined using unpaired two-tailed Student's t test. The P values were indicated (***$p<0.0005$). No statistical tool was used to pre-determine sample size. No blinding was done, no randomization was used, and no sample was excluded from analysis.

Cell permeability assay with MCF7 cell. For reference traces of LC-MS, 5 mM stocks of SIS7, SIS26, and SIS17 were prepared in DMSO. 1 µl of each stock was dissolved in 99 µl of acetonitrile. After checking there was no precipitation in acetonitrile (1 µl of 5 mM SIS7, SIS26, and SIS17 are all soluble in 99 µl of acetonitrile), each diluted sample was injected into LC-MS. UV (280 nm) intensity was measured as a representative value indicating the amount of each compound (A_{ref}). For sample traces of LC-MS, 50mM stocks of SIS7, SIS26, and SIS17 were prepared in DMSO. In 80% confluent MCF7 15 cm dish in 8ml DMEM media, 8 µl of each compound was treated per a cell plate. MCF7 cells were incubated for 6hrs at 37^{o}C. After 6hrs, MCF7 cells were collected, washed with 1X PBS three times and lysed cells with cold 200 µl water and 200 µl dichloromethane by vortexing at maximum power for 2 mins three times. All samples were centrifuged at 17,000 g for 20 mins at 4^{o}C. The water layer was gently removed using a pipette then

dichloromethane layer was transferred into a new 1.5 ml tube to prevent cell pellets interrupted buffer flow in a column of LC-MS. We evaporated dichloromethane in a fume hood. After all dichloromethane was evaporated, white powders were stuck in 1.5ml tubes. Those compounds were dissolved in 100 µl of acetonitrile. After checking all white powders were dissolved, samples were injected in LC-MS and their UV (280 nm) intensity was measured (A_{sample}). 50 µl of reference and sample was injected in LC-MS.

Supplementary data for synthesis routes, characterization and IC_{50} curves of key compounds.

A. Procedure for the Synthesis of Fatty acylated UF010 (SIS4).

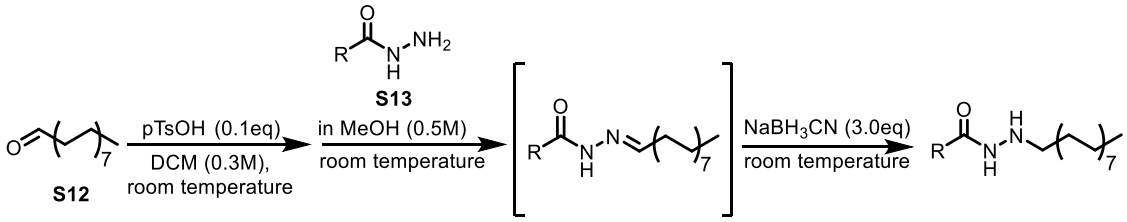

Hexadecanal **S12** and substituted benzoic hydrazide **S13** are commercially available from Sigma-Aldrich, VWR chemical and Combi-block and they were used directly without further purification.

In a 10 mL round bottom flask equipped with a stir bar, hexadecanal **S12** (56 mg, 0.233 mmol, 1.0 equiv) and p-TsOH•H_2O (5 mg, 0.025 mmol, 0.1 equiv) were dissolved in CH_2Cl_2 (0.8 mL) at room temperature. After stirring for 30 min at room temperature, 4-bromobenzoic hydrazide **S13** (50 mg, 0.232 mmol, 1.0 equiv) in methanol (0.47 mL) was added into hexadecanal and p-TsOH reaction mixture. This mixture was stirred for 1 h at room temperature and then $NaCNBH_3$ (44 mg, 0.699 mmol, 3.0 equiv) in MeOH (0.8 mL) was added. After further stirring for 1 hr at room temperature, the reaction was quenched by $NaHCO_3$ (1M, aq) until there is no hydrogen gas generated from remaining $NaCNBH_3$. The organic phase was separated from the aqueous phase, and the aqueous phase was extracted with CH_2Cl_2 (5 mL × 2). The combined organic phase was dried over Na_2SO_4 and concentrated *in vacuo* to

afford the crude product **SIS4**. After concentration in vacuo, the residue was subsequently purified through column chromatography (hexane/EtOAc: 2:8) to afford SIS4 as white powder (58mg, 57% yield from **S12**).

Compounds **SIS2, 5, 7, 10, 17, 21, 39, 40, 49, 50 and 51** were synthesized following the same procedure as that for **SIS4**.

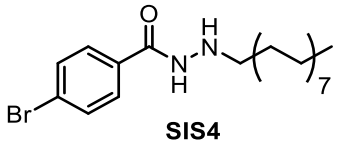

SIS4

4-bromo-N'-hexadecylbenzohydrazide (SIS4): yield: 43%, white powder; ^{1}H NMR (500 MHz, $CDCl_3$) δ 7.62 (d, *J* = 8.3 Hz, 2H), 7.58 (d, *J* = 8.2 Hz, 2H), 3.31 (s, 1H), 2.92 (t, *J* = 7.3 Hz, 2H), 1.62 – 1.51 (m, 2H), 1.25 (s, 34H), 0.88 (t, *J* = 6.8 Hz, 4H); ^{13}C NMR (126 MHz, $CDCl_3$) δ 166.3, 132.0, 131.7, 128.5, 126.6, 104.6, 77.3, 77.0, 76.8, 52.6, 52.3, 34.3, 32.5, 31.9, 29.71, 29.70, 29.68, 29.62, 29.58, 25.08, 24.62, 29.5, 29.5, 29.4, 29.2, 28.0, 27.3, 27.1, 25.1, 24.6, 22.7, 14.1; HRMS (DART Orbitrap, m/z): calcd for $C_9H_9Br_2O_2^+$ ([M + H]$^+$) 439.2312, found 439.2307.

SIS2

4-(tert-butyl)-N'-hexadecyl benzohydrazide (**SIS2**): yield: 48%, white powder; ^{1}H NMR (500 MHz, $CDCl_3$) δ 7.81 (s, 1H), 7.69 (d, J = 8.4 Hz, 2H), 7.45 (d, J = 8.4 Hz, 2H), 2.92 (t, J = 7.3 Hz, 2H), 1.59 – 1.48 (m, 2H), 1.33 (s, 9H), 1.31 – 1.17 (m, 26H), 0.88 (t, J = 6.9 Hz, 3H); ^{13}C NMR (126 MHz, $CDCl_3$) δ 167.2, 155.4, 130.0, 126.7, 125.6, 52.4, 35.0, 31.9, 31.2, 31.15, 29.71, 29.68, 29.67, 29.63, 29.60, 29.57, 29.4, 28.1, 27.1, 22.7, 14.1; HRMS (DART Orbitrap, m/z): calcd for $C_{27}H_{48}N_2O^+$ ([M+H]$^+$) 417.3839, found. 417.3828.

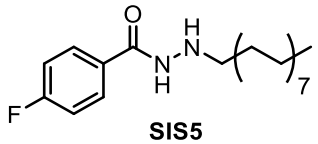

SIS5

4-fluoro-N'-hexadecylbenzohydrazide yield (**SIS5**): yield: 36%, white powder; ^{1}H NMR (500 MHz, $CDCl_3$) δ 7.82 – 7.72 (m, 2H), 7.64 (s, 1H), 7.16 – 7.08 (m, 2H), 2.92

(t, *J* = 7.3 Hz, 2H), 1.57 – 1.46 (m, 2H), 1.32 – 1.21 (m, 26H), 0.88 (t, *J* = 6.9 Hz, 3H); ^{13}C NMR (126 MHz, $CDCl_3$) δ 166.3, 165.9, 163.9, 129.3, 115.8, 52.4, 31.9, 29.71, 29.90, 29.67, 29.59, 29.5, 29.4, 28.1, 27.1, 22.7, 14.1. HRMS (DART Orbitrap, m/z): calcd for $C_{23}H_{40}FN_2O^+$([M+H]$^+$) 379.3119, found 379.3110.

SIS7

4-(dimethylamino)-N'-hexadecylbenzohydrazide (**SIS7**):yield: 64%, white powder; ^{1}H NMR (300 MHz, $CDCl_3$) δ 7.65 (d, J = 8.8 Hz, 2H), 6.66 (d, J = 8.8 Hz, 2H), 3.02 (s, 6H), 2.90 (t, J = 7.2 Hz, 2H), 1.38-1.25 (m, 29H), 0.87 (t, J = 6.5 Hz, 3H); ^{13}C NMR (126 MHz, $CDCl_3$) δ 167.4, 152.7, 128.3, 119.5, 111.1, 52.5, 40.1, 31.9, 29.71, 29.69, 29.67, 29.63, 29.60, 29.58, 29.38, 28.1, 27.2, 22.7, 14.1; HRMS (DART Orbitrap, m/z): calcd for $C_{25}H_{46}N_3O^+$ ([M + H]$^+$) 404.3635, found 404.3626.

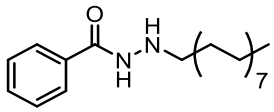

SIS10

N'-hexadecylbenzohydrazide (**SIS10**): yield: 39%, white powder; ^{1}H NMR (500 MHz, $CDCl_3$) δ 7.75 (d, *J* = 7.4 Hz, 2H), 7.52 (d, *J* = 7.4 Hz, 1H), 7.44 (t, *J* = 7.6 Hz, 2H), 2.93 (t, *J* = 7.3 Hz, 2H), 1.53 (dd, *J* = 14.8, Hz, 2H), 1.42 – 1.20 (m, 28H), 0.88 (t, *J* = 6.9 Hz, 3H); ^{13}C NMR (126 MHz, $CDCl_3$) δ 167.2, 132.9, 131.8, 128.7, 126.8, 52.4, 31.9, 29.71, 29.70, 29.67, 29.62, 29.59, 29.4, 28.1, 27.1, 22.7, 14.1; HRMS (DART Orbitrap, m/z): calcd for $C_{23}H_{41}N_2O^+$ ([M + H]$^+$) 361.3213, found 361.3205.

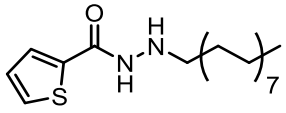

SIS17

N'-hexadecylthiophene-2-carbohydrazide (**SIS17**): yield: 51%, white powder; ^{1}H NMR (500 MHz, $CDCl_3$) δ 7.53 (dd, *J* = 18.0, 4.4 Hz, 2H), 7.11 (t, *J* = 4.4 Hz, 1H), 2.95 (t, *J* = 7.3 Hz, 2H), 1.67 – 1.48 (m, 2H), 1.46 – 1.07 (m, 28H), 0.90 (t, *J* = 6.8 Hz, 3H); ^{13}C NMR (126 MHz, $CDCl_3$) δ 162.0, 136.6, 130.1, 128.4, 127.7, 77.3, 77.0, 76.8, 52.4, 31.9, 31.9, 29.71, 29.68, 29.62, 29.53, 29.47, 29.4, 29.2, 28.0, 28.0, 27.6,

27.3, 27.1, 26.4, 22.7, 14.1; HRMS (DART Orbitrap, m/z): calcd for $C_{21}H_{39}N_2OS^+$ ($[M + H]^+$) 367.2778, found 367.2768.

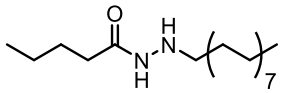

SIS18

N'-hexadecylpentanehydrazide (**SIS18**): yield 42%, white powder; ^{1}H NMR (400 MHz, $CDCl_3$) δ 6.91 (s, 1H), 2.80 (t, J = 7.1 Hz, 2H), 2.13 (t, J = 7.6 Hz, 2H), 1.76 – 1.54 (m, 2H), 1.51 – 1.41 (m, 2H), 1.37 – 1.16 (m, 26H), 0.95 – 0.81 (m, 6H); ^{13}C NMR (126 MHz, $CDCl_3$) δ 172.5, 52.3, 34.5, 31.9, 29.71, 29.69, 29.67, 29.62, 29.58, 29.54, 29.5, 29.4, 28.0, 27.6, 27.1, 22.7, 22.4, 14.14, 13.76; HRMS (DART Orbitrap, m/z): calcd for $C_{21}H_{45}N_2O^+$ ($[M + H]^+$) 341.3526, found 341.3518.

SIS21

N'-hexadecyl-4-(trifluoromethyl)benzohydrazide (**SIS21**): yield 55%, white powder; ^{1}H NMR (500 MHz, $CDCl_3$) δ 7.86 (d, *J* = 8.1 Hz, 2H), 7.72 (d, *J* = 8.2 Hz, 2H), 2.95 (t, *J* = 7.2 Hz, 2H), 1.59 – 1.50 (m, 2H), 1.38 – 1.21 (m, 26H), 0.88 (t, *J* = 6.8 Hz, 3H); ^{13}C NMR (126 MHz, $CDCl_3$) δ 165.9, 136.15, 133.6, 128.2, 127.3, 125.8, 123.6, 52.3, 31.9, 29.71, 29.67, 29.61, 29.57, 29.52, 29.4, 28.0, 27.1, 22.7, 14.1; ^{19}F NMR (376 MHz, $CDCl_3$) δ -63.1; HRMS (DART Orbitrap, m/z): calcd for $C_{24}H_{40}F_3N_2O^+$ ($[M + H]^+$) 429.3087, found 429.3025.

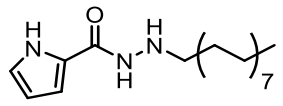

SIS39

N'-hexadecyl-^{1}H-pyrrole-2-carbohydrazide (**SIS39**): yield 29%, white powder; ^{1}H NMR (500 MHz, $CDCl_3$) δ 10.31 (s, 1H, pyrrole NH), 7.24 (q, *J* = 1.8 Hz, 1H, amide NH), 7.02 – 6.86 (m, 1H), 6.27 (ddd, *J* = 11.9, 6.1, 3.0 Hz, 1H), 5.78 (s, 1H), 2.96 – 2.68 (m, 3H), 2.55 (ddd, *J* = 12.3, 9.9, 5.3 Hz, 1H), 1.67 – 1.44 (m, 10H), 1.45 – 1.11 (m, 57H), 0.90 (t, *J* = 6.8 Hz, 7H); ^{13}C NMR (126 MHz, $CDCl_3$) δ 162.6, 161.3, 160.6, 124.6, 124.6, 124.3, 122.0, 121.1, 116.9, 109.9, 109.7, 109.7, 109.5, 108.7, 77.3, 77.1,

76.8, 59.8, 58.7, 31.9, 29.72, 29.68, 29.64, 29.61, 29.58, 29.56, 29.54, 29.46, 29.4, 28.0, 27.4, 27.3, 27.2, 27.1, 26.6, 22.7, 14.1; HRMS (DART Orbitrap, m/z): calcd for $C_{21}H_{40}N_3O^+$ ([M + H]$^+$) 350.3166, found 350.3159.

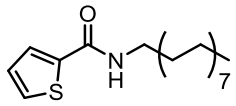

SIS40

N-hexadecylthiophene-2-carboxamide (**SIS40**): yield 48%, white powder; ^{1}H NMR (500 MHz, $CDCl_3$) δ 7.49 (dd, *J* = 12.5, 4.3 Hz, 2H), 7.09 (t, *J* = 4.3 Hz, 1H), 5.96 (s, 1H), 3.45 (q, *J* = 6.8 Hz, 2H), 1.73 – 1.51 (m, 5H), 1.28 (s, 25H); ^{13}C NMR (126 MHz, $CDCl_3$) δ 161.8, 139.2, 129.6, 127.8, 127.6, 77.3, 77.0, 76.8, 40.1, 31.9, 29.71, 29.69, 29.67, 29.66, 29.60, 29.55, 29.4, 29.3, 27.0, 22.7, 14.1; HRMS (DART Orbitrap, m/z): calcd for $C_{21}H_{38}NOS^+$ ([M + H]$^+$) 352.2669, found 352.2663.

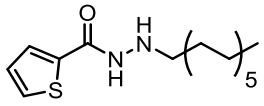

SIS49

N'-dodecylthiophene-2-carbohydrazide (**SIS49**): yield 56%, white powder; ^{1}H NMR (500 MHz, $CDCl_3$) δ 7.64 – 7.42 (m, 2H), 7.19 – 7.04 (m, 1H), 3.47 – 3.25 (m, 3H), 1.68 – 1.49 (m, 2H), 1.43 – 1.08 (m, 22H), 0.90 (t, *J* = 6.8 Hz, 3H); ^{13}C NMR (126 MHz, $CDCl_3$) δ 162.1, 162.0, 136.6, 130.1, 128.4, 127.7, 125.9, 104.6, 77.3, 77.0, 76.8, 52.6, 52.4, 51.4, 34.1, 33.6, 32.5, 31.9, 30.0, 29.90, 29.71, 29.70, 29.67, 29.66, 29.63, 29.61, 29.58, 29.54, 29.52, 29.50, 29.4, 29.2, 28.4, 28.0, 27.5, 27.3, 27.1, 26.6, 26.4, 25.0, 24.7, 24.6, 22.7, 20.8, 18.5, 16.8, 14.1; HRMS (DART Orbitrap, m/z): calcd for $C_{17}H_{31}N_2OS^+$ ([M + H]$^+$) 311.2152, found 311.2143.

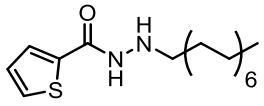

SIS50

N'-tetradecylthiophene-2-carbohydrazide (**SIS50**): yield 44%, white powder; ^{1}H NMR (500 MHz, $CDCl_3$) δ 7.53 (dd, *J* = 14.8, 4.4 Hz, 2H), 7.11 (t, *J* = 4.3 Hz, 1H), 3.33 (s, 1H), 2.95 (t, *J* = 7.1 Hz, 1H), 1.58 (ddt, *J* = 34.1, 14.7, 6.8 Hz, 3H), 1.48 – 1.08 (m, 31H), 0.90 (t, *J* = 6.8 Hz, 5H); ^{13}C NMR (126 MHz, $CDCl_3$) δ 162.0, 130.1,

128.4, 127.7, 104.6, 77.3, 77.0, 76.8, 52.6, 52.4, 32.5, 31.9, 30.4, 29.7, 29.62, 29.59, 29.4, 29.3, 29.2, 28.9, 28.7, 28.0, 27.4, 27.1, 26.0, 25.8, 25.1, 24.6, 23.8, 23.6, 23.0, 22.7, 14.1; HRMS (DART Orbitrap, m/z): calcd for $C_{19}H_{35}N_2OS^+$ ($[M + H]^+$) 339.2465, found 339.2456.

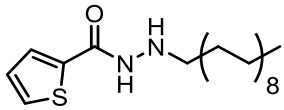

SIS52

N'-octadecylthiophene-2-carbohydrazide (**SIS52**): yield 32%, white powder; ^{1}H NMR (500 MHz, $CDCl_3$) δ 7.61 – 7.45 (m, 2H), 7.17 – 7.10 (m, 1H), 4.38 (t, *J* = 5.8 Hz, 2H), 3.33 (s, 11H), 2.95 (t, *J* = 7.3 Hz, 1H), 2.74 (q, *J* = 7.2 Hz, 8H), 1.66 – 1.51 (m, 6H), 1.22 (d, *J* = 52.6 Hz, 89H), 0.91 (d, *J* = 6.6 Hz, 6H); ^{13}C NMR (126 MHz, $CDCl_3$) δ 130.2, 130.1, 128.5, 128.4, 127.8, 127.7, 104.6, 77.3, 77.0, 76.8, 52.6, 52.4, 45.8, 32.5, 31.9, 29.7, 29.6, 29.5, 29.4, 28.0, 27.1, 24.6, 22.7, 14.1, 8.6; HRMS (DART Orbitrap, m/z): calcd for $C_{23}H_{43}N_2OS^+$ ($[M + H]^+$) 395.3370, found. 395.3081.

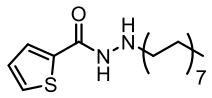

SIS65

N'-pentadecylthiophene-2-carbohydrazide (SIS65): yield 62%, white powder; ^{1}H NMR (500 MHz, Chloroform-d) δ 7.62 – 7.45 (m, 2H), 7.11 (t, J = 4.3 Hz, 1H), 2.95 (t, J = 7.4 Hz, 2H), 1.55 (t, J = 7.4 Hz, 2H), 1.27 (s, 25H), 0.90 (t, J = 6.8 Hz, 4H); ^{13}C NMR (126 MHz, $CDCl_3$) δ 161.98, 136.62, 133.69, 130.93, 130.10, 128.84, 128.36, 127.71, 77.29, 77.04, 76.78, 52.36, 34.38, 31.94, 29.71, 29.70, 29.67, 29.62, 29.59, 29.53, 29.38, 29.24, 28.00, 27.11, 22.71, 14.14; HRMS (DART Orbitrap, m/z): calcd for $C_{20}H_{36}N_2OS^+$ ($[M + H]^+$) 353.2621, found. 353.2613.

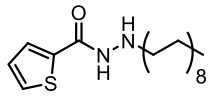

SIS66

N'-heptadecylthiophene-2-carbohydrazide (SIS66): yield 58%, white powder; ^{1}H NMR (500 MHz, Chloroform-*d*) δ 7.63 – 7.42 (m, 1H), 7.12 (dt, *J* = 11.9, 4.4 Hz, 1H), 4.14 (q, *J* = 7.2 Hz, 0H), 2.95 (t, *J* = 7.3 Hz, 1H), 1.27 (d, *J* = 2.3 Hz, 22H), 0.90 (t, *J* = 6.9 Hz, 3H); ^{13}C NMR (126 MHz, $CDCl_3$) δ 161.98, 161.57, 161.52, 137.34, 137.00,

136.62, 133.41, 130.23, 130.12, 128.38, 128.31, 128.14, 127.79, 127.76, 127.71, 126.49, 77.29, 77.04, 76.78, 65.25, 63.09, 60.42, 52.36, 32.84, 31.94, 30.25, 29.96, 29.74, 29.72, 29.68, 29.62, 29.59, 29.53, 29.46, 29.38, 27.96, 27.79, 27.25, 27.10, 22.71, 14.21, 14.14; HRMS (DART Orbitrap, m/z): calcd for $C_{22}H_{40}N_2OS^+$ ($[M + H]^+$) 381.2934, found. 381.2926.

B. Procedure for the Synthesis of fatty acylated SAHA S(S1S15).

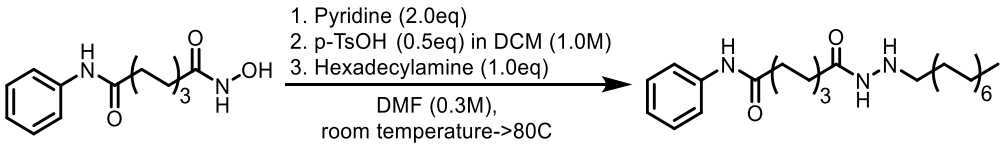

S14

N^1-hydroxy-N^8-phenyloctanediamide (**S14)** is commercially available from Combi-Block and they were used directly without further purification.

To a stirred solution of N^1-hydroxy-N^8-phenyloctanediamide (**S14**) (100 mg, 0.38 mmol, 1.0 equiv) and pyridine (0.76 mL, 0.76 mmol, 2.0 equiv) in anhydrous DMF (0.76 mL, 0.5 M) was added dropwise a solution of p-TsOH (36 mg, 0.19 mmol, 0.5 equiv) in anhydrous dichloromethane (0.19 mL,) at room temperature. The mixture was refluxed for 1 h. Addition of water (5 mL) caused the intermediate to separate. Then, the crude was used for further reaction without purification. To a stirred solution of intermediate in anhydrous CH_2Cl_2 (1.3 ml) was gradually added a solution of hexadecylamine (92 mg, 0.38 mmol, 1.0 equiv) in anhydrous CH_2Cl_2 at room temperature under N_2. The mixture was refluxed for 12 hours, washed with 1% aqueous sodium hydrogen carbonate and water, dried with $MgSO_4$ and evaporated to dryness *in vacuo*. The residue was subsequently purified through column chromatography with (hexane:EtOAc=8:2). (57 mg, 31% yield from S14).

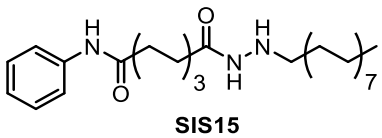

SIS15

8-(2-hexadecylhydrazineyl)-8-oxo-N-phenyloctanamide (SIS15): ^{1}H NMR (500 MHz, $CDCl_3$) δ 7.55 (d, *J* = 7.9 Hz, 1H), 7.34 (t, *J* = 7.7 Hz, 2H), 7.12 (t, *J* = 7.4 Hz, 1H), 3.91 (d, *J* = 7.3 Hz, 1H), 2.38 (t, *J* = 7.4 Hz, 2H), 1.83 – 1.57 (m, 10H), 1.28 (s,

35H), 1.06 – 0.77 (m, 9H); ^{13}C NMR (126 MHz, $CDCl_3$) δ 171.4, 138.0, 129.0, 124.2, 119.7, 77.3, 77.0, 76.8, 32.8, 31.9, 30.4, 30.1, 29.71, 29.69, 29.67, 29.6, 29.5, 29.4, 29.4, 29.3, 28.9, 28.3, 28.0, 27.1, 22.7, 19.8, 14.1, 14.1; HRMS (DART Orbitrap, m/z): calcd for $C_{30}H_{54}N_3O_2^+$ ([M + H]$^+$) 488.4832, found 488.4279.

C. Procedure for the Synthesis of FT895[23].

The compound **FT895** was synthesized according to a known procedure[6] but with several modifications as described below.

Overall Synthetic Scheme of FT895.

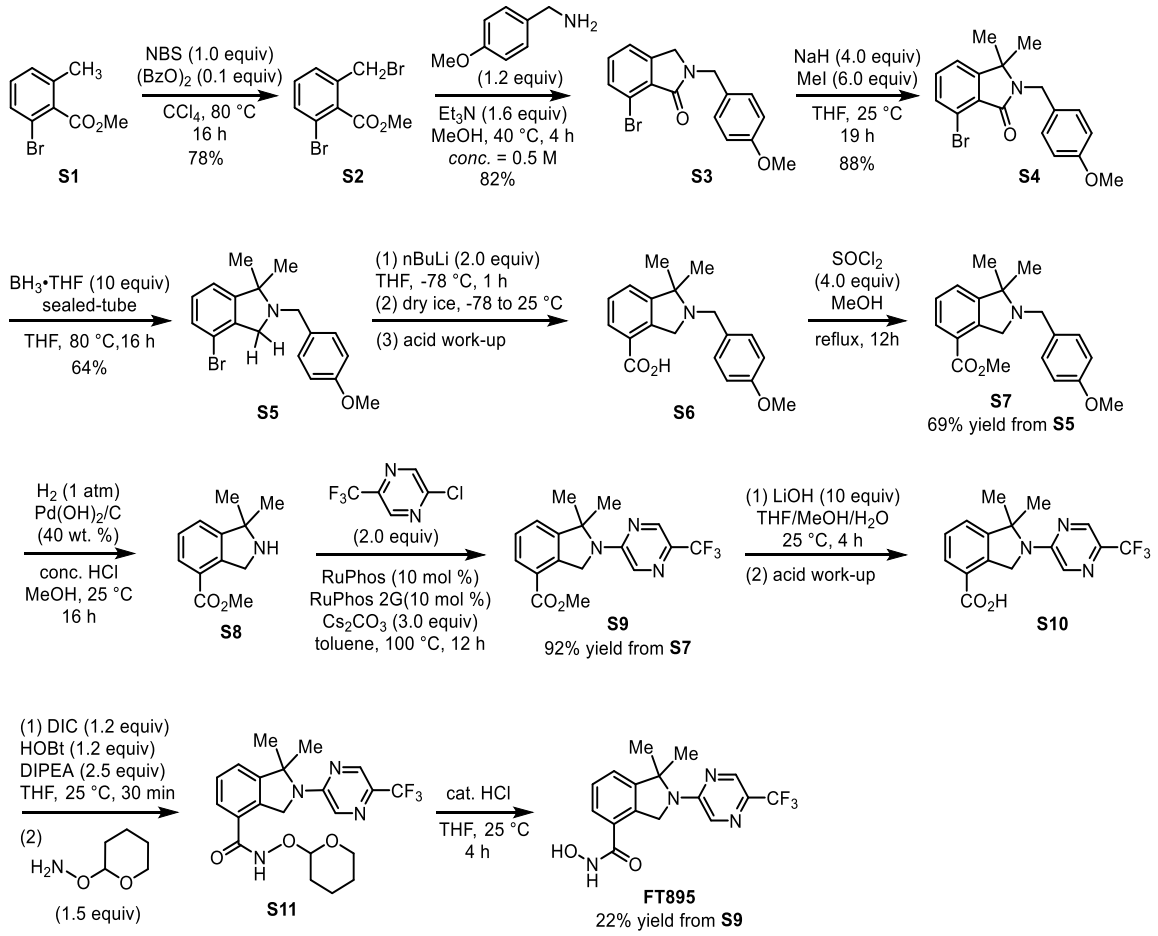

Detailed Procedures for FT895 Preparation.

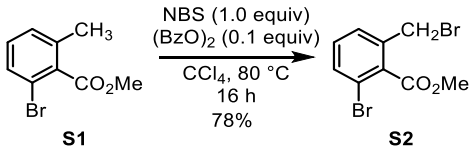

Methyl 2-bromo-6-(bromomethyl)benzoate **S2** was synthesized from methyl 2-bromo-6-methylbenzoate **S1** through a known procedure.[6] **S1** is commercially available and it was used directly without further purification.

In a 250 mL round bottom flask equipped with a stir bar, methyl 2-bromo-6-methylbenzoate **S1** (6.7 g, 29.3 mmol, 1.0 equiv) was dissolved in CCl_4 (140 mL). Subsequently, NBS (5.21 g, 29.3 mmol, 1.0 equiv) and benzoyl peroxide (0.7 g, 2.9 mmol, 0.1 equiv) were added and the resulting mixture was vigorously stirred at 80 °C for 16 h. The reaction was cooled down to room temperature and filtered to remove solid. The filtrate was washed with brine (100 mL× 3) and dried over anhydrous Na_2SO_4. After concentration *in vacuo*, the desired product methyl 2-bromo-6-(bromomethyl)benzoate **S2** was obtained as light yellow oil, which was used in the next step without further purification (7.0 g, 78% yield).

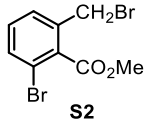

Methyl 2-bromo-6-(bromomethyl)benzoate (**S2**): ^{1}H NMR (500 MHz, $CDCl_3$) δ 7.57 (d, *J* = 8.0 Hz, 1H), 7.41 (d, *J* = 7.7 Hz, 1H), 7.28 (dd, *J* = 8.7, 7.1 Hz, 1H), 4.51 (s, 2H), 4.02 (s, 3H); LC-MS (ESI, m/z): calcd for $C_9H_9Br_2O_2^+$([M + H]$^+$) 305.89, found 305.90.

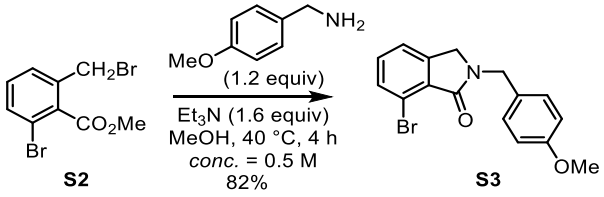

7-Bromo-2-(4-methoxybenzyl)isoindolin-1-one **S3** was synthesized from **S2** through a known procedure with modifications.[6]

To an oven-dried 100 mL round bottom flask equipped with a stir bar was added **S2** (5.6 g, 18.1 mmol, 1.0 equiv). After the flask was evacuated and backfilled with N_2 twice, anhydrous MeOH (36 mL), 4-methoxybenzylamine (2.9 mL, 22 mmol, 1.2

equiv) and Et_3N (4.0 mL, 29 mmol, 1.6 equiv) were added via syringes. The reaction was warmed up to 40 °C and stirred at this temperature for 4 h. The mixture was cooled to room temperature and concentrated under reduced pressure. H_2O (50 mL) was added and the solution was extracted with CH_2Cl_2 (100 mL× 3). The organic phase was separated from the aqueous phase, and dried over Na_2SO_4. After concentration *in vacuo*, the residue was subsequently purified through column chromatography (hexanes/EtOAc: from 10:1 to 2:1) to afford the product 7-bromo-2-(4-methoxybenzyl)isoindolin-1-one **S3** as white solid (4.8 g, 82% yield).

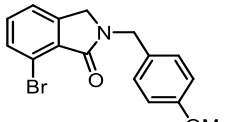

S3

7-Bromo-2-(4-methoxybenzyl)isoindolin-1-one (**S3**): ^{1}H NMR (300 MHz, $CDCl_3$) δ 7.59 (d, *J* = 6.7 Hz, 1H), 7.39 – 7.22 (m, 5H), 6.86 (d, *J* = 8.2 Hz, 2H), 4.72 (s, 2H), 4.19 (s, 2H), 3.79 (s, 3H); LC-MS (ESI, m/z): calcd for $C_{16}H_{15}BrNO_2^+$([M + H]$^+$) 332.02, found 332.03.

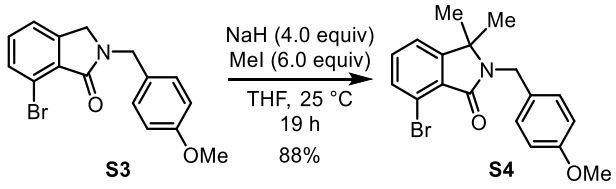

S3 **S4**

7-Bromo-2-(4-methoxybenzyl)-3,3-dimethylisoindolin-1-one **S4** was synthesized from **S3** through a known procedure with modifications.[6]

To a flame-dried 100 mL round bottom flask equipped with a stir bar was added NaH (60%, 576 mg, 14.4 mmol, 4.0 equiv). After the flask was evacuated and backfilled with N_2 twice, anhydrous THF (10 mL) was added via a syringe. Subsequently, **S3** (1.2 g, 3.6 mmol, 1.0 equiv) in THF (10 mL) was added dropwise and the mixture was stirred at room temperature for 3 h. MeI (1.34 mL, 21.6 mmol, 6.0 equiv) was added and the reaction mixture was kept stirring for additional 16 h until **S3** was fully consumed (monitored by TLC). The reaction was cooled down in ice-bath and quenched by adding H_2O (10 mL) slowly. EtOAc (50 mL) was added and the organic phase was separated from the aqueous phase, which was extracted with EtOAc

(50 mL × 2). The combined organic layers were dried over anhydrous Na_2SO_4. After concentration *in vacuo*, the residue was subsequently purified through column chromatography (hexanes/EtOAc: from 10:1 to 4:1) to afford the product 7-bromo-2-(4-methoxybenzyl)-3,3-dimethylisoindolin-1-one **S4** as colorless oil (1.14 g, 88% yield).

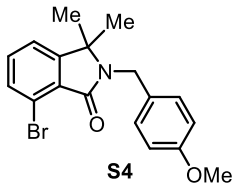

S4

7-Bromo-2-(4-methoxybenzyl)-3,3-dimethylisoindolin-1-one (**S4**): ^{1}H NMR (300 MHz, $CDCl_3$) δ 7.63 – 7.54 (m, 1H), 7.40 – 7.28 (m, 4H), 6.82 (d, *J* = 8.7 Hz, 2H), 4.67 (s, 2H), 3.77 (s, 3H), 1.35 (s, 6H); LC-MS (ESI, m/z): calcd for $C_{18}H_{19}BrNO_2^+$([M + H]$^+$) 360.05, found 360.07.

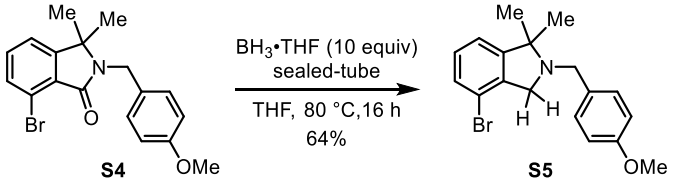

S4 **S5**

4-Bromo-2-(4-methoxybenzyl)-1,1-dimethylisoindoline **S5** was synthesized from **S4** through a known procedure.[6]

To a 500 mL sealed tube equipped with a stir bar were added substrate **S4** (1.2 g, 3.3 mmol, 1.0 equiv) and borane-THF complex solution (1.0 M, 33 mL, 33 mmol, 10 equiv). The reaction mixture was tightly sealed and stirred for 19 h at 80 °C. After cooling down to room temperature, MeOH (50 mL) was added to quench the reaction and the resulting mixture was stirred for additional 1 h at room temperature. After concentration *in vacuo*, the residue was subsequently purified through column chromatography (hexanes/EtOAc: from 50:1 to 10:1) to afford 4-bromo-2-(4-methoxybenzyl)-1,1-dimethylisoindoline **S5** as yellow oil (0.73 g, 64% yield).

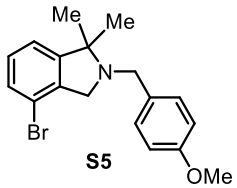

S5

4-Bromo-2-(4-methoxybenzyl)-1,1-dimethylisoindoline (**S5**) ^{1}H NMR (400 MHz, $CDCl_3$) δ 7.34 – 7.26 (m, 3H), 7.09 – 7.05 (m, 2H), 6.86 (d, *J* = 8.5 Hz, 2H), 3.80 (s, 3H), 3.75 (s, 2H), 3.73 (s, 2H), 1.35 (s, 6H); LC-MS (ESI, m/z): calcd for $C_{18}H_{21}BrNO^+$ ($[M + H]^+$) 346.07, found 346.07.

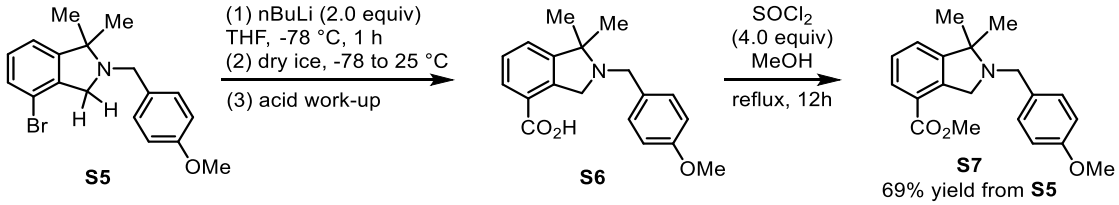

To a flame-dried 100 mL round bottom flask equipped with a stir bar was added **S5** (346 mg, 1.0 mmol, 1.0 equiv). After this flask was evacuated and backfilled with N_2 twice, anhydrous THF (20 mL) were added via a syringe and the mixture was cooled down to -78 °C. nBuLi (2.5 M in hexanes, 0.8 mL, 2.0 mmol, 2.0 equiv) was added dropwise and the mixture was stirred for 1 h at -78 °C. N_2 was removed and CO_2 (generated from dry-ice and dried over conc. H_2SO_4) was bubbled into the reaction mixture at -78 °C for 20 min. CO_2 was replaced by N_2 and the mixture was allowed to gradually warm up to room temperature and vigorously stirred for 8 h. 1.0 M HCl (10 mL) and EtOAc (40 mL) were added to quench the reaction. The organic phase was separated from the aqueous phase, and the aqueous phase was extracted with EtOAc (50 mL × 2). The combined organic phase was dried over Na_2SO_4 and concentrated *in vacuo* to afford the crude product **S6**, which was directly used in the next step without further purification.

To a 50 mL round bottom flask equipped with a stir bar and reflux condenser was added the crude **S6** (1.0 mmol, 1.0 equiv) and anhydrous MeOH (20 mL). At 0 °C, $SOCl_2$ (0.29 mL, 4.0 mmol, 4.0 equiv) was added and the mixture was warmed up to reflux for 12 h. After concentration *in vacuo*, the residue was subsequently purified through column chromatography (hexanes/EtOAc: from 50:1 to 10:1) to afford methyl 2-(4-methoxybenzyl)-1,1-dimethylisoindoline-4-carboxylate **S7** as colorless oil (225 mg, 69% yield from **S5**).

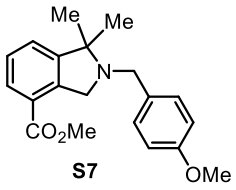

S7

Methyl 2-(4-methoxybenzyl)-1,1-dimethylisoindoline-4-carboxylate (**S7**): ^{1}H NMR (300 MHz, $CDCl_3$) δ 7.83 (dd, *J* = 7.1, 1.1 Hz, 1H), 7.37 – 7.29 (m, 4H), 6.87 (d, *J* = 8.4 Hz, 2H), 4.11 (s, 2H), 3.82 (s, 3H), 3.81 (s, 3H), 3.78 (s, 2H), 1.37 (s, 6H); LC-MS (ESI, m/z): calcd for $C_{20}H_{24}NO_3^+$ ($[M + H]^+$) 326.16, found 326.14.

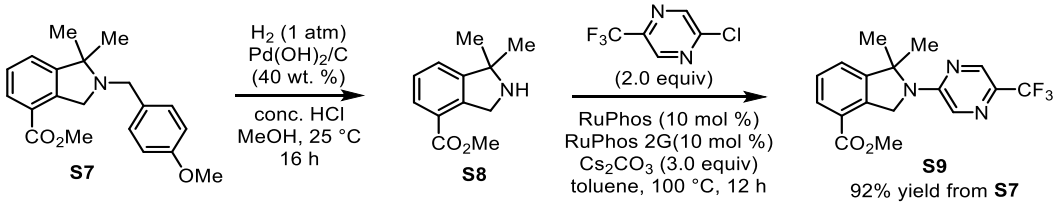

S7 **S8** **S9**

92% yield from **S7**

Methyl 1,1-dimethyl-2-(5-(trifluoromethyl)pyrazin-2-yl)isoindoline-4-carboxylate **S9** was synthesized from **S7** through a known procedure.[6]

To a 10 mL 2-neck round bottom flask equipped with a stir bar and a three-way adapter was added $Pd(OH)_2/C$ (80 mg, 40 wt. %). After the flask was evacuated and backfilled twice with N_2, a solution of **S7** (200 mg, 0.61 mmol, 1.0 equiv) in MeOH (5 mL) and conc. HCl (0.2 mL) were added via syringes. The mixture was degassed with brief evacuation and backfilled three times with H_2, and then vigorously stirred under H_2 balloon at 22 °C for 16 h (monitored by TLC until the substrate **S7** was fully consumed). The solution was filtered through a Celite pad and washed with MeOH (10 mL). The filtrate was concentrated *in vacuo* and the residue was dissolved in CH_2Cl_2 (20 mL) and washed with 10% K_2CO_3 (3 mL). The organic phase was separated from the aqueous phase, and the aqueous phase was extracted with CH_2Cl_2 (10 mL × 3). The combined organic phase was dried over Na_2SO_4 and concentrated *in vacuo* to afford the crude product **S8**, which was directly used in the next step without further purification.

To a flame-dried sealable 3-dram vial equipped with a stir bar was added **S8** (120 mg,

0.583 mmol, 1.0 equiv), 2-chloro-5-(trifluoromethyl)pyrazine (215 mg, 1.18 mmol, 2.0 equiv), RuPhos Pd G2 (47 mg, 0.06 mmol, 10 mol%), RuPhos (28 mg, 0.06 mmol, 10 mol%) and $CsCO_3$ (570 mg, 1.75 mmol, 3.0 equiv). After this vial was evacuated and backfilled with N_2 twice, anhydrous toluene (3.0 mL) were added via syringe and the mixture was warmed up to 110 °C and stirred for 12 h. The reaction was cooled down to room temperature. EtOAc (4 mL) and H_2O (3 mL) were added to quench the reaction. The organic phase was separated from the aqueous phase, and the aqueous phase was extracted with EtOAc (10 mL × 3). The combined organic phase was dried over Na_2SO_4. After concentration *in vacuo*, the residue was subsequently purified through column chromatography (hexanes/EtOAc: from 20:1 to 5:1) to afford methyl 1,1-dimethyl-2-(5-(trifluoromethyl)pyrazin-2-yl)isoindoline-4-carboxylate **S9** as light yellow solid (186 mg, 92% yield form **S7**).

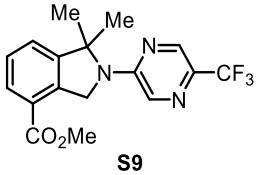

S9

Methyl 1,1-dimethyl-2-(5-(trifluoromethyl)pyrazin-2-yl)isoindoline-4-carboxylate (**S9**): ^{1}H NMR (400 MHz, $CDCl_3$) δ 8.46 (s, 1H), 8.10 (s, 1H), 8.02 (d, *J* = 6.5 Hz, 1H), 7.52 – 7.42 (m, 2H), 5.13 (s, 2H), 3.97 (s, 3H), 1.84 (s, 6H); ^{19}F NMR (376 MHz, $CDCl_3$) δ -66.23 (s); LC-MS (ESI, m/z): calcd for $C_{17}H_{17}F_3N_3O_2^+$ ($[M + H]^+$) 352.12, found 352.13.

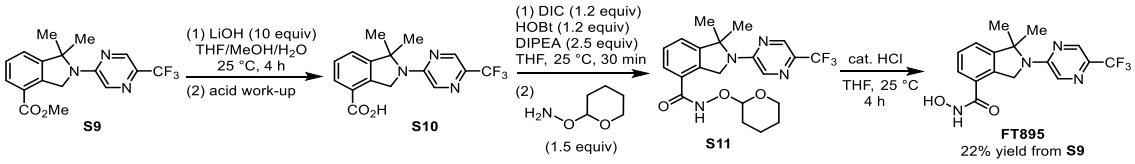

In a 2-dram vial equipped with a stir bar, compound **S9** (35 mg, 0.1 mmol, 1.0 equiv) was dissolved in a mixed solvent of MeOH/THF (1:4) (1.5 mL) and cooled to 0 °C. LiOH (42 mg, 1.0 mmol, 10 equiv) in 0.5 mL H_2O was added and the reaction was vigorously stirred for 4 h until the starting material was fully consumed (monitored by TLC). The organic solvent was removed *in vacuo* and the residue was diluted with

H_2O (5 mL) and Et_2O (1 mL). The organic phase was separated from the aqueous phase, and the aqueous phase was acidified with aqueous 1.0 M HCl. EtOAc (5 mL) was added. The organic phase was separated from the aqueous phase, and the aqueous phase was extracted with EtOAc (10 mL × 3). The combined organic phase was dried over Na_2SO_4 and concentrated *in vacuo* to afford the crude product **S10**, which was used directly in the next step without purification.

To an oven-dried 3-dram vial equipped with a stir bar were added the crude compound **S10** (25 mg, 0.074 mmol, 1.0 equiv) obtained in last step and anhydrous THF (1.5 mL). Subsequently, N, N-diisopropylcarbodiimide (DIC, 14 µL, 0.09 mmol, 1.2 equiv), hydroxybenzotriazole (HOBt, 14 mg, 0.09 mmol, 1.2 equiv) and N, N-diisopropylethylamine (DIPEA, 32 µL, 0.185 mmol, 2.5 equiv) were added and the mixture was stirred at room temperature for 30 min. *O*-(tetrahydro-2*H*-pyran-2-yl)hydroxylamine (11 mg, 0.09 mmol, 1.2 equiv) in THF (0.5 mL) was then added and reaction mixture was kept stirring at room temperature for 2 h. The reaction was diluted with EtOAc (4 mL) and H_2O (2 mL). The organic phase was separated from the aqueous phase, and it was washed with brine (2 mL) and dried over Na_2SO_4. After concentration *in vacuo*, the residue was re-dissolved in THF (2 mL) and concentrated HCl (50 µL) was added. The mixture was stirred at room temperature for 2 h until the starting material **S11** was fully consumed (monitored by TLC). EtOAc (5 mL) and saturated $NaHCO_3$ solution (1 mL) were added to quench the reaction and to remove any residual hydrochloric acid. The organic phase was separated from the aqueous phase, and the aqueous phase was extracted with EtOAc (10 mL × 3) and dried over Na_2SO_4. The combined organic phase was dried over Na_2SO_4. After concentration *in vacuo*, the residue was purified through column chromatography (hexanes/EtOAc: from 4:1 to 1:2) to afford N-hydroxy-1,1-dimethyl-2-(5-(trifluoromethyl)pyrazin-2-yl)isoindoline-4-carboxamide **FT895** as white solid (7.7 mg, 22% yield form **S9**), which is a known compound.[6]

N-Hydroxy-1,1-dimethyl-2-(5-(trifluoromethyl)pyrazin-2-yl)isoindoline-4-carboxamide (FT895): ^{1}H NMR (400 MHz, DMSO-d_6) δ 11.19 (s, 1H), 9.11 (s, 1H), 8.55 (s, 1H), 8.12 (s, 1H), 7.55 (d, J = 7.6 Hz, 2H), 7.43 (t, J = 7.7 Hz, 1H), 5.05 (s,

2H), 1.76 (s, 6H); ^{13}C NMR (126 MHz, DMSO-d_6) δ 164.7, 153.4, 149.2, 139.8, 133.7, 131.7, 129.0 (q, J = 34.4 Hz), 128.7, 128.1, 126.3, 124.7, 123.3 (q, J = 271.3 Hz), 67.8, 53.3, 26.5; ^{19}F NMR (376 MHz, DMSO-d_6) δ -64.54 (s); LC-MS (ESI, m/z): calcd for $C_{16}H_{16}F_3N_4O_2^+$ ($[M + H]^+$) 353.11, found 353.07.

D. Supplementary Figures and Table.

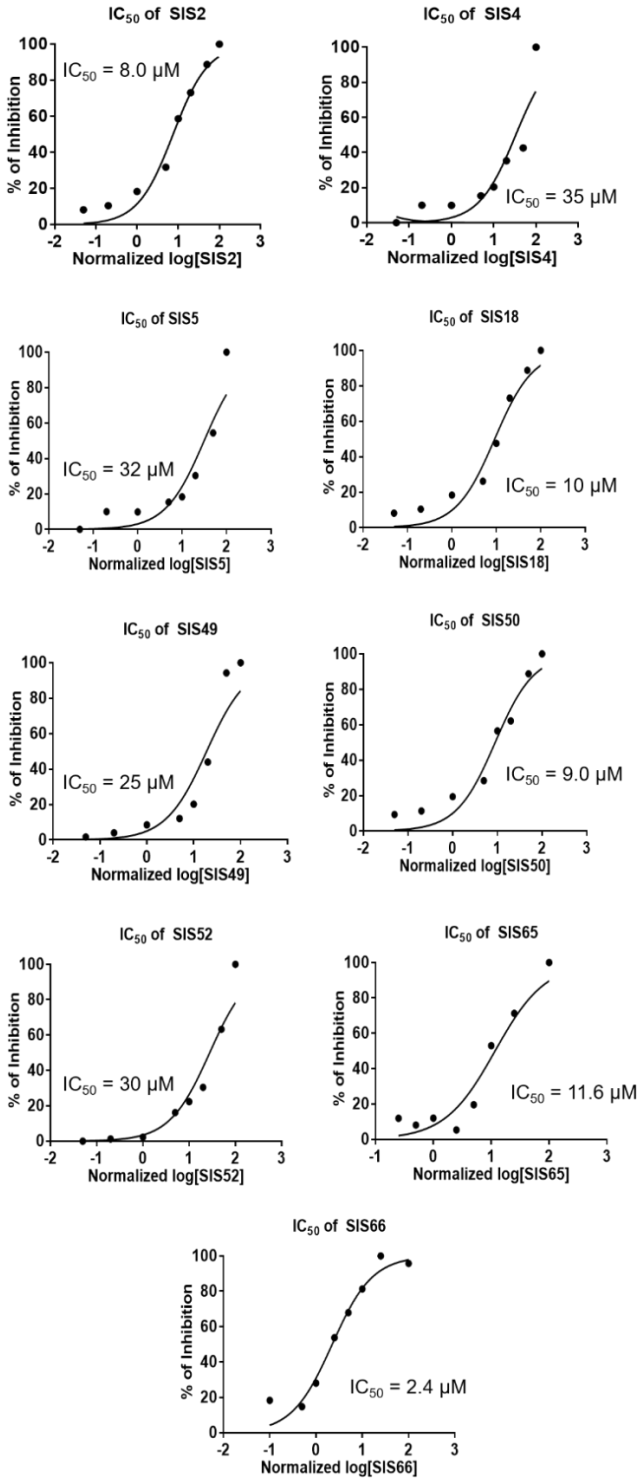

d1. IC_{50} curves of SIS2, SIS4, SIS5, SIS18, SIS49, SIS50, SIS52, SIS65 and SIS66 with myristoyl-H3K9.

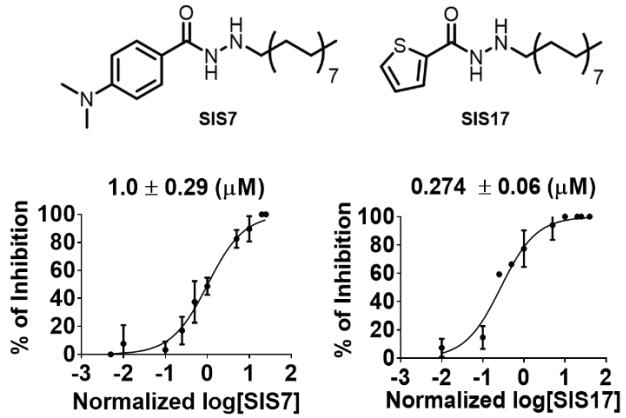

d2. IC_{50} curves of SIS7 and SIS17 myristoyl-SHMT2.

References

1. Falkenberg, K. J.; Johnstone, R. W., Histone deacetylases and their inhibitors in cancer, neurological diseases and immune disorders., *Nat Rev Drug Discov*., **13**, 673-691, doi: 10.1038/nrd4360, (2014).

2. Yang, X. J.; Seto, E., The Rpd3/Hda1 family of lysine deacetylases: from bacteria and yeast to mice and men., *Nat Rev Mol Cell Biol.*, **9**, 206-218. doi: 10.1038/nrm2346, (2008).

3. Finnin, M. S.; Donigian, J. R.; Cohen, A.; Richon, V. M.; Rifkind, R. A.; Marks, P. A.; Breslow, R.; Pavletich, N. P., Structures of a histone deacetylase homologue bound to the TSA and SAHA inhibitors. *Nature*, **401**, 188-193, doi: 10.1038/43710, (1999).

4. Lombardi, P. M.; Cole, K. E.; Dowling, D. P.; Christianson, D. W., Structure, Mechanism, and Inhibition of Histone Deacetylases and Related Metalloenzymes., *Curr. Opin. Struct. Biol.*, **21**, 735-743, doi: 10.1016/j.sbi.2011.08.004, (2011).

5. Moreno-Yruela, C.; Galleano, I.; Madsen, A. S.; Olsen, C. A., Histone Deacetylase 11 Is an ε-N-Myristoyllysine Hydrolase, *Cell Chem. Biol.*, 25, 849-856, doi: 10.1016/j.chembiol.2018.04.007, (2018).

6. Kutil, Z.; Novakova, Z.; Meleshin, M.; Mikesova, J.; Schutkowski, M.; Barinka, C. Histone Deacetylase 11 Is a Fatty-Acid Deacylase, *ACS Chem Biol*., **13**, 685-693, doi: 10.1021/acschembio.7b00942, (2018).

7. Cao, J.; Sun, L.; Aramsangtienchai, P.; Spiegelman, N. A.; Zhang, X.; Seto, E.; Lin, H., HDAC11 regulates type I interferon signaling through defatty-acylation of SHMT2, *PNAS*, **116,** 5487-5492, doi: 10.1073/pnas.1815365116, (2019).

8. Deubzer, H. E.; Schier, M. C.; Oehme, I.; Lodrini, M.; Haendler, B.; Sommer, A.; Witt, O., HDAC11 is a novel drug target in carcinomas, *Int J Cancer.*, **132**, 2200-2208, doi: 10.1002/ijc.27876, (2013).

9. Buglio, D.; Khaskhely, N. M.; Voo, K. S.; Martinez-Valdez, H.; Liu, Y. J.; Younes, A. HDAC11 plays an essential role in regulating OX40 ligand expression in Hodgkin lymphoma, *Blood*, **117**, 2910-2917, doi: 10.1182/blood-2010-08-303701, (2011).

10. Thole, T. M.; Lodrini, M.; Fabian, J.; Wuenschel, J.; Pfeil, S.; Hielscher, T.; Kopp-Schneider, A.; Heinicke, U.; Fulda, S.; Witt, O.; Eg-gert, A.; Fischer, M.; Deubzer, H. E. Neuroblastoma cells depend on HDAC11 for mitotic cell cycle progression and survival., *Cell Death Disease*, **8**, e2635-e2635, doi: 10.1038/cddis.2017.49, (2017).
11. Sun, L.; Telles, E.; Karl, M.; Cheng, F.; Luetteke, N.; Sotomayor, E. M.; Miller, R. H.; Seto, E., Loss of HDAC11 ameliorates clinical symptoms in a multiple sclerosis mouse model, *Life Science Alliance*, **1**, e201800039-e201800039. doi: 10.26508/lsa.201800039, (2018).
12. Bagchi, R. A.; Ferguson, B. S.; Stratton, M. S.; Hu, T.; Cavasin, M. A.; Sun, L.; Lin, Y. H.; Liu, D.; Londono, P.; Song, K.; Pino, M. F.; Sparks, L. M.; Smith, S. R.; Scherer, P. E.; Collins, S.; Seto, E.; McKinsey, T. A., HDAC11 suppresses the thermogenic program of adipose tissue via BRD2, *JCI Insight*, **3**, 120159-12067, doi: 10.1172/jci.insight.120159, (2018).
13. Sun, L.; Marin de Evsikova, C.; Bian, K.; Achille, A.; Telles, E.; Pei, H.; Seto, E. Programming and Regulation of Metabolic Homeostasis by HDAC11, *EBioMedicine.*, **33**, 157-168, doi: 10.1016/j.ebiom.2018.06.025, (2018).
14. James E Bradner, Nathan West, Melissa L Grachan, Edward F Greenberg, Stephen J Haggarty, Tandy Warnow, Ralph Mazitschek, Chemical Phylogenetics of Histone Deacetylases, *Nat Chem Biol.*, **6**, 238-243. doi: 10.1038/nchembio.313, (2010).
15. Matthew J Bottomley 1, Paola Lo Surdo, Paolo Di Giovine, Agostino Cirillo, Rita Scarpelli, Federica Ferrigno, Philip Jones, Petra Neddermann, Raffaele De Francesco, Christian Steinkühler, Paola Gallinari, Andrea Carfí, Structural and Functional Analysis of the Human HDAC4 Catalytic Domain Reveals a Regulatory Structural Zinc-Binding Domain, *J Biol Chem*., **283**, 26694-26704, doi: 10.1074/jbc.M803514200, (2008); Mohamed A Abdallah Elbadawi, Mohamed Khalid Alhaj Awadalla, Muzamil Mahdi Abdel Hamid, Magdi Awadalla Mohamed, Talal Ahmed Awad, Valproic Acid as a Potential Inhibitor of Plasmodium Falciparum Histone Deacetylase 1 (PfHDAC1): An in Silico Approach, *Int. J. Mol. Sci.*, **16**, 3915-3931, doi: 10.3390/ijms16023915, (2015).
16. Wang, Y.; Stowe, R. L.; Pinello, C. E.; Tian, G.; Madoux, F.; Li, D.; Zhao, L. Y.;

Li, J. L.; Wang, Y.; Wang, Y.; Ma, H.; Hodder, P.; Roush, W. R.; Liao, D., Identification of histone deacetylase inhibitors with benzoyl hydrazide scaffold that selectively inhibit class I histone deacetylases, *Chem. Biol.*, **22**, 273-284, doi: 10.1016/j.chembiol.2014.12.015, (2015).

17. Corwin. HanschA., LeoR. W. Taft, A survey of Hammett substituent constants and resonance and field parameters, *Chem. Rev.*, **91**, 165-195, doi: https://doi.org/10.1021/cr00002a004, (1991).

18. Linda Lauinger, Jing Li, Anton Shostak, Ibrahim Avi Cemel, Nati Ha, Yaru Zhang, Philipp E Merkl, Simon Obermeyer, Nicolas Stankovic-Valentin, Tobias Schafmeier, Walter J Wever, Albert A Bowers, Kyle P Carter, Amy E Palmer, Herbert Tschochner, Frauke Melchior, Raymond J Deshaies , Michael Brunner, Axel Diernfellner, Thiolutin Is a Zinc Chelator That Inhibits the Rpn11 and Other JAMM Metalloproteases, *Nat. Chem. Biol.*,
13, 709-714, doi: 10.1038/nchembio.2370, (2017).

19. Martin, M. W.; Lee, J. Y.; Lancia, D. R., Jr.; Ng, P. Y.; Han, B.; Thomason, J. R.; Lynes, M. S.; Marshall, C. G.; Conti, C.; Collis, A.; Mo-rales, M. A.; Doshi, K.; Rudnitskaya, A.; Yao, L.; Zheng, X. Discovery of novel N-hydroxy-2-arylisoindoline-4-carboxamides as potent and selective inhibitors of HDAC11, *Bioorg Med Chem Lett.*, **28**, 2143-2147, doi: 10.1016/j.bmcl.2018.05.021, (2018).

20. Jing, H.; Zhang, X.; Wisner,S.A.; Chen, X.; Spiegelman, N.A.; Linder, M.E.; Lin, H. SIRT2 and lysine fatty acylation regulate the trans-forming activity of K-Ras4a, *eLife*, **6**, e32436-e32468, doi: 10.7554/eLife.32436, (2017).

21. Zhang, X.; Spiegelman, N.A.; Nelson, O.D.; Jing, H.; Lin, H. SIRT6 regulates Ras-related protein R-Ras2 by lysine defatty-acylation, *eLife*, **6**, e25158-e25174, doi: 10.7554/eLife.25158, (2017).

22. Zhang, X.; Khan, S.; Hong, J.; Antonyak, M.A.; Chen, X.; Spiegel-man, N.A.; Shrimp, J.H.; Cerione, R.A.; Lin, H. Identifying the functional contribution of the defatty-acylase activity of SIRT6, *Nat. Chem. Biol.*, **12**, 614-620, doi: 10.1038/nchembio.2106, (2016); Aramsangtienchai, P.; Spiegelman, N.A.; He, B.; Miller, S.P.; Dai, L.; Zhao, Y.; Lin, H. HDAC8 Catalyzes the Hydrolysis of Long

Chain Fatty Acyl Lysine, *ACS Chem. Biol.*, **11**, 2685-2692, doi: 10.1021/acschembio.6b00396, (2016).
23. Synthesis of FT895 was done with Chengliang Zhu.
24. (a) Charron, G.; Zhang, M. M.; Yount, J. S.; Wilson, J.; Raghavan, A. S.; Shamir, E.; Hang, H.C., Robust fluorescent detection of protein fatty-acylation with chemical reporters., *J. Am. Chem. Soc.*, **131**, 4967-4975, doi: 10.1021/ja810122f. (2009) (b) Jiang, H.; Kim, J. H.; Frizzell, K. M.; Kraus, W. L.; Lin, H., Clickable NAD analogues for labeling substrate proteins of poly(ADP-ribose) polymerases, *J. Am. Chem. Soc.*, **132,** 9363-9372, doi: 10.1021/ja101588r, (2010).

CHAPTER 3

GARCINOL IS AN HDAC11 INHIBITOR

Abstract

Garcinol is a natural product from the *Garcinia indica* fruit and is well-known as an anti-oxidant, anti-inflammation, and anti-cancer agent. However, the understanding for its mechanism of action is still incomplete. It has been reported to be a histone acetyltransferase (HAT) inhibitor Here, we surprisingly found that Garcinol is a potent HDAC11 inhibitor (HDAC11 IC_{50} ~5 μM in vitro HPLC assay and IC_{50} ~10 μM in cell SHMT2 fatty acylation assay) which is comparable to previously reported HDAC11 inhibitors. Additionally, among all the HDACs tested, Garcinol specifically inhibits HDAC11 over other HDACs. HDAC11 is the only class IV HDACs and there are very few inhibitors available for it. Therefore, this study provides a new HDAC11 inhibitor lead from natural products and may help explain the various biological activities of Garcinol.

Introduction

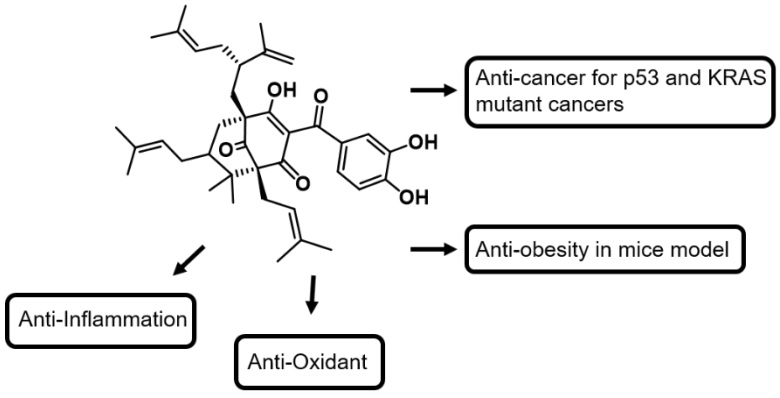

Figure 3.1. Structure and biological activities of Garcinol.

Natural product, Garcinol, is a poly-isoprenylated benzophenone compound extracted from the *Garcinia indica* fruit. It has been reported to have various interesting

biological properties, such as anti-cancer, anti-inflammation, and anti-oxidant activities (Figure 3.1).[1-3] Its mechanism of action, however, remains largely unknown. It has been reported to decrease the expression of COX2, iNOS, and NF-kB.[1] In the cell-free extract, it could inhibit 5-lipoxygenase and microsomal prostaglandin E2 synthase 1 (mPGES-1).[2] It could also inhibit STAT3 activation and suppresses tumorigenesis.[3] However, the exact protein targets underlying its various biological functions is rather unclear. The only reported direct target is histone acetyltransferases, p300 and PCAF.[4] It has been reported to be a histone acetyltransferase inhibitor, but the biological activities do not really fit HAT inhibition.[5,6]

Surprisingly, here we found that Garcinol is a potent HDAC11 inhibitor. HDAC11 is the only class IV HDAC member. Recently, several reports showed that it does not have deacetylation activity but instead can hydrolyze long-chain fatty acyl groups from protein lysine residues.[7-9] The first reported physiological substrate of HDAC11 is SHMT2, and HDAC11 regulates type I interferon signaling by defatty-acylating SHMT2 and promoting type I interferon receptor ubiquitination and degradation.[7] Several recent reports showed that HDAC11 knockout in mice displays beneficial effects, including increased thermogenesis in adipose tissue, increased resistance to high-fat diet-induced obesity, as well as protection from symptoms of multiple sclerosis.[10,11] The interesting phenotypes of HDAC11 knockout warrants the development of HDAC11 inhibitors. Currently, only a few HDAC11 inhibitors are known. The finding that Garcinol is an HDAC11 inhibitor will not only provide an opportunity to understand the mechanism underlying Garcinol's various biological activities but also provide a new HDAC11 inhibitor scaffold to develop new inhibitors to explore the therapeutic potential of targeting HDAC11.

Results and discussion

New strategy to discover a new HDAC11 inhibitor

Since Class I, II, and IV HDACs have a Zinc dependent catalytic mechanism, all previous HDAC inhibitors targeting Class I and II HDACs possess a Zinc-binding

group which is essential for HDAC inhibition.[12,13] Previously, known HDAC inhibitors were examined as potential HDAC11 inhibitors. However, we and others soon discovered that this strategy does not work for developing HDAC11 inhibitors.[9,14,15] Most known HDAC inhibitors turned out to be unable to inhibit HDAC11, while a few (such as trapoxin) can inhibit HDAC11, but it does not have the desired selectivity for HDAC11. Hence, a new strategy to discover HDAC11 inhibitors is needed.

We previously used an activity-based design approach and discovered a potent and selective HDAC11 inhibitor, SIS17, which is similar to FT895, an HDAC11 inhibitor developed by Forma Therapeutics. This approach focuses on compounds that contain zinc-chelating groups and long hydrophobic groups to occupy the acyl pocket of HDAC11 that accommodate long-chain fatty acyl groups. Guided by similar principles, we turned our attention to natural products with similar properties (zinc-chelating groups and large hydrophobic groups). We noticed that several natural products (curcumin, garcinol, and anacardic acid) with interesting biological activities contain potential Zinc binding groups (Figure 3.2), which is indispensable for HDAC11 inhibition. Furthermore, these natural products also contain large hydrophobic moieties, which could potentially bind the active site pocket of HDAC11 that accommodate long-chain fatty acyl groups.

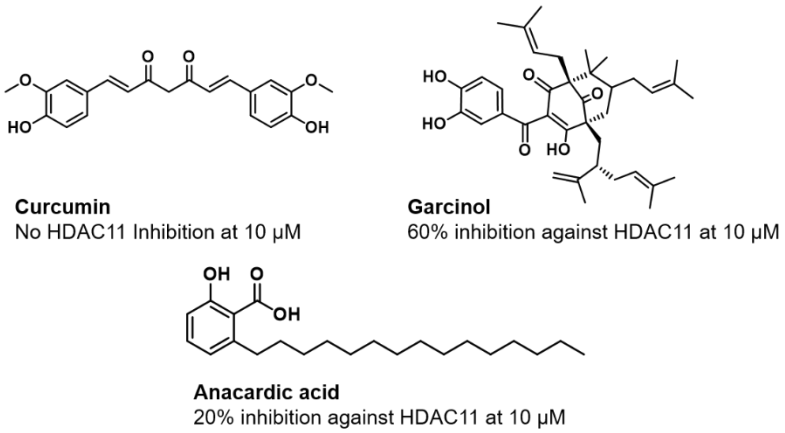

Figure 3.2. Structures of metal-chelating groups-containing natural products tested for HDAC11 inhibition. The percent of inhibition at 10 μM concentration is indicated.

We tested whether they could inhibit HDAC11 with an in vitro HPLC assay using myristoyl-H3K9 peptide. Anacardic acid showed weak inhibition at 10 µM (20% inhibition against HDAC11) while Curcumin showed no inhibition at 10 µM. Garcinol, on the other hand, exhibited 60% inhibition at 10 µM (Figure 3.2).

Selective HDAC11 inhibition of Garcinol

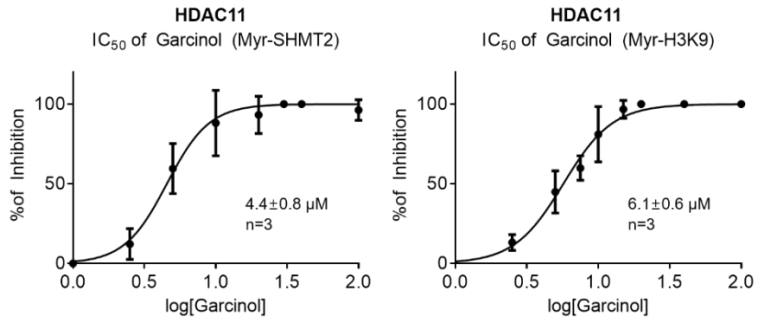

In vitro HPLC IC_{50} with H3K9 peptide	
Garcinol	
Sirtuin2	>50 µM
Sirtuin3	>50 µM
HDAC1	>100 µM
HDAC4	>100 µM
HDAC6	>100 µM
HDAC8	~25 µM
HDAC11	**6.1 µM**

Figure 3.3. IC_{50} curves with Garcinol against HDAC11 and in vitro HPLC assay results against other HDACs.

We further examined its IC_{50} values of Garcinol against HDAC11 with myristoyl-SHMT2 and myristoyl-H3K9 peptides. Garcinol showed 4.4 µM (Myristoyl-SHMT2) and 6.1 µM (Myristoyl-H3K9) of IC_{50} based on our HPLC assay (Figure 3.3). Next, we tested its selectivity against other HDACs using the same HPLC assay. Given that Garcinol has been reported to inhibit HATs, we initially expected that Garcinol might be a pan-assay interfering compound and may inhibit many HDACs. Surprisingly, to our delight, Garcinol showed a remarkable selectivity among the HDACs tested. It only showed 10% inhibition against SIRT3 demyristoylation activity at 50 µM and 43% inhibition against HDAC8 demyristoylation activity at 25 µM. For other HDACs tested, we could not detect any inhibition at 50 µM (Figure 3.3).

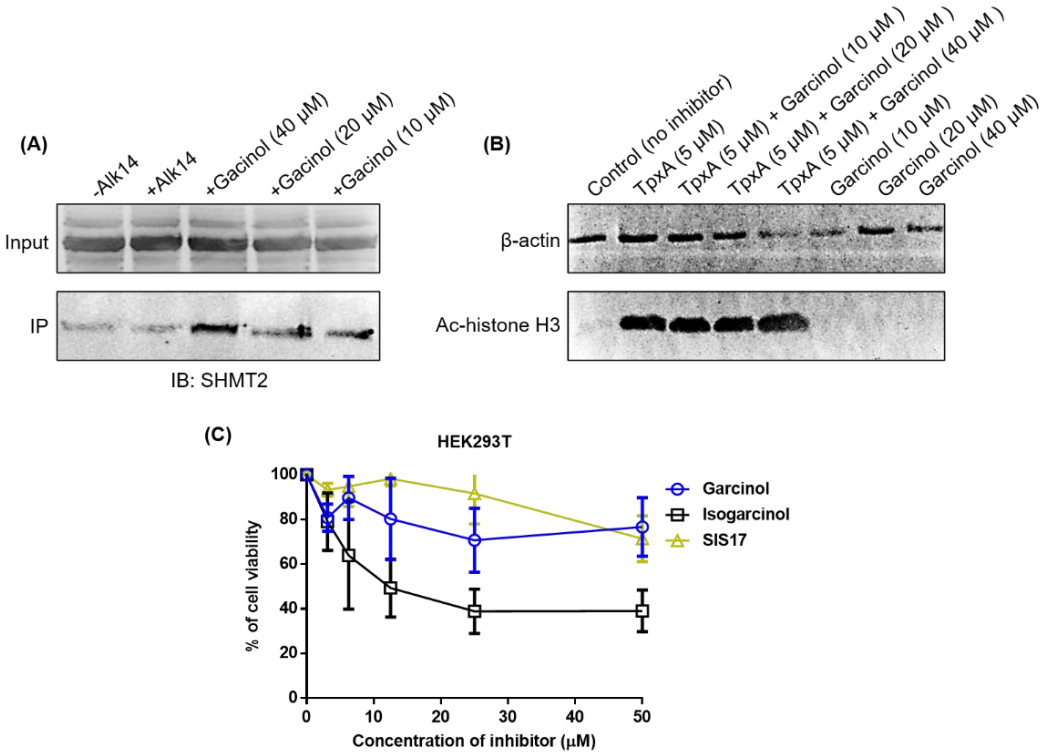

Figure 3.4. Garcinol effects in cells. (A) Garcinol effect on defatty acylation of SHMT2 by HDAC11 (B) Garcinol effect on acetylation of Histone H3. (C) 2D Cell Cytotoxicity with Garcinol, Isogarcinol and SIS17.

Given the surprising selectivity of Garcinol towards HDAC11, we then proceeded to test its ability to inhibit HDAC11 in cells. We measured the palmitoylation of the known HDAC11 physiological substrate, SHMT2, in cells. The acylation of SHMT2 was detected using an alkyne tagged palmitic acid analog (Alk14, 50 μM). HEK 293T cells were incubated with Alk14 and after cell lysis, the Alk14-labeled proteins were conjugated with biotin-azide using click chemistry. Biotinylated proteins were immunoprecipitated with streptavidin beads and immunoblotted against SHMT2. Higher western blot signal would indicate a higher fatty acylation level on SHMT2. At 10, 20, and 40 μM of Garcinol, we could see a clear increase of fatty acylation on SHMT2 (Figure 3.4.A). Thus, Garcinol can inhibit HDAC11 in cells.

Garcinol has been reported to inhibit HATs with IC_{50} values ranged from 25 to 100 uM. To test whether Garcinol indeed inhibits HATs in cells, we also measured the

histone acetylation levels in the presence of Garcinol. DMSO and a pan-HDAC inhibitor, TpxA (trapoxin A), were used as controls. Garcinol did not change histone acetylation levels at 10, 20, and 40 µM, while TpxA increased the acetylation level of histone H3 drastically even at 5 µM (Figure 3.4.B). Since the base level of acetyl-histone H3 is low, we co-treated TpxA (5 µM) with Garcinol to see more clear change in acetylation. However, Garcinol did not change the acetylation level with co-treatment of TpxA (Figure 3.4.B). Thus, our data showed that Garcinol potently inhibits HDAC11 in cells and it does not seem to inhibit HATs under the conditions we used. Furthermore, inhibition on other HDACs is well-known to be toxic to normal cells. Hence, there should be no cell cytotoxicity on normal cells if Garcinol did not target other HDACs in cells. We examined the cell cytotoxicity of Garcinol along with SIS17 and isogarcinol. Garcinol did not cause normal cell death with HEK293T cells and this result could be another evidence that Garcinol may not inhibit other HDACs (Figure 3.4.C).

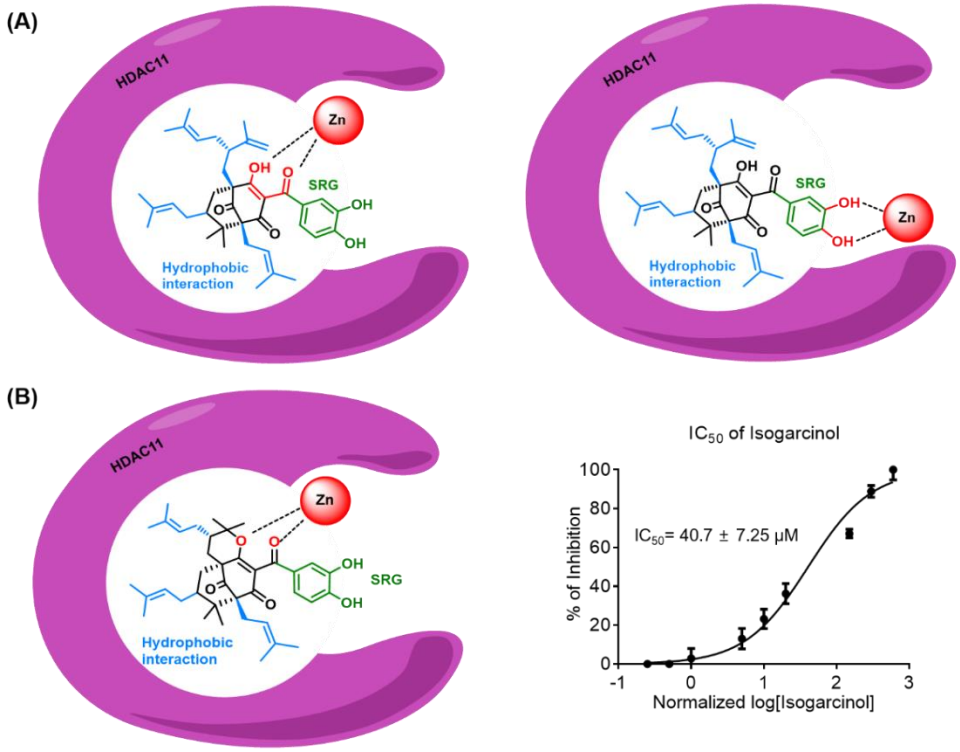

Figure 3.5. Potential Zinc binding sites of Garcinol. (A) Speculation of ZBG in Garcinol. (B) Possible ZBG based on IC_{50} of isogarcinol.

There are two potential Zinc-chelating groups in Garcinol (Figure 3.5.A), the enol-ketone structure, or the dihydroxy group on the benzene ring. One of the commercially available Garcinol-derived compounds is isogarcinol. Isogarcinol also has the dihydroxy group on the phenyl ring but does not contain the enol ketone group. Using the same HPLC assay, we found that isogarcinol has much weaker HDAC11 inhibition activity (IC_{50} = 40.7±7.25 μM). This result support that the enol ketone part of Garcinol is important for HDAC11 inhibition and is likely a ZBG of Garcinol (Figure 3.5.B). This speculation could help to modify the Garcinol structure to obtain even better HDAC11 inhibitors.

Summary

By examining three natural products with potential zinc-chelating groups and large hydrophobic groups, we surprisingly found that Garcinol efficiently inhibits HDAC11. Furthermore, Garcinol showed selectivity toward HDAC11 among all the HDACs tested. In cells, it did not affect the acetylation of histone H3, but efficiently increased the fatty acylation level of SHMT2, a previously established HDAC11 substrate. These results are comparable to the best HDAC11 inhibitors we previously developed, SIS17. Thus, our data established Garcinol as a potent and selective HDAC11 inhibitor.

Garcinol has been reported to have many beneficial biological activities, including anticancer[1], anti-oxidant[2], and anti-inflammation[3] activities. Interestingly, several in vivo effects of Garcinol showed similarity with HDAC11 knockout phenotypes. Garcinol treatment in the experimental autoimmune encephalomyelitis (EAE) mice model exhibited a decreased level of demyelination in the spinal cord which is the key step for treating multiple sclerosis. Loss of HDAC11 also significantly inhibited demyelination of the spinal cord in the EAE mice model.[4] Additionally, dietary Garcinol has been reported to reduce obesity and diabetes in the high-fat-diet mice model, correlating with the phenotypes of HDAC11 knockout in mice on a high-fat diet.[5] These striking phenotypic similarities provide further support that Garcinol is an HDAC11 inhibitor. Our study thus not only provides a novel HDAC11 inhibitor to further investigate the biological function of HDAC11 and therapeutic potential of targeting HDAC11, but also an opportunity to understand the mechanism of action of a complex natural product with an interesting history and biological activities.

Methods

General Information

Reagents. Commercially available Curcumin (#81025.1), Anacardic acid (#13144), Garcinol (#10566) and Isogarcinol (#21164) were purchased from Cayman. Anti-Flag affinity gel (#A2220) and anti-Flag antibody conjugated with horseradish peroxidase (#A8592) were purchased from Sigma-Aldrich. Acetyl-Histone H3 Antibody (#9675) was purchased from Cell Signaling Technology. SHMT2 (mSHMT Antibody (F-11): sc-390641- Non-conjugated), ß-actin antibody (SC-47778 HRP) and goat anti-mouse IgG-HRP (sc-2005) were purchased from Santa Cruz. Triple Flag peptide for eluting Flag-tagged HDAC11 enzyme and protease inhibitor cocktail were purchased from Sigma-Aldrich. ECL plus western blotting detection reagent and universal nuclease for cell lysis were purchased from Thermo Scientific Pierce. Acyl peptides (myristoyl-H3K9) and Alk14 were synthesized.[16] The peptide sequence for the H3K9 peptide is KQTARK(myristoyl)STGGWW with uncapped N-terminal and SHMT2 peptide is SDEVK(myristoyl)AHLLAWW with capped acetyl N-terminal.

Instrumentation. Analytical HPLC analysis was carried out on a SHIMADZU LC with Kinetex 5u EVO C18 100A column (100 mm × 4.60 mm, 5 μm, Phenomenex) monitoring at 215 nm and 280 nm. Solvents for analytical HPLC were water with 0.1% (v/v) trifluoroacetic acid (TFA) as solvent A and acetonitrile with 0.1% (v/v) TFA as solvent B. Compounds were analyzed at a flow rate of 0.5 mL/min.

Cell culture. HEK293T cells were cultured in designated DMEM media with 10% (v/v) heat-inactivated at 56 ^{o}C FBS. The cell lines used for experiments had been passaged no more than 20 times and all cell lines were tested for and showed no mycoplasma contamination.

Expression and purification of HDACs and sirtuins from HEK293T Cells. Full-length human HDACs and sirtuins were inserted into the pCMV-Tag 4a vector with a C-terminal Flag tag. All plasmids were transfected into HEK293T cells using FuGene

6 Transfection Reagent according to the manufacturer's protocol (from Promega). Eight 10-cm plates of cells were collected by centrifugation at 500 × g for 5 min and then lysed in 2 ml of Nonidet P-40 lysis buffer (25 mM Tris-HCl, pH 7.4, 150 mM NaCl, 10% (v/v) glycerol and 1% (v/v) Nonidet P-40) with protease inhibitor cocktail (1:100 dilution) at 4 °C for 30 min. After centrifugation at 15,000 × g for 15 min, the supernatant was collected and incubated with 20 μL anti-Flag affinity gel at 4 °C for 2 h. The affinity gel was washed three times with 1 ml of washing buffer (25 mM Tris-HCl, pH 7.4, 150 mM NaCl, 0.2% (v/v) Nonidet P-40) and then eluted with 100 μl of 300 μM 3× FLAG peptide (dissolved in 25 mM Tris-HCl, pH 7.4, 150 mM NaCl and 10% (v/v) glycerol) twice (total 200 μL) for 1 hr each time. The eluted proteins were checked by 12% SDS-PAGE to be at least 80% pure.

HDACs and sirtuins deacylase activity assay. All inhibitors were dissolved in DMSO. For the deacylation assay using the zinc-dependent HDACs, HDAC1, HDAC4, HDAC6 and HDAC8 was incubated in 40 μL reaction mixtures (25 mM Tris-HCl, pH 8.0, 50 mM NaCl, 25 μM H3K9 acetyl (HDAC1), trifluoacetyl (HDAC4), myristoyl (HDAC8) and 25 μM p53 acetyl (HDAC6) peptide) at 37 °C for 20 min with 64 nM of HDAC11. To quench the reactions, 40 μL cold acetonitrile was mixed with the reaction mixture. After centrifuging at 15,000 × g for 15 min, the supernatant was collected and analyzed by HPLC using Kinetex 5u EVO C18 100A column (150 mm × 4.6 mm, Phenomenex). Solvents used for HPLC were water with 0.1% (v/v) trifluoroacetic acid (solvent A) and acetonitrile with 0.1% (v/v) trifluoroacetic acid (solvent B). The gradient for HPLC condition was 0% B for 2 min, 0–20% B in 2 min, 20–40% B in 13 min, 40–100% B in 2 min, and then 100% B for 5 min. The flow rate was 0.5 mL/min. Procedure for HPLC assay with SHMT2 myristoyl peptide is the same as H3K9 myristoyl procedure described above except 120 mins incubation time used instead of 20mins.

For the deacylation assay using sirtuin2 and sirtuin3, sirtuins were incubated in 40 μL reaction mixtures (25 mM Tris-HCl, pH 8.0, 50 mM NaCl, 1 mM DTT, 1 mM NAD+, 25 μM H3K9 myristoyl peptide) at 37 °C for (sirtuin2 and 3 for 5 mins and sirtuin 6

for 30 mins with 2 μM). To quench the reactions, 40 μL of cold acetonitrile was mixed with the reaction mixture. After centrifuging at 15,000 g for 15 min, the supernatant was collected and analyzed by HPLC following the same conditions described above.

Detection of histone H3 acetylation in cells. HEK293T cells cultured in 15-cm dishes were treated with the corresponding inhibitors for 6 h. The cells were scraped off the plates and collected at 500 g for 5 min. Cells from each plate were then lysed in 200 μL of 4% SDS lysis buffer (50 mM triethanolamine at pH 7.4, 150 mM NaCl, 4% (w/v) SDS) with protease inhibitor cocktail (1:100 dilution) and nuclease (1:1000 dilution) at room temperature for 15 min. The protein concentration in the total cell lysate was determined using a BCA assay and equal amount of protein was loaded onto a 15% SDS-PAGE gel and resolved. The gel was used for western blot analysis with acetyl histone H3 antibodies.

Western Blot. Proteins were resolved by 12% or 15% SDS-PAGE and transferred to PVDF membranes. The membrane was blocked with 5% (w/v) BSA in PBS with 0.1% (v/v) Tween-20 (TPBS) at room temperature for 60 min. The primary antibody was diluted with fresh 5% (w/v) BSA in TPBS (1:5,000 dilution for antibodies to Flag, Ac-histone H3, Ac-α-tubulin and mSHMT2) and incubated with the membrane at room temperature for 1 h or at 4 °C for 12 h. After washing the membrane three times with TPBS, the secondary antibody (1:3,000 dilution with 5% (w/v) BSA in TPBS) was added and then incubated at room temperature for 1 h. The chemiluminescence signal in the membrane was recorded after developing in ECL Plus Western Blotting detection reagents using a Typhoon 9400 Variable Mode Imager (GE Healthcare Life Sciences).

Detection of Lysine Fatty Acylation on Endogenous SHMT2 by Western Blot. HEK293T cells were treated with 50 μM of Alk14 and inhibitors or DMSO for 6 h. One 80-90% confluent 15-cm plate of cells (approximately $2*10^6$ cells per 15-cm dish) were collected by centrifugation at 1000 g for 5 min and lysed in 4% SDS lysis

buffer (50 mM triethanolamine at pH 7.4, 150 mM NaCl, 4% (w/v) SDS) with protease inhibitor cocktail (1:100 dilution) and nuclease (1:1000 dilution) at room temperature for 15 min. The proteins were precipitated with cold methanol (200 µL per sample), cold chloroform (75 µL per sample), and cold water (150 µL per sample). After vortexing to mix well, samples were spun down at 17,000 g for 15 min. Proteins should be located between the upper layer and bottom layer. The upper layer of the solvents was gently removed. Then 1 mL of cold methanol was added to each sample to wash the proteins by vortexing. Samples were centrifuged at 17,000g for 5 min and the solvent was removed. The washing was repeated once more. After methanol washing, methanol was removed from tubes and protein pellets in tubes were air-dried for 5-10 min. Proteins were dissolved in 100 µL of click chemistry buffer (25 mM HEPES, pH 7.4, 150 mM NaCl, and 4% (w/v) SDS). The proteins were sonicated for 30 min at room temperature to be resolubilized. The concentration of the resolubilized proteins was determined using the BCA assay. For each sample, 800 µg of proteins were used for click chemistry (for samples that have higher protein concentration, the reaction volume was adjusted with click chemistry buffer). Biotin-N_3 (5 µL of 5 mM solution in DMF), Tris[(1-benzyl-1H-1,2,3-triazole-4-yl)methyl]amine (5 µL of 2 mM solution in DMF), CuSO4 (5 µL of 50 mM solution in H_2O) and Tris(2-carboxyethyl)phosphine (5 µL of 50 mM solution in H_2O) were added into the reaction mixture. The click chemistry reaction was allowed to proceed at 30^oC for 60 min. Proteins were then precipitated using cold methanol, chloroform, and water as described above. After washing two times with cold methanol, the proteins were resolubilized in 120 µL of 4% SDS lysis buffer. Again, the concentrations of proteins were measured by BCA, and 10 µg of proteins for each sample were set aside as input. Then, 400 µg of proteins for each sample was added into 10 mL of IP washing buffer (25 mM Tris-HCl pH 8.0, 150 mM NaCl, 0.2% (v/v) NP-40) (making sure that SDS is lower than 0.1% in IP washing buffer for efficient affinity purification with streptavidin beads). Streptavidin agarose beads (Thermo Fisher, 20 µl) were added into each sample. The mixture was agitated for 1 h at room temperature. After washing the beads three times with 1 mL of IP washing buffer, 24 µL of 4% (w/v)

SDS lysis buffer and 6 µL of 6× loading dye were added into each sample and boiled for 10 min. The samples and inputs were resolved using 12% SDS-PAGE gel, transferred to nitrocellulose membrane, and analyzed by western blot for SHMT2. The signal was recorded using a Typhoon 9400 Variable Mode Imager (GE Healthcare Life Sciences).

References

1. Mantelingu K., Reddy BA., Swaminathan V., Kishore AH., Siddappa NB., Kumar GV., Nagashankar G., Natesh N., Roy S., Sadhale PP., Ranga U., Narayana C., Kundu TK.,
Specific inhibition of p300-HAT alters global gene expression and represses HIV replication, *Chem. Biol.*, **14**, 645-657, doi: 10.1016/j.chembiol.2007.04.011, (2007)
2. Koeberle A., Northoff H., Werz O., Identification of 5-lipoxygenase and microsomal prostaglandin E2 synthase-1 as functional targets of the anti-inflammatory and anti-carcinogenic garcinol, *Biochemical Pharmacology*, **77**, 1513-1521, DOI: 10.1016/j.bcp.2009.02.005 PMID: 1942668, (2009).
3. Sethi, G., Chatterjee, S., Rajendran, P., Li, F., Shanmugam, M. K., Wong, K. F., Kumar, A. P., Senapati, P., Behera, A. K., Hui, K. M., Basha, J., Natesh, N., Luk, J. M., & Kundu, T. K., Inhibition of STAT3 dimerization and acetylation by garcinol suppresses the growth of human hepatocellular carcinoma in vitro and in vivo, *Mol. cancer*, **13**, doi: 10.1186/1476-4598-13-66, (2014).
4. Karanam B., M Altaf, Radhika AV., V Swaminathan, Aarti R., Parag P S., Tapas K K., Polyisoprenylated Benzophenone, Garcinol, a Natural Histone Acetyltransferase Inhibitor, Represses Chromatin Transcription and Alters Global Gene Expression, *J. Biol. Chem*., **279**, 33716-33726, doi: 10.1074/jbc.M402839200, (2004)
5. Mengyuan Huang, Jiangkun Huang, Yongcheng Zheng, Qiu Sun, Histone Acetyltransferase Inhibitors: An Overview in Synthesis, Structure-Activity Relationship and Molecular Mechanism, Eur J Med Chem, 178, 259-286. doi: 10.1016/j.ejmech.2019.05.078, (2019).
6. Hannah Wapenaar, Frank J Dekker, Histone Acetyltransferases: Challenges in Targeting Bi-Substrate Enzymes, *Clin Epigenetics*, **8**, 59-61, doi: 10.1186/s13148-016-0225-2, (2016).
7. Ji Cao, Lei Sun, Pornpun Aramsangtienchai, Nicole A Spiegelman, Xiaoyu Zhang, Weishan Huang, Edward Seto, Hening Lin, HDAC11 Regulates Type I Interferon Signaling Through Defatty-Acylation of SHMT2, *Proc Natl Acad Sci U S A*, **116**,

5487-5492. doi: 10.1073/pnas.1815365116, (2019).
8. Kutil, Z.; Novakova, Z.; Meleshin, M.; Mikesova, J.; Schutkowski, M.; Barinka, C. Histone Deacetylase 11 Is a Fatty-Acid Deacylase, *ACS Chem Biol.*, **13**, 685-693, doi: 10.1021/acschembio.7b00942, (2018).
9. Moreno-Yruela, C.; Galleano, I.; Madsen, A. S.; Olsen, C. A., Histone Deacetylase 11 Is an ε-N-Myristoyllysine Hydrolase, *Cell Chem. Biol.*, **25,** 849-856, doi: 10.1016/j.chembiol.2018.04.007, (2018).
10. Sun, L.; Telles, E.; Karl, M.; Cheng, F.; Luetteke, N.; Sotomayor, E. M.; Miller, R. H.; Seto, E., Loss of HDAC11 ameliorates clinical symptoms in a multiple sclerosis mouse model, *Life Science Alliance,* **1**, e201800039-e201800039. doi: 10.26508/lsa.201800039, (2018).
11. Bagchi, R. A.; Ferguson, B. S.; Stratton, M. S.; Hu, T.; Cavasin, M. A.; Sun, L.; Lin, Y. H.; Liu, D.; Londono, P.; Song, K.; Pino, M. F.; Sparks, L. M.; Smith, S. R.; Scherer, P. E.; Collins, S.; Seto, E.; McKinsey, T. A., HDAC11 suppresses the thermogenic program of adipose tissue via BRD2, *JCI Insight*, **3**, 120159-12067, doi: 10.1172/jci.insight.120159, (2018).
12. Mengqi Wang, Yufei Xie, Youxiu Zhong, Juren Cen, Lei Wang, Yuanyuan Liu, Ying Zhu, Li Tong, Qun Wei, Amelioration of Experimental Autoimmune Encephalomyelitis by Isogarcinol Extracted From Garcinia Mangostana L. Mangosteen, J Agric Food Chem, 64, 9012-9021. doi: 10.1021/acs.jafc.6b04145, (2016).
13. Rainer Schobert, Bernhard Biersack, Chemical and Biological Aspects of Garcinol and Isogarcinol Recent Developments, Chemistry & Biodiversity, 16, e1900366, https://doi.org/10.1002/cbdv.201900366, (2019).
14. Son SI, Cao J, Zhu CL, Miller SP, Lin H., Activity-Guided Design of HDAC11-Specific Inhibitors, *ACS Chem. Biol*., **14**, 1393–1397, doi: 10.1021/acschembio.9b00292, (2019).
15. Martin, M. W.; Lee, J. Y.; Lancia, D. R., Jr.; Ng, P. Y.; Han, B.; Thomason, J. R.; Lynes, M. S.; Marshall, C. G.; Conti, C.; Collis, A.; Mo-rales, M. A.; Doshi, K.; Rudnitskaya, A.; Yao, L.; Zheng, X. Discovery of novel N-hydroxy-2-arylisoindoline-

4-carboxamides as potent and selective inhibitors of HDAC11, *Bioorg. Med. Chem. Lett.*, **28**, 2143-2147, doi: 10.1016/j.bmcl.2018.05.021, (2018).
16. (a) Charron, G.; Zhang, M. M.; Yount, J. S.; Wilson, J.; Raghavan, A. S.; Shamir, E.; Hang, H.C., Robust fluorescent detection of protein fatty-acylation with chemical reporters., *J. Am. Chem. Soc.*, **131**, 4967-4975, doi: 10.1021/ja810122f. (2009) (b) Jiang, H.; Kim, J. H.; Frizzell, K. M.; Kraus, W. L.; Lin, H., Clickable NAD analogues for labeling substrate proteins of poly(ADP-ribose) polymerases, *J. Am. Chem. Soc.*, **132,** 9363-9372, doi: 10.1021/ja101588r, (2010).

CHAPTER 4

THE EFFECTS OF HDAC11 INHIBITORS ON KRAS-DRIVEN CANCERS

Abstract

Up to date, physiological roles of HDAC11 in regulating immune responses and metabolic pathways have been established. However, little is known about its roles in tumorigenesis. Also, the few papers that reported on a role of HDAC11 in cancer relied on monitoring deacetylation activity instead of the actual catalytic activity of HDAC11 as a defatty-acylase. Here, we screened cancer cells for sensitivity with our HDAC11-specific inhibitor (SIS17) to find that the anchorage-independent growth of KRAS-driven cancers cells are hypersensitive to HDAC11 inhibition. We attempted to investigate the mechanism behind this sensitivity and uncovered preliminary evidence that HDAC11 may regulate CDC42 lysine fatty acylation.

Introduction

There have been several reports that HDAC11 suppression could affect cancer cell proliferation. Deubzer et al. reported that HDAC11 knockdown using siRNA can increase levels of cleaved caspases and induce cancer cell death.[1] With a similar inducing apoptosis mechanism, Thole et al. reported that HDAC11 knockdown causes cell death in neuroblastoma.[2] In contrast to the tumor suppressing role of HDAC11 knockdown, Leslie et al. showed HDAC11 inhibition may facilitate breast cancer cell metastasis through lymph nodes.[3] Since underlying mechanism of each reported phenotypes is mostly based on deacetylation activity, the exact role of HDAC11 as a defatty acylase in different types cancers is still unknown.

In this chapter, we tested the activity of our HDAC11-specific inhibitor SIS17 in many cancer cells and found that HDAC11 suppression is detrimental for the anchorage-independent growth of KRAS-driven cancers. Furthermore, we suggest a possible

mechanism with small GTPases, CDC42 as a potential HDAC11 substrate regarding this phenotype.

Results and Discussion

Testing the effect of an HDAC11-specific inhibitor in various cancer cell lines

To test our HDAC11-specific inhibitor in several cancer cell lines, two different assays were used, a normal 2D cell proliferation assay (anchorage-dependent growth assay) and a soft-agar assay (anchorage-independent growth assay). The soft agar assay that measures anchorage-independent growth has been considered to more closely mimic the in vivo system than 2D assay.[4] Also, the oncogenic signal that promotes colony formation on soft agar is a distinct characteristic for cancerous cells since normal cells generally do not form colonies on soft agar. We used a number of cell lines, including colon cancer cells (HT29, HCT8, HCT116, SW948, SW480, SW620, and SKCO1), pancreatic cancer cells (BxPC3, Caco2, MIAPACA2, and HPAFII), and normal cells (HEK293T, 3T3, and CRL-1790). These cells were treated with different concentrations of inhibitors (0, 6.3, 12.5, 25.0, 50.0 μM) in the 2D proliferation assay and (0, 1.6, 3.1, 6.3, 12.5, 25.0 μM) in the soft agar assay.

A.

	Cell Line	KRAS Dependency	IC_{50} in 2D SIS17 (μM)	IC_{50} in 3D SIS17 (μM)	Inhibition in colony formation with HDAC11 knockdown
Colon cancer	HT29	Weak	~50	~ 25	N
	HCT8	Weak	~50	>25	N
	HCT116	Moderate	~50	~ 25	N
	SW948	Moderate	~50	12	N
	SW480	Strong	~50	1.6	Y
	SW620	Strong	~50	1.6	Y
	SK-CO-1	Strong	~50	6	
Pancreatic cancer	BxPC3	Weak	~50	>25	N
	Caco2	Weak	~50	>25	
	MIAPACA2	Strong	~50	10	Y
	HPAFII	Strong	~50	3	Y
	AsPC3	Unknown	~50	6	
Normal cell	293T	Normal Cell	~50	NA	NA
	3T3	Normal Cell	~50	NA	NA
	CRL-1790	Normal Cell	~50	NA	NA

B.

	Cell Line	IC_{50} in 3D SIS17 (μM)
3T3	KRAS4a G12D	6
	KRAS4a G12C	6
	KRAS4b G12D	12
	HRAS G12D	12
Breast cancer	MCF7	50
	MDA-MB-231	12
	SKBR3	6
	BE2C (Brain)	25
	A549 (Lung)	25

Figure 4.1. Cancer cells screening with SIS17. (A) IC_{50} values in 2D growth and 3D growth with SIS17. (B) Transformed 3T3 cells and cancer cells other than pancreatic and colon cancers with SIS17.

Based on the 2D assay, SIS17 showed mild cell toxicity on cancer cells and normal cells even at the high concentration (50 μM). This result is not consistent with literature reports suggesting that HDAC11 knockdown inhibit 2D cell proliferation in several cancer cell lines. One possibility was that the bioavailability of SIS17 was low and could not reach the concentrations needed to inhibit HDAC11 in these cell lines (Figure 4.1.A). However, this is unlikely as we previously shown that even at 12.5 uM, SIS17 could inhibit HDAC11 in cells (described in Chapter 2). Regarding the 2D growth, one research group recently reported that HDAC11 knockdown would inhibit 2D growth of HCT116 colon cancer cell and MCF7 breast cancer cell through increasing apoptotic gene expression.[1] However, SIS17 did not inhibit 2D growth of HCT116 and MCF7 (Figure 4.2). To confirm whether the results with SIS17 are consistent with HDAC11 knockdown, we knocked down HDAC11 in HCT116 and MCF7 cells. However, we did not see any inhibition of 2D cell growth with HDAC11 knockdown in the cells (Figure 4.2).

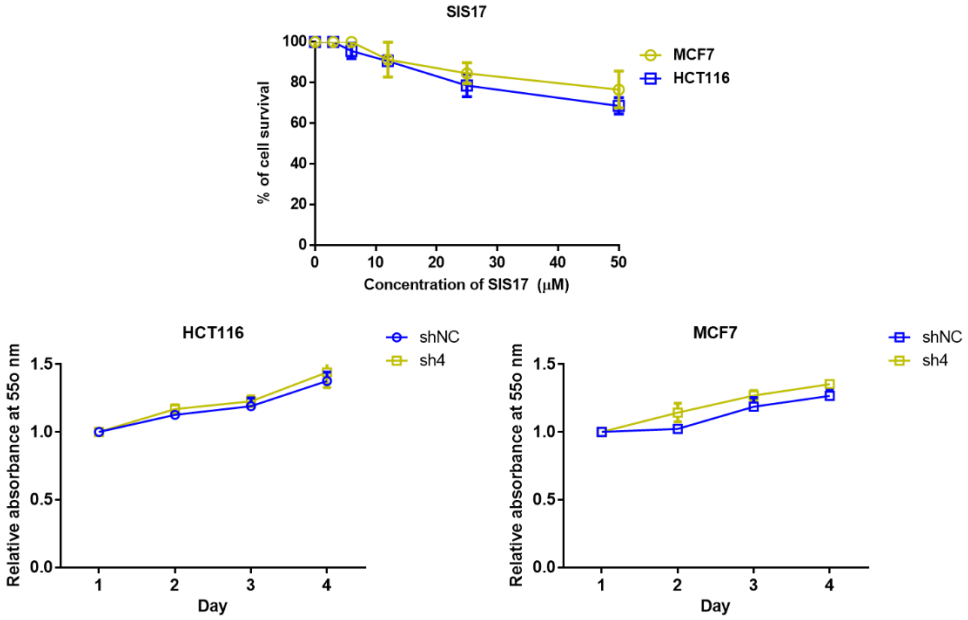

Figure 4.2. 2D proliferation assay results of HCT116 and MCF7 with SIS17 and HDAC11 knockdown. (HDAC11 knockdown efficiency based on mRNA level: HCT116 (62%) and for MCF7 (74%)).

On contrary, in the 3D soft agar assay, we could see noticeable inhibition on several

cancer cells with SIS17 treatment (colon cancer cells: SW480, SW620, and SKCO1 and pancreatic cancer cells: HPAFII, and MIAPACA2). To further confirm that this inhibitor's effect on the specific cancer cells is through HDAC11 inhibition, stable HDAC11 knockdown cancer cells were generated with shRNA and selected with puromycin. The same 3D soft agar assay was performed on the generated HDAC11 stable knockdown cells. Consistently with the SIS17 and transient knockdown results, stable knockdown efficiently impedes the colony formation of these cancer cells (Figure 4.1.A and 4.3).

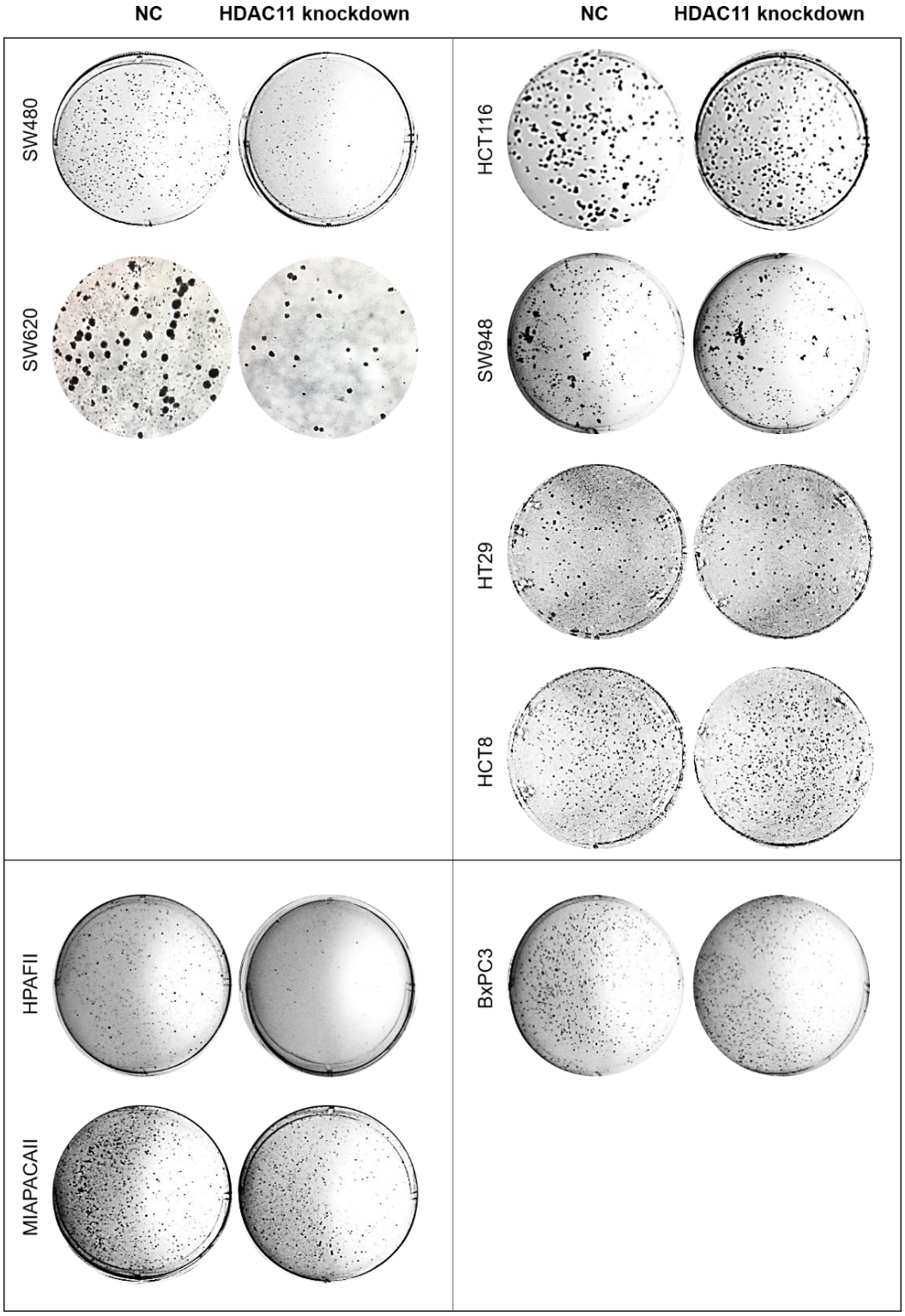

Figure 4.3. Colony formation (Soft Agar) assay results with HDAC11 knockdown. Left column shows cancer cells with high dependency on KRAS and right column

shows cancer cell with low dependency on KRAS. Knockdown efficiency for each cell line based on mRNA level: 63% (SW480), 62% (SW620), 64% (HCT8), 62% (HCT116), 61% (SW948), 75% (HT29), 62% (HPAFII), 54% (MIAPACAII), 70% (BxPC3).

Mechanistic investigation in the HDAC11-sensitive cancer cells

To understand why certain cell lines are more sensitive to HDAC11 inhibition, we checked the mutation status of p53, KRAS, and HRAS in these cell lines. Interestingly, SW480, SW620, SKCO1, HPAFII, and MIAPACA2 have KRAS mutations and they have been reported to highly depend on KRAS among KRAS mutant cancer cells.[5]

The small GTPase – CDC42 has been reported to be a downstream effector of KRAS and related to cell cytoskeleton. Disruption of cell cytoskeleton has been well-known to be crucial for cancer cell proliferation including colony formation. To validate CDC42 as a potential HDAC11 substrate in endogenous system, we knocked down HDAC11 in SW620 cells and HPAFII cells. Consistent with the SIS17 data, knockdown of HDAC11 also increased CDC42 lysine fatty acylation (Figure 4.4).

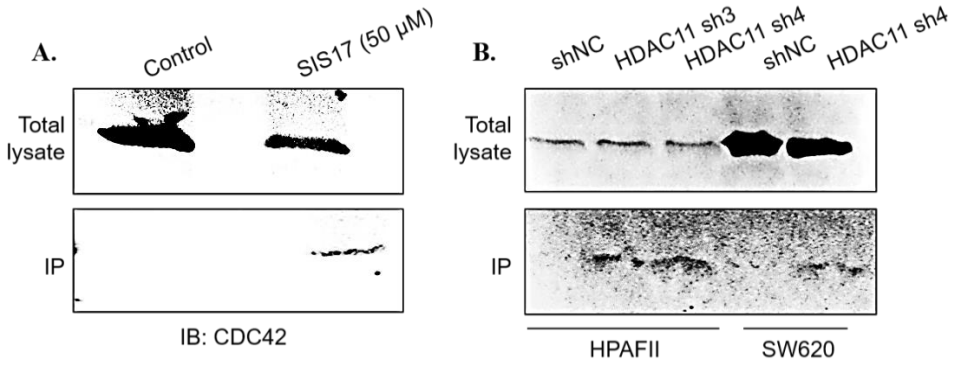

Figure 4.4. Fatty acylation of CDC42 in cells. (A) Endogenous fatty acylated CDC42 level with SIS17 in SW620 cells. (B) Endogenous fatty acylated CDC42 level with HDAC11 knockdown in HPAFII and SW620.

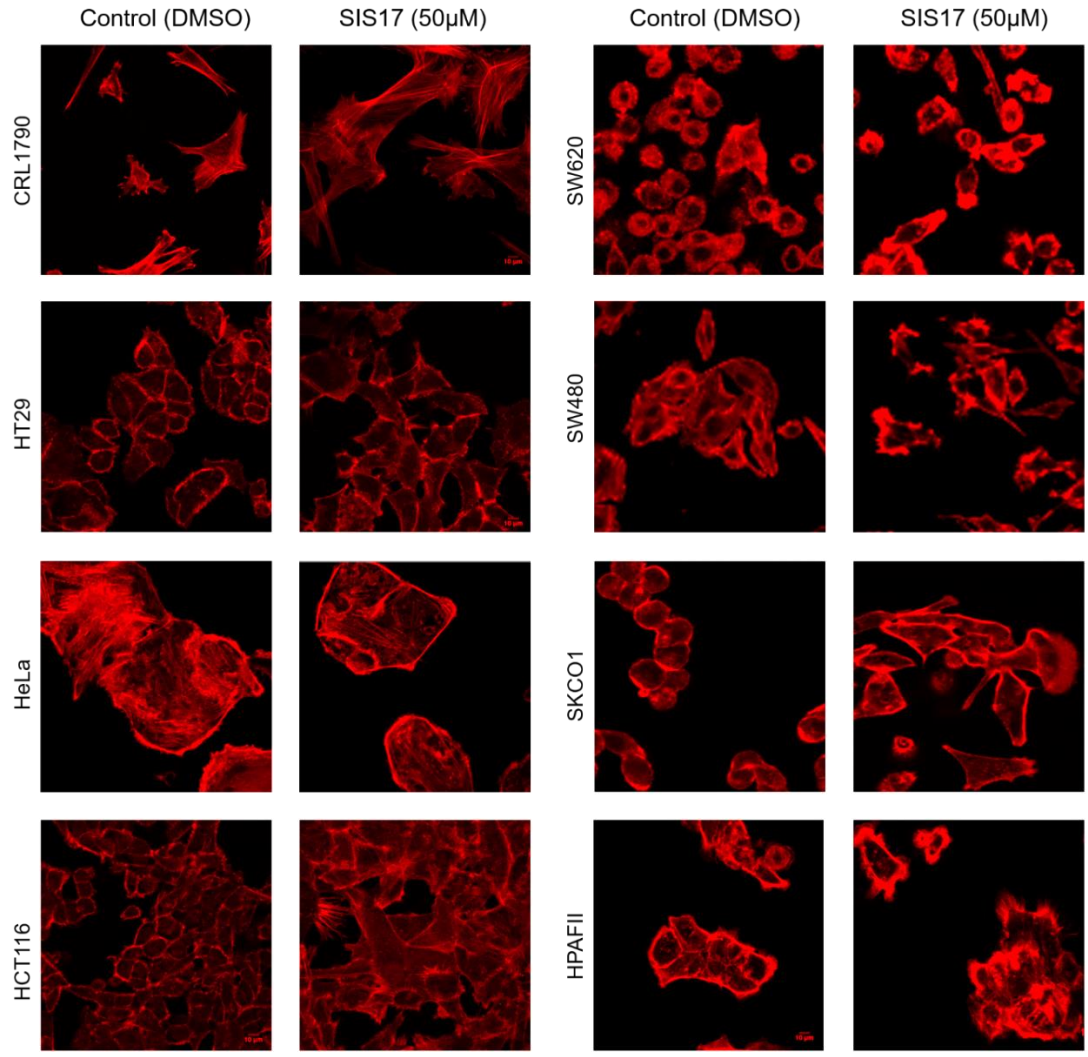

Figure 4.5. Actin morphology change with SIS17 treatment in different cell lines.

Next, since CDC42 is highly involved in formation of cell cytoskeleton as a KRAS downstream gene, we examined actin morphology with and without HDAC11 suppression. Most of the colon and pancreatic cancer cells which are used for 2D cell proliferation and 3D soft agar assays was examined for actin morphology. SIS17 treatment and HDAC11 knockdown showed more pronounced actin disruption in cancer cells that are more sensitive to HDAC11 inhibition in the soft agar assay (Figure 4.5). For example, in SW480 and SW620 cells that are sensitive to SIS17, we could notice that actin was located evenly on cell envelope without HDAC11 inhibition but clusters of increased actin staining were clearly visible after HDAC11

inhibition (Figure 4.5). In contrast, with cells that are less sensitive to SIS17, there is not much different in actin staining with and without SIS17 (Figure 4.5).

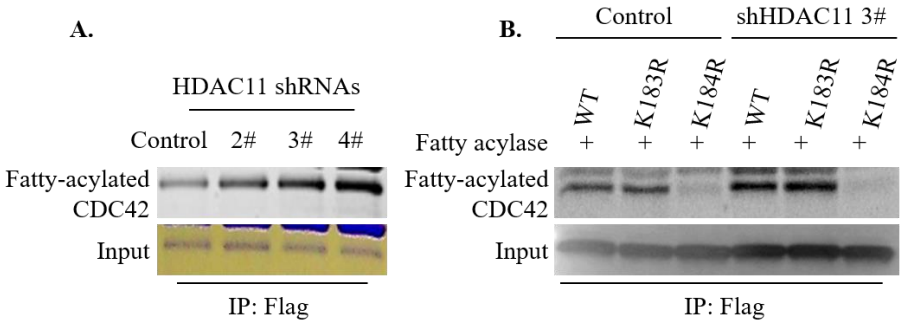

Figure 4.6. Fluorescence gel results to demonstrate lysine defatty acylation site on CDC42. (A) HDAC11 knockdown increased fatty acylation level of CDC42. (B). Lysine to Arginine mutant on K184 drastically decreased fatty acylation signal of CDC42.[7]

To demonstrate that the actin staining change is due to defatty acylation activity of HDAC11 on CDC42, HDAC11 catalytic site on CDC42 was examined by Dr. Ji Cao (Figure 4.6).[7] Dr. Cao first demonstrated that CDC42 is a potential HDAC11 substrate through fluorescence gel assay with HDAC11 knockdown (Figure 4.6.A). He then performed site directed mutagenesis converting lysine to arginine on CDC42 to show that lysine 184 (K184) position is the catalytic activity site of HDAC11 (Figure 4.6.B). After fluorescence gel assays with WT and KR mutants, he concluded that the K184R mutant cannot be fatty acylated. Hence, K184 could be the main fatty acylation site on CDC42 (Figure 4.6.B).[7]

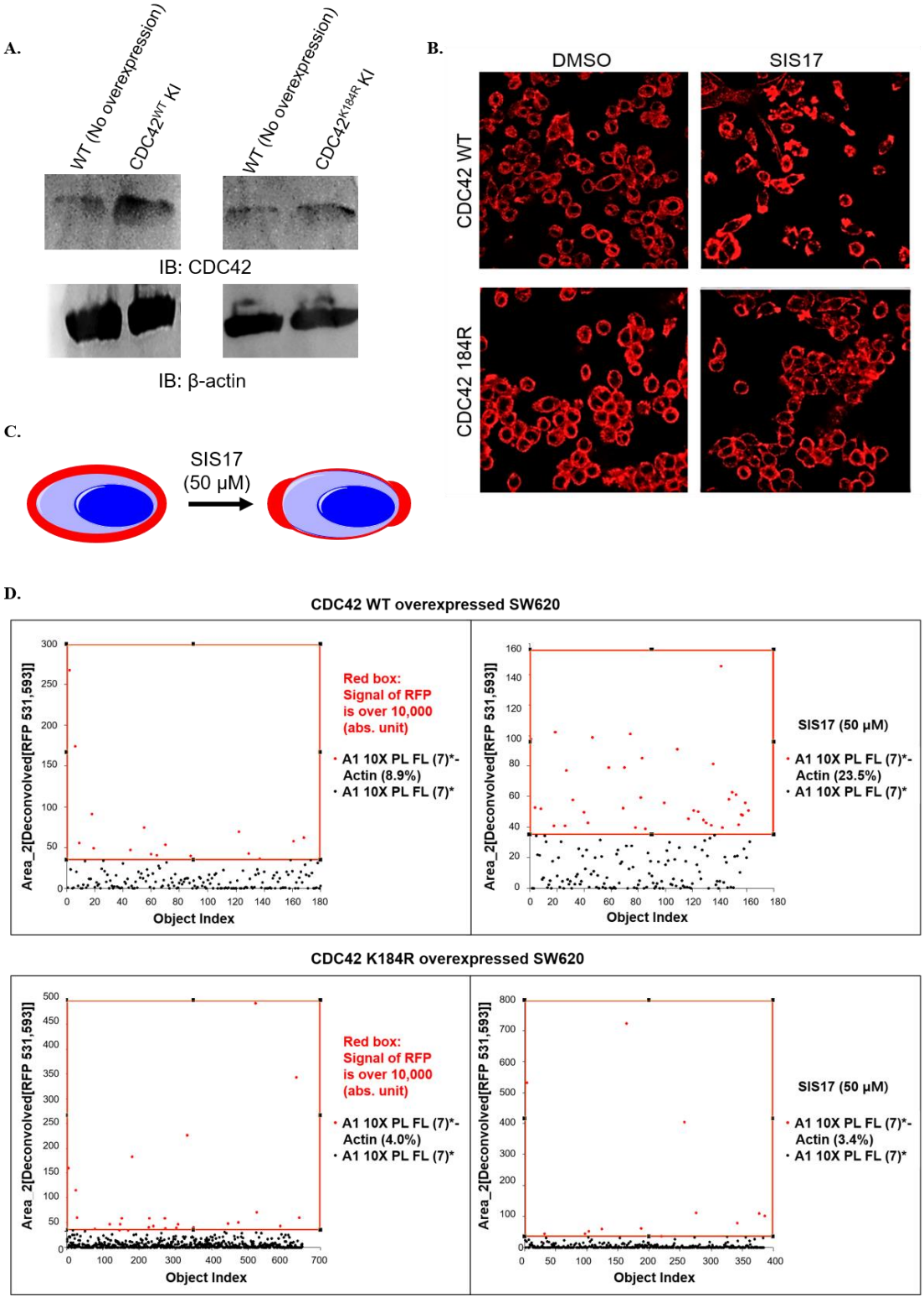

Figure 4.7. Actin morphology change with SIS17 treatment in CDC42 WT and

K184R overexpressed SW620. (A) CDC42 Overexpression level through western blot. (B) Actin morphology change in SIS17 treated CDC42 WT overexpressed SW620. (C) Schematic drawing showing the effect of SIS17 on actin morphology. (D) Quantification of actin area (y-axis) and intensity of red fluorescence signal (RFP) of Rhodamine Phalloidin - (Indicated as Red dots).

We then checked whether the expression of the K184R mutant could rescue the actin morphology change induced by SIS17. With CDC42 K184R overexpression, actin morphology disruption by SIS17 was not observed, but with CDC42 WT overexpression, the same actin morphology disruption by SIS17 was observed. This result supports that SIS17 inhibits HDAC11 to increase CDC42 lysine 184 fatty acylation, leading to actin distribution in cells (Figure 4.7.B). To quantify the actin morphology disruption results, we considered both area and signal intensity of red fluorescence signal (Rhodamine Phalloidin; F-actin signal) (Figure 4.7.C and D). With the treatment of SIS17 in CDC42 WT overexpressed SW620, F-actin signal became stronger while the area of the signal became smaller since the signal is dense at the edges of cells. Hence, we put an index for each cell which is indicated on the x-axis and the area of F-actin signal was plotted on the y-axis (Figure 4.7.D). We could see that in CDC42 WT overexpressed cells, the area of F-actin with SIS17 was smaller than without SIS17. Additionally, we set up the threshold of signal intensity of F-actin as 10,000 (abs.unit) and calculated how much cells showed intensity over 10,000 (abs.unit) for each group. CDC42 WT overexpressed SW620 cells with SIS17 showed stronger F-actin signal in more localized area than without SIS17 (8.9% of cells with actin signal over the threshold without SIS17 and 23.5% with SIS17). On the other hand, CDC42 K184R overexpressed SW620 cells showed no difference with and without SIS17 (4.0% of cells with actin signal over the threshold without SIS17 and 3.4% with SIS17) (Figure 4.7.D).

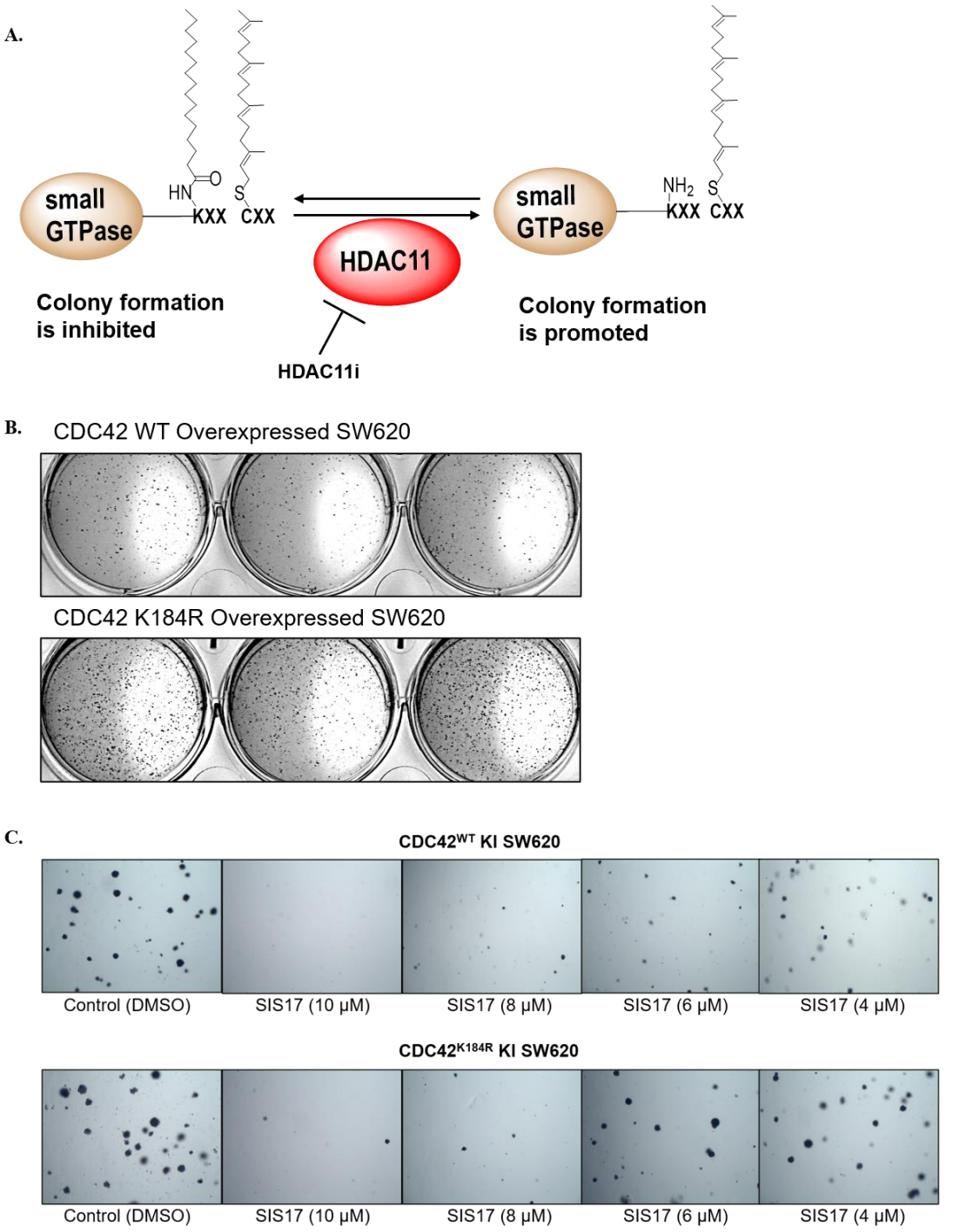

Figure 4.8. Colony formation affected by CDC42 lysine fatty acylation. (A) Working model how the loss of lysine fatty acylation on K184 would affect colony formation. (B) Soft agar colony formation of SW620 cells overexpressing CDC42 WT or K184R. Cells (8000 per well) were cultured for 2.5 weeks. (C) CDC42 K184R overexpression

desensitized SIS17 effects on colony formation. With CDC42 K184R overexpression, colony size is bigger than with CDC42 WT overexpression.

Last, we examined whether CDC42 fatty acylation on K184 is important for anchorage-independent growth by comparing the soft agar colony formation of SW620 cells overexpressing CDC42 WT or K184R mutant. Since HDAC11 inhibitors decreased colony formation of SW620 cells, we predicted that increased population of CDC42 lysine fatty acylation would inhibit colony formation (Figure 4.8A). Thus, SW620 cells overexpressing CDC42 K184R, which cannot be fatty acylated, would better form colonies on soft agar. As a result, with the same amounts of cells and time periods, SW620 with CDC42 K184R overexpression formed more colonies compared to that with CDC42 WT overexpression (Figure 4.8B).

To further demonstrate that the effect of SIS17 on anchorage-independent growth is through HDAC11's regulation of CDC42 lysine fatty acylation, we examined the effect of SIS17 cells on anchorage-independent growth in SW620 cells overexpressing either CDC42 WT or the K184R mutant (Figure 4.8.C). CDC42 WT expressing cells, SIS17 was able to decrease both the size and the number of colonies formed. In contrast, in CDC42 K184R expressing cells, SIS17 was only able to decrease the number of colonies formed (Figure 4.8.C). The data suggest that lysine fatty acylation of CDC42 regulates the colony size, while the colony number may be regulated through other substrates of HDAC11.

Summary

By testing different cancer cell lines with HDAC11 inhibition and knockdown, we discovered that transformation of KRAS-dependent cancers is efficiently inhibited by the HDAC11-specific inhibitor, SIS17, or by HDAC11 knockdown. Mechanistically, we found HDAC11 removes CDC42 lysine fatty acylation and this is important for the anchorage-independent growth of KRAS-dependent cancer cells. We validated CDC42 as an HDAC11 substrate and identified K184 as the fatty acylation site. Since CDC42 is well-known as a downstream effector of KRAS and regulates cell cytoskeleton, it is not surprising that we found HDAC11 inhibition affects actin morphology in the KRAS-dependent cancer cells. KRAS mutation is found in many human tumors and is a well-known tumor driver. However, efforts to directly target KRAS mutants have so far found only very limited success. Our findings here may provide a novel strategy, HDAC11 inhibition, to target KRAS-dependent cancers. Given that HDAC11 knockout in mice displayed no major harmful effect, this strategy may be much safer than other methods that target KRAS-dependent cancers.

Methods

A. General Information

Reagents. SIS17 was prepared as previously described in Chapter 2. CDC42 (#2462) and anti-rabbit IgG-HRP were purchased from Cell Signaling Technology (CST). Protease inhibitor cocktail for lysing cells was purchased from Sigma-Aldrich. ECL plus western blotting detection reagent and universal nuclease for cell lysis were purchased from Thermo Scientific Pierce.

Cell culture. HEK293T cells were cultured in DMEM with 10% (v/v) heat-inactivated at 56 ^{o}C (HI) FBS and SW620 cells were cultured in Leibovitz 15 with 10% HI FBS. The cell lines used for experiments had been passaged no more than 20 times and all cell lines were tested for and showed no mycoplasma contamination.

Stable overexpression of CDC42 WT and K184R mutant in SW620 cells

Human CDC42 WT was inserted into pCDH-CMV-MCS-EF1-Puro vector with flag tag. SIRT6 K184R mutants were made by the sited-mutagenesis. CDC42 lentivirus was generated by co-transfection of CDC42, pCMV-dR8.2, and pMD2.G into HEK 293T cells. After transfection for 48 hr, the medium was collected and used for infecting SW620 cells. SW620s with stable expressed CDC42 WT and K184R was selected by 2.0 mg/mL of puromycin.

Detection of lysine fatty acylation on CDC42 by in-gel fluorescence

CDC42, HDAC11 and fatty acylase were co-transfected into HEK 293T cells by fugene-6 transfection reagent. After 24 hr, the cells were treated with 50 μM of Alk14 and the inhibitor (DMSO for no inhibitor groups) for 6 hr. The cells were collected at 500 g for 5 min and then lysed in Nonidet P-40 lysis buffer (25 mM Tris-HCl pH 7.4, 150 mM NaCl, 10% glycerol, and 1% Nonidet P-40) with protease inhibitor cocktail in ice. The total lysate was incubated with anti-FLAG affinity gel at 4°C for 2 hr. The affinity gel was then washed three times by immunoprecipitation (IP) washing buffer (25 mM Tris-HCl pH 7.4, 150 mM NaCl and 0.2% Nonidet P-40) and then re-

suspended in 18 µL of IP washing buffer. The click chemistry reaction was performed by adding the following reagents: 520-BODIPY azide (0.8 µL of 1.5 mM solution in DMF), TBTA (1.2 µL of 10 mM solution in DMF), $CuSO_4$ (1 µL of 40 mM solution in H_2O) and TCEP (1 µL of 40 mM solution in H_2O). The reaction was allowed to proceed at room temperature for 30 mins in dark. Then, the SDS loading buffer was added and heated at 95°C for 10 min. After centrifugation at 15,000 g for 2 min, the supernatant was collected and treated with 400 mM hydroxylamine at 95°C for 5 min. The samples were resolved by 15% SDS-PAGE. In-gel fluorescence signal was recorded by Typhoon 9400 Variable Mode Imager (GE Healthcare Life Sciences) and CDC42 bands were right under the light chain.

Detection of Lysine Fatty Acylation on Endogenous CDC42 by Western Blot. SW620 cells were treated with 50 µM of Alk14 and inhibitor or DMSO for 6 hours. Two of 80-90% confluent 15-cm SW620 cells (approximately $2*10^6$ cells per 15-cm dish) cells were collected by centrifugation at 1000 g for 5 min and lysed in 4% SDS lysis buffer (50 mM triethanolamine at pH 7.4, 150 mM NaCl, 4% (w/v) SDS) with protease inhibitor cocktail (1:100 dilution) and nuclease (1:1000 dilution) at room temperature for 15 min. The proteins were precipitated with cold methanol (200 µL per sample), cold chloroform (75 µL per sample), and cold water (150 µL per sample). After vortexing to mix well, samples were spun down at 17,000 g for 15 min. Proteins should be located between the upper layer and bottom layer. The upper layer of the solvents was gently removed. Then 1 mL of cold methanol was added to each sample to wash the proteins by vortexing them. Samples were centrifuged at 17,000g for 5 min. The washing was repeated once more. After methanol washing, methanol was removed from tubes and protein pellets in tubes were air-dried for 5-10 min. Proteins were dissolved in 100 µL of click chemistry buffer (25 mM HEPES, pH 7.4, 150 mM NaCl, and 4% (w/v) SDS). The proteins were sonicated for 30 min at room temperature to be resolubilized. The concentration of the resolubilized proteins was determined using a BCA assay. For each sample, 800 µg of proteins were used for click chemistry (for samples that have higher protein concentration, the volume was

adjusted with click chemistry buffer). Biotin-N_3 (5 μL of 5 mM solution in DMF), Tris[(1-benzyl-1H-1,2,3-triazole-4-yl)methyl]amine (5 μL of 2 mM solution in DMF), $CuSO_4$ (5 μL of 50 mM solution in H_2O) and Tris(2-carboxyethyl)phosphine (5 μL of 50 mM solution in H_2O) were added into the reaction mixture. The click chemistry reaction was allowed to proceed at 30^oC for 3 hrs. Proteins were then precipitated using cold methanol, chloroform (and water as described above. After washing two times with cold methanol, the proteins were resolubilized in 120 μL of 4% SDS lysis buffer. Again, the concentrations of proteins were measured by BCA, and 10 μg of proteins for each sample were set aside as input. Then, 400μg of proteins for sample was added into 10 mL of IP washing buffer (25 mM Tris-HCl pH 8.0, 150 mM NaCl, 0.2% (v/v) NP-40) (making sure that SDS is lower than 0.1% in IP washing buffer for efficient affinity purification with streptavidin beads). Streptavidin agarose beads (Thermo Fisher, 20 μl) were added into each sample. The mixture was agitated for overnight at room temperature. After washing the beads three times with 1 mL of IP washing buffer, 24 μL of 4% (w/v) SDS lysis buffer and 6 μL of 6× loading dye were added into each sample and boiled for 10 min. The samples and inputs were resolved using 12% SDS-PAGE gel, transferred to nitrocellulose membrane, and analyzed by western blot for CDC42 (samples; IP) and (input). The signal was recorded using a Typhoon 9400 Variable Mode Imager (GE Healthcare Life Sciences).

Confocal microscopy

Cells were seeded in 35 mm glass bottom dishes (MatTek) and the inhibitor was treated when cells were seeded. After 24hrs, cells were attached to the plate. For immunofluorescence, cells were rinsed with 1 × PBS twice and fixed with 4% paraformaldehyde (v/v in 1 × PBS) for 15 min. The fixed cells were washed twice with 1 × PBS, permeabilized and blocked with 0.1% Saponin/5% BSA/1 × PBS for 30 min. The cells were then incubated for 1 hr at 4°C in dark with rhodamine phalloidin at 1/50 - 1/100 dilution (in 0.1% Saponin/5% BSA/1 × PBS). Samples were washed with 0.1% Saponin/1 × PBS three times and mounted with Fluoromount-G® (0100–01) from Southern Biotech before imaging with Zeiss 710 inverted confocal

microscopy. Images were processed with Fiji software.

Soft agar colony formation assay

To assess the effect of the inhibitor and knockdown in anchorage-independent growth, 0.6% base low-melting point agarose (LMP) and 0.3% top LMP were prepared by mixing 1.2% LMP in H_2O and 0.6% LMP in H_2O, respectively, with 2 × complete medium in 1:1 (v/v) ratio. 1.5 mL of 0.6% base LMP was added to each well of 6-well plate and allowed to solidify for 30 min at room temperature. Then 5.0×10^3 cells were resuspended in 0.3% LMP top LMP and plated onto 6-well plate pre-coated with the base LMP. 150 μL of complete medium was added on top of the 0.3% LMP and refreshed every 3 days. After at least 14 days of culture, colonies were stained with 200 μl of nitro blue tetrazolium chloride solution in 1X PBS (1mg/ml) per well for overnight incubation at 37 ºC.

Cell proliferation assay for inhibitor screening

Cells were seeded in 96-well plate at a density of 1.0×10^3 cells/well (100 μl) 24 hr before being treated with the inhibitor. The inhibitor in 100 μl of media was treated for each well and incubated for next 48 hrs at 37 ºC. Cell-titer blue reagent (40 μl per well) was treated and incubated until cell media turned into violet. It is important to stop incubating before the color of media turned into light violet/ pink to avoid the saturation of signal. The viable cell population was measured by the indicating emission UV wavelength from a vendor. (It could be various from a vendor and a lot number of the reagent.)

Cell proliferation assay for HDAC11 knockdown

HCT116 and MCF7 cells were seeded in 12-well plate at a density of 1.5×10^4 cells/well 24 hr before being infected with luciferase (Ctrl) shRNA- or HDAC11 shRNA-carrying lentivirus for 0 or 4 days. After knocking down HDAC11 for the indicated time, cells were washed with 1 × PBS, fixed with ice-cold methanol for 10 min and then stained with 0.25% crystal violet (m/v, in 25% methanol) for 10 min.

The stained cells were washed with running distilled water, air-dried and solubilized in 200–800 μL of 0.5% SDS in 50% ethanol. Absorbance of the resulting solution was measured at 550 nm.

Cloning and mutagenesis

The human CDC42 lentiviral vector was obtained by inserting FLAG-CDC42 into pCDH-CMV-MCS-EF1-Puro vector. The expression vector for CDC42 K184R was generated by QuikChange site-directed mutagenesis

References

1. Hedwig E Deubzer, Marie C Schier, Ina Oehme, Marco Lodrini, Bernard Haendler, Anette Sommer, Olaf Witt, HDAC11 Is a Novel Drug Target in Carcinomas, *Int. J. Cancer*, **132**, 2200-2208, doi: 10.1002/ijc.27876, (2013).
2. Theresa M Thole, Marco Lodrini, Johannes Fabian, Jasmin Wuenschel, Sebastian Pfeil, Thomas Hielscher, Annette Kopp-Schneider, Ulrike Heinicke, Simone Fulda, Olaf Witt, Angelika Eggert, Matthias Fischer, Hedwig E Deubzer, Neuroblastoma Cells Depend on HDAC11 for Mitotic Cell Cycle Progression and Survival, *Cell Death Dis.*, **8**, e2635. doi: 10.1038/cddis.2017.49, (2017).
3. Patrick L Leslie, Yvonne L Chao, Yi-Hsuan Tsai, Subrata K Ghosh, Alessandro Porrello, Amanda E D Van Swearingen, Emily B Harrison, Brian C Cooley, Joel S Parke, Lisa A Carey, Chad V Pecot, Histone Deacetylase 11 Inhibition Promotes Breast Cancer Metastasis From Lymph Nodes, *Nat. Commun.*, **10**, 4192, doi: 10.1038/s41467-019-12222-5, (2019).
4. Marta Kapałczyńska, Tomasz Kolenda, Weronika Przybyła, Maria Zajączkowska, Anna Teresiak, Violetta Filas, Matthew Ibbs, Renata Bliźniak, Łukasz Łuczewski, Katarzyna Lamperska, 2D and 3D Cell Cultures - A Comparison of Different Types of Cancer Cell Cultures, *Arch Med Sci.*, **14**, 910-919, doi: 10.5114/aoms.2016.63743, (2018); Kenny Chitcholtan 1, Eric Asselin, Sophie Parent, Peter H Sykes, John J Evans, Differences in Growth Properties of Endometrial Cancer in Three Dimensional (3D) Culture and 2D Cell Monolayer, *Exp Cell Res.*, **319**, 75-87. doi: 10.1016/j.yexcr.2012.09.012, (2012).
5. di Magliano MP, Logsdon CD., Roles for KRAS in Pancreatic Tumor Development and Progression, *Gastroenterology*, **144**, 1220-1229, doi: 10.1053/j.gastro.2013.01.071, (2013); Anurag Singh, Michael F Sweeney, Min Yu, Alexa Burger, Patricia Greninger, Cyril Benes, Daniel A Haber, Jeff Settleman, TAK1 Inhibition Promotes Apoptosis in KRAS-dependent Colon Cancers, *Cell*, **148**, 639-650, doi: 10.1016/j.cell.2011.12.033, (2012).
6. Cao, J.; Sun, L.; Aramsangtienchai, P.; Spiegelman, N. A.; Zhang, X.; Seto, E.; Lin,

H., HDAC11 regulates type I interferon signaling through defatty-acylation of SHMT2, *PNAS*, **116,** 5487-5492, doi: 10.1073/pnas.1815365116, (2019); Shanglei Ning, Siquan Ma, Abdul Qahar Saleh, Lingyu Guo, Zixiao Zhao, Yuxin Chen, SHMT2 Overexpression Predicts Poor Prognosis in Intrahepatic Cholangiocarcinoma, *Gastroenterol Res. Pract.*, 4369253. doi: 10.1155/2018/4369253, (2018); Zhen Wei, Jinglue Song, Guanghui Wang, Ximao Cui, Jun Zheng, Yunlan Tang, Xinyuan Chen, Jixi Li, Long Cui, Chen-Ying Liu, Wei Yu, Deacetylation of Serine Hydroxymethyl-Transferase 2 by SIRT3 Promotes Colorectal Carcinogenesis, *Nat. Commun.*, **9**, 4468. doi: 10.1038/s41467-018-06812-y, (2018).

7. The fluorescence gel experiments were done by Dr. Ji Cao.

CONCLUSIONS AND FUTURE DIRECTIONS

In my thesis work, I first focused on developing selective HDAC11 inhibitors based on the defatty-acylation function of HDAC11 as described in Chapter 2. I introduced a long fatty acyl group into previous pan-HDAC inhibitors which are composed of zinc-binding groups, linkers, and surface recognition groups. Although such a strategy did work for SAHA and Mocetinostat, using UF010, which does not have a linker part, I was able to obtain several HDAC11-specific inhibitors. The key finding for my HDAC11 inhibitor is that the electron-donating group is essential for potent HDAC11 inhibition. Through a series of assays, I confirmed that SIS17 inhibits HDAC11 selectively both in vitro and in cells.

In Chapter 3, I presented results from screening natural products as a potential HDAC11 inhibitor. Surprisingly, Garcinol, which was reported as an HAT inhibitor turned out to be potent HDAC11 inhibitor. Garcinol exhibits potent HDAC11 inhibition based on both in vitro HPLC assay and in cell SHMT2 fatty acylation assay. In addition, Garcinol is selective for HDAC11 and does not affect the acetylation level of histone in cells. This study provides a new HDAC11 inhibitor from natural product and provide key insights to understand the underlying mechanism of Garcinol's various biological effects.

In Chapter 4, I described the results of screening cancer cells with HDAC11 inhibitor and HDAC11 knockdown. HDAC11 inhibitor (SIS17) can efficiently impede colony formation of colon and pancreatic cancer cells that are highly dependent on KRAS. I connected this phenotype to CDC42, which is a HDAC11 substrate. CDC42 was discovered as a HDAC11 substrate by Dr. Ji Cao. By mutagenesis (Lysine to Arginine) in CDC42, he concluded that lysine 184 (K184) site of fatty acylation. Following his findings, I confirmed that CDC42 is an HDAC11 substrate the KRAS-dependent cancer cell line SW620. In addition, because CDC42 is a downstream effector of KRAS and regulates the cell cytoskeleton, I showed that HDAC11

inhibition affects the actin morphology in KRAS-dependent cancer cells. This finding could explain the inhibition of colony formation since cytoskeleton change is well-known to be related to the transformation of cancer cells. Furthermore, to demonstrate that this cytoskeleton changes and inhibition of colony formation is due to inhibition of HDAC11 lysine defatty acylation on CDC42, I generated SW620 cells overexpressing CDC42 WT or K184R mutant. K184R overexpression could rescue the effect of SIS17 on actin morphology and colony formation.

These studies suggest that HDAC11 inhibitors could be a potential therapeutic strategy for KRAS-driven cancers. However, to further establish this, we would need to further understand the underlying mechanism of this phenotype, namely how CDC42 fatty acylation affects its activity. Also, we need to demonstrate that HDAC11 inhibitors can effectively suppress tumor growth in mouse models. The challenge is the availability of potent HDAC11 inhibitors that work in animals.

APPENDIX A: PERMISSION FOR REPRODUCTION

Chapter 2: Reproduced with permission from Son et al, *ACS Chem. Biol.*, **2019**, 14 (7), pp 1393-1397.

The publisher terms and conditions are available by accessing the website below:

https://pubs.acs.org/page/copyright/permissions_otherpub.htm